NMR solution structure of C2 domain of MFG-E8 and insights into its recognition with phosphatidylserine

Li, Baihong

2013

Li,B. (2013). NMR solution structure of C2 domain of MFG-E8 and insights into its recognition with phosphatidylserine.. Doctoral thesis, Nanyang Technological University, Singapore.

https://hdl.handle.net/10356/54855

https://doi.org/10.32657/10356/54855

NMR Solution Structure of C2 Domain of MFG-E8 and Insights into Its Recognition with Phosphatidylserine

Li Baihong

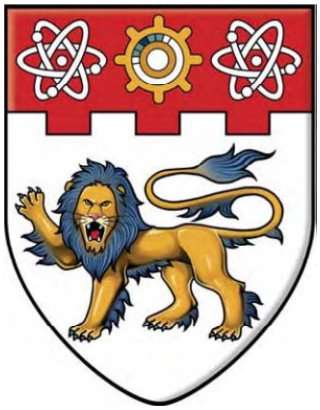

SCHOOL OF BIOLOGICAL SCIENCES

NANYANG TECHNOLOGICAL UNIVERSITY

A thesis submitted to the Nanyang Technological University

in fulfillment of the requirement for the degree of

Doctor of Philosophy

2012

Abstract

MFG-E8 (also known as lactadherin), which is a secreted glycoprotein from a variety of cell types, possesses two EGF domains and tandem C domains with sequence homology to that of blood coagulation proteins factor V and factor VIII. MFG-E8 binds to phosphatidylserine (PS) in membranes with high affinity. We have recently shown that the C2 domain of MFG-E8 bears more specificity toward PS when compared with phophatidylcholine (PC), another phospholipid thought to be involved in the immune function of phagocytes. In our current study, we have determined the solution structure of the C2 domain by nuclear magnetic resonance (NMR) spectroscopy, characterized the molecular basis of binding between the C2 domain and PS by ^{31}P-NMR spectroscopy. Furthermore, we also verified that positively charged and aromatic residues clustered in loops 1-3 of the C2 domain play key roles in recognizing PS in apoptotic cells. Last but not least, the influence of C1 domain on PS binding was also tested in our new Co-culture FACS analysis and confirmed its role in the binding event.

Acknowledgements

I would like to express my sincere thanks to my supervisor Prof. Yoon Ho Sup for his supervision, guidance, encouragement and support in work and in life during my staying in the school of biological sciences.

I am also thankful to Dr. Choi Bo Hwa for her help as my first mentor and teaching in the field of cell culture and FACS analysis; Dr. Ye Hong for her help in NMR data collection and processing; and Dr. Xu Huibin and Dr Liang yu for teaching me all aspects of protein engineering.

I am also deeply indebted to all the other colleagues and ex-colleagues in the lab. They are: Dr. Kang Congbao, Dr. Shin Joon, Dr. B. S. R. Naga, Dr. Souvik Chattopadhaya, Dr. Goutam Chakraborty, Dr. Reema Alag, Dr. A. V. K. H. Kishore, Dr. Sreekanth Rajan, Mr. Liu Wei, Mr. Nguyen Quoc Toan, Mr. Ajit Prakash, Ms. Toh Hui Ting, Ms. Choi Minjoo and Ms. Chin Hui Li.

My special thanks go to my partner Zhao Jing, for her help on the lab experiments, her understanding in our life and her love and support in the past few years.

I deeply thank my parents for their love, encouragement and support in my life.

ABBREVIATIONS

2D	Two-dimensional
3D	Three-dimensional
β_2-GPI	β_2-glycoprotein I
ACAMPs	Apoptotic-cell-associated-molecular-patterns
Apaf-1	Apoptosis-activating factor 1
APLT	Aminophospholipid transporter / translocase
APS	Ammonium persulfate
ATP	Adenosine-5'-triphosphate
Caspases	Cysteine Aspartate–Specific ProteASEs
CBL	Ca^{2+}-binding loops
CD95	Fas Receptor
cPLA2α	Cytosolic phospholipase A2
CRP	C-reactive protein
CSI	Chemical Shift Index
DAG	Diacylglycerol
DC	Dendritic cells
DMEM	Dulbecco's modified Eagle's medium
DMSO	Dimethyl sulfoxide
DNA	Deoxyribonucleic acid
dNTP	Deoxyribonucleotide
DS	Discoidin
DSS	2,2-dimethyl-2-silapentane-5-sulonate, sodium salt
DTT	1,4-Dithiothreitol
ER	Endoplasmic reticulum
EDTA	ethylene glycol-bis (β-aminoethylether)-N, N' tetraacetic acid
FACS	Fluorescence Activated Cell Sorting
FADD	Fas-associated death domain
FAK	Focal adhesion kinase
FPLC	Fast protein liquid chromatography

FSC	Forward-scattering signal
Gas6	Growth arrest specific gene 6
GFP	Green fluorescent protein
GST	Glutathione-S-transferase
HeLa	Human cervical cancer cell line
HMQC	Heteronuclear multiple-quantum correlation spectroscopy
HSQC	Heteronuclear single quantum correlation
ICAM3	Intercellular adhesion molecule 3
IL-10	Interleukin-10
IPTG	Isopropyl-Thio-B-D-galactopyranoside
Jurkat	Immortalized line of T lymphocyte cells
K_d	Dissociation constants
kDa	kilo Daltons
LB	Luria-Bertani or Lysogeny Broth
LOX1	Oxidised low-density lipoprotein receptor 1
LPS	Lipopolysaccharide
LR	Lower-right quadrant
LTP	Lipid-transfer protein
MALDI	Matrix-assisted laser desorption/ionization
MFG-E8	Milk fat globule EGF-factor 8
MW	Molecular weight
MS	Mass spectrometry
NMR	Nuclear magnetic resonance
NOE	Nuclear Overhauser effect
NOESY	Nuclear Overhauser effect spectroscopy
nt	Nucleotide
oxLDL	Oxidized low-density lipoprotein
OD	Optical density
PA	Phosphatidic acid
PAF	Platelet activating factor
PAMPs	Pathogen-associated-molecular-patterns

PBS	Phosphate buffer saline
PC	Phosphatidylcholine
PCR	Polymerase chain reaction
PE	Phosphatidylethanolamine
PI	Propidium iodide
PKC	Protein kinases C
PLC	Phospholipase C
PLSCR	Phosholipid scramblase
PM	Plasma membrane
PMSF	Phenylmethylsulfonyl fluoride
PS	Phosphatidylserine
PSR	PS receptor
PSS1	PS-synthase 1
PSS2	PS-synthase 2
PtdIns, or PI	Phosphatidylinositol
PtdIns(4,5)P_2	Phosphatidylinositol-4,5-biphosphate
PtdSer	Phosphatidylserine
PtdSerR	Phosphatidylserine receptor
RGD motif	(Arg-Gly-Asp) motif
RMSD	Root-mean-square-deviation
rpm	Revolutions per minute
RPMI	Roswell Park Memorial Institute medium
SDS-PAGE	Sodium dodecyl dulphate-polyacrylamide gel electrophoresis
SRA	Class-A scavenger receptor
SSC	Side-scattering signal
SUMO	Small Ubiquitin-like Modifier
TALOS	Torsion Angle Likelihood Obtained from Shift and sequence similarity
TCEP	Tris-(2-carboxyethyl)-phosphine
TEMED	N,N,N',N'-Tetramethylethylenediamine
TGF-β1	Transforming growth factor-β1

THP-1	Human acute monocytic leukemia cell line
TNF	Tumor-necrosis factor
TOCSY	Total correlation spectroscopy
TSP1	Thrombospondin 1
UL	Upper-left quadrant
UV	ultraviolet
v/v	Volume per volume
WT	Wild type

Table of Contents

List of Figures

List of Tables

1 INTRODUCTIONS

1.1 Apoptosis

Apoptosis is a process that removes unhealthy and unwanted cells, which is essential for mammalian homeostasis (Jacobson et al., 1997).The concept and terminology of apoptosis were first proposed by Kerr et al 40 years ago (Kerr et al., 1972). ‘Shrinkage necrosis’ was used when they first observed this morphologically distinct cell death phenomenon during the research about the rapid shrinkage of liver tissue after interruption of its port alvenous blood supply (Kerr, 2002; O'Rourke and Ellem, 2000). Repeated observation of this death type from following studies on basal cell carcinomas (Kerr and Searle, 1972), adrenal cortex of rats treated with prednisolone (Wyllie et al., 1973), and some other studies led to a new term consisting of the Greek words ‘apo’ and ‘ptosis’, with meaning of ‘from’ and ‘falling’ respectively, coined ‘Apoptosis’ (Kerr, 2002). It differs significantly in morphology from the typical necrosis, in which membrane integrity is compromised and cells begin to swell up, followed by the spillage of their contents into surrounding tissues and subsequent incitement of local inflammation (Blankenberg, 2008). Cells undergoing apoptosis exhibit following morphological changes: the cells rounding up, cellular volume reducing, chromatin condensed, nuclear-fragmented, few or no ultra-structural modifications of cytoplasmic organelles, and plasma membrane loosing asymmetry, but the cells remain integrated until the final stage of the process (Kroemer et al., 2005), as shown in Figure 1. These morphological changes, especially the maintenance of the integrity of various membrane

structures, retain intracellular toxic substances, and thus do not induce local inflammations nor release the self-antigens (Blankenberg, 2008).

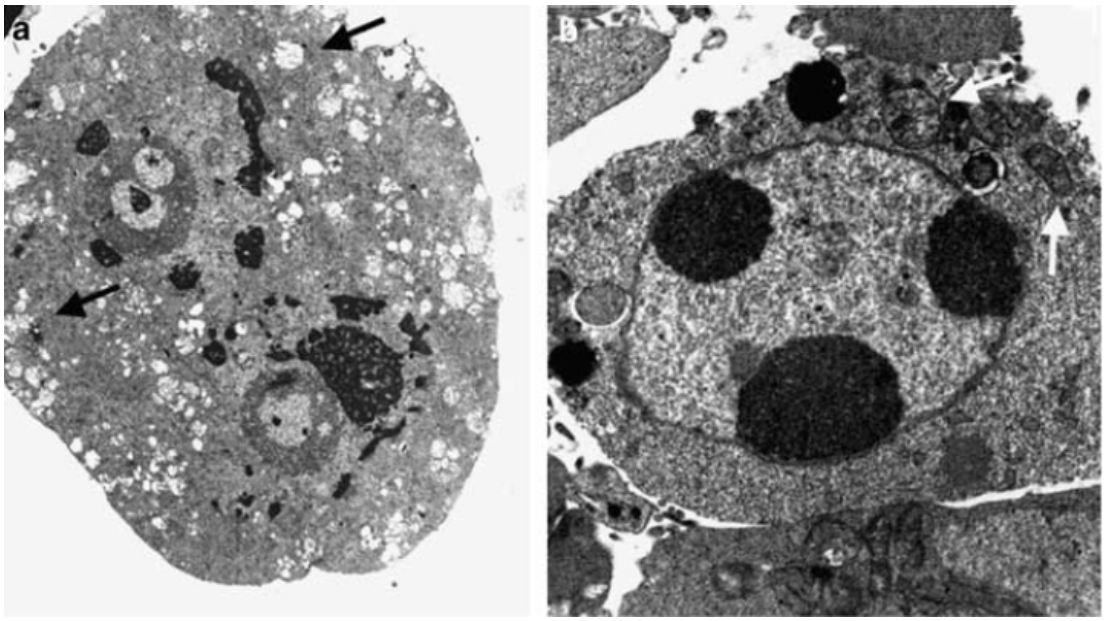

Figure 1. Transmission electron microscope images of the morphological ultrastructural appearance of cell death
(Adapted from Kroemer et al., 2005) **(a)** Necrotic human epithelial cell in response to oxidative stress. Swelling of intracellular vesicle, rupture of plasma membrane and disappearance of mitochondrial ultra-structure were present (arrows). Magnification: × 4000. **(b)** Apoptotic human epithelial cell caused by radiation. Clumping of chromatin was present and mitochondria integrity was maintained (arrow). Magnification × 4000

1.1.1 Activation of Apoptosis

As a well regulated and genetically controlled process of cell death, apoptosis is also known as type I programmed cell death (Kroemer et al., 2005). The omnipresence of this phenomenon suggests its importance in maintaining homeostasis as well as in developmental process of multicellular organisms (Kerr et al., 1972). Through intense researches and studies over the decades, a large number of genes and their protein

products have been identified to be involved in apoptosis in a well-orchestrated manner. The initiation of apoptosis could rise from various triggers through several pathways, and the signals converge on a cascade of Cysteine Aspartate–Specific ProteASEs, which are called as the 'caspases' collectively (Hengartner, 2000). Each caspase possesses a cysteine residue at the active-site, and cleaves substrates after aspartic acid residues. The four residues preceding the cleavage site are believed to be responsible for substrate specificity determination (Thornberry et al., 1997). This proteolytic cleavage could lead to inactivation of the targeted substrates in most cases, but could also activate the substrate directly by removing inhibitory domains or peptides, or indirectly through the inactivation of the inhibiting regulator of the substrate. Based on this mechanism, members of the caspase family are able to exhibit opposing capabilities in apoptosis pathways and exhibit strict regulations on the whole process (Blankenberg, 2008).

As shown in Figure 2, the initiation of the apoptosis could be triggered through two main pathways originated from either extrinsic or intrinsic stimuli (Hengartner, 2000). Death signals coming from extracellular compartments could activate several specific death receptors, inducing apoptosis in extrinsic (death-receptor) pathway. Fas ligand (CD95 ligand) and Fas Receptor (CD95) binding was an example of this pathway (Blankenberg, 2008; Wajant, 2002). Death inducing complex was formed by receptor clustering and Fas-associated death domain (FADD) recruitment, resulting in the activation of initiator group of caspases (including caspase 8 and 10) through induced proximity. The executioner group of caspases (including caspase 3,6, and 7) was then activated by the initiator group of caspases and triggered downstream array of over hundred effectors, eliciting those distinct morphological changes that differentiate apoptosis from necrosis

(Blankenberg, 2008). On the other side, various insults coming from inside of the cell, including oxidative stress and DNA damage, triggered a range of signaling pathways that converged on mitochondria and induced apoptosis in intrinsic (mitochondria) pathway (Hengartner, 2000). The released cytochrome *c* resulted from the activation of pro-apoptosis bcl-2 family proteins formed a structure called apoptosome together with apoptosis-activating factor 1 (Apaf-1) and pro-caspase 9. Executioner caspases activation following caspase 9 activation would eventually mark the onset of apoptosis.

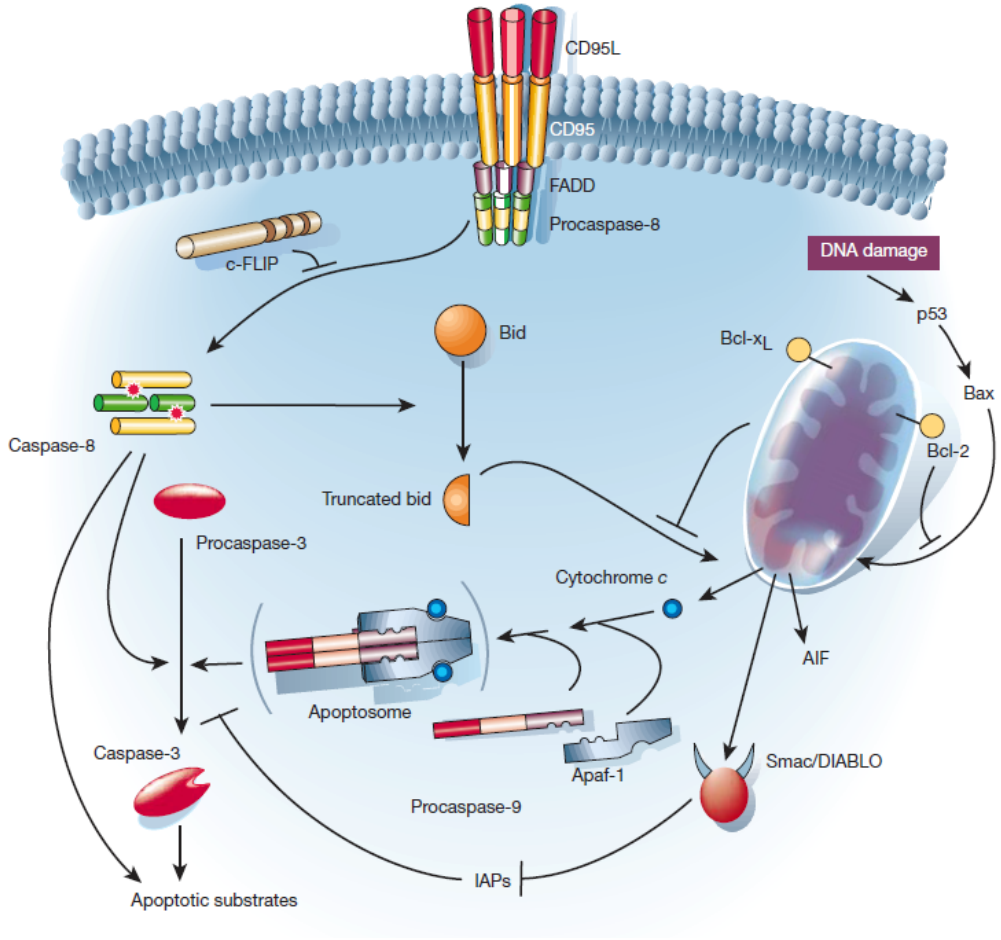

Figure 2. Two major apoptotic pathways in mammalian cells
(Adapted from Hengartner, 2000) **(Left)** The death-receptor pathway: recognition and association of CD95 ligand to CD95 induces clustering of receptor and formation of a death inducing signaling complex, recruits multiple procaspase-8 molecules through FADD (Fas-associated death domain protein), and activates caspase-8 in the form of induced proximity. **(Right)** The mitochondrial pathway: Extracellular stimulations and internal impingement such as DNA damage (Rich et al., 2000) induced different responsive pathways converging on mitochondria, achieved through pro-apoptotic members of the Bcl-2 family protein activation in most cases, leading to the release of cytochrome *c* and the formation of apoptosome. Both pathways converged on the activation of caspase-3 for the induction of apoptosis.

1.1.2 Apoptotic Body Recognition and Clearance

As mentioned previously, apoptosis differs greatly from necrosis not only in the morphological outcomes, but also in the resulting downstream immune responses, namely inflammation and antigen-presentation (Blankenberg, 2008). Since its discovery, apoptosis is known for its clearance *in vivo* - rapid phagocytosis that is almost non-immunogenic and undetectable histologically by either neighboring cells or activated macrophages and other professional phagocytes (Savill et al., 2002). In this process, several questions raised and attracted much attention. How did phagocytes differentiate dying cells or apoptotic bodies from normal healthy cells? And as phagocytes take up both necrotic debris and apoptotic bodies in similar manner, how were these almost opposite immune responses triggered? Although these questions remained researches in progress and were found to be remarkably complex, a great deal of information had been revealed. As shown in Figure 3, the specific recognition of apoptotic cells and their differentiation from normal cells were achieved through the combined efforts from different factors, including the surface patterns on apoptotic cell surface, exposed signals during apoptosis, receptors on phagocyte membrane surface, and those adaptors and bridging molecules that associated with both cells at the same time (Savill et al., 2002). There were generally three types of interactions based on the nature of the signals exposed.

It was interesting that the first type of recognition resembled the innate immune response to a large extent, or the so-called innate recognition of non-self. Similar to the recognition of non-self pathogen-associated-molecular-patterns (PAMPs), members of innate immunity, like complement fragments (Mevorach et al., 1998; Taylor et al., 2000) and

CD14 (Devitt et al., 1998), could also recognize the Apoptotic-cell-associated-molecular-patterns (ACAMPs) and facilitate apoptotic engulfment. How this originally pro-inflammatory mechanics participated in a non-inflammatory or even anti-inflammatory process is unclear. Associated binding of pentraxin-related C-reactive protein (CRP) was found to prevent the formation of membrane attacking complex (Gershov et al., 2000), and was believed to be one of the mechanisms by which innate immune response separated from its downstream events.

The second type of apoptotic recognition made use of the receptors and proteins known for the clearance of damaged or altered self cellular components, or the so-called recognition of altered-self. For example, CD36 was first found as a class-B scavenger receptor responsible for clearance of oxidized low-density lipoprotein (oxLDL) through phagocytosis (Canton et al., 2013). Later researches suggested its participation in apoptotic cell clearance recognizing the oxLDL-like sites displayed on the outer surface of apoptotic cells (Ren et al., 1995). Other scavenger receptors were also found to perform similar tasks, represented by the classical class-A scavenger receptor (SRA) (Platt et al., 2000; Platt et al., 1996). As the most characteristic apoptotic phenomenon, phosphatidylserine (PS) exposure on the outer leaflet of the plasma membrane represented the best-studied altered-self pattern that was utilized for the recognition. Several phagocyte membrane receptors and secreted proteins were known to bind with the exposed PS and facilitate the engulfment and clearance, including the PS receptor (PSR) (Fadok et al., 2000), the plasma protein β_2-glycoprotein I (β_2-GPI, apolipoprotein H) (Balasubramanian et al., 1997), the milk fat globule EGF-factor 8 (MFG-E8) (Hanayama et al., 2002), and the growth arrest specific gene 6 (Gas6) (Scott et al., 2001).

MFG-E8 secreted by phagocytes also bridged the apoptotic cells with phagocytes through the associations with the exposed PS on apoptotic cell side and with $\alpha_v\beta_3$ integrin on the phagocytes side, allowing the uptake of the apoptotic cells (Hanayama et al., 2002). At the same time, Mer receptor tyrosine kinase, named from its original distribution in Myeloid cells, Epithelial cells and Reproductive tissues, bound with exposed PS through the opsonization of Gas6, i.e. Gas6 bound with both PS and Mer at the same time to bridge the two together to facilitate recognition (Scott et al., 2001). The MFG-E8 bound $\alpha_v\beta_3$ integrin and Gas6 bound Mer were shown to cross-talk between each other, through the phosphorylations at different tyrosine residues on focal adhesion kinase (FAK) causing the amplification of the activation signals, and lead to the final activation of a Rho GTPase, Rac1, which activated the downstream signaling and mechanics for internalization (Wu et al., 2006).

The last type of recognition happened through the receptors that normally promoted cell-cell adhesion and movement away of normal cells from phagocytes, or the so-called recognition of non-detaching self. This type of recognition was somehow contradictory. The intercellular adhesion molecule 3 (ICAM3) promoted phagocytosis of apoptotic leucocytes when bound by macrophages through unknown type of integrins, but did not do so in healthy leucocytes (Moffatt et al., 1999). Another bridging molecule thrombospondin 1 (TSP1) showed similar functions. It could present apoptotic leucocytes to phagocytes through linking with apoptotic cell surface binding sites and $\alpha_v\beta_3$ integrin on the phagocyte surface (Savill et al., 1992). However, it could also get normal leucocytes away from phagocytes (Hughes et al., 1997). It was believed by some researchers that the apoptosis machineries disabled the downstream signaling of move-

away signals, rendering the otherwise detached cells to be non-detachable from phagocytes (Parnaik et al., 2000). Apoptosis in leucocytes was shown to convert the repulsive signals from CD31 to adhesive signals, thus allowing homophilic binding (binding with the CAMs of the same kind) between CD31s from leucocytes and phagocytes, promoting uptake of these apoptotic leucocytes (Brown et al., 2002). Non-detachment of apoptotic cells provided prolonged exposure towards phagocytes, but mightstill need other factors in triggering engulfment.

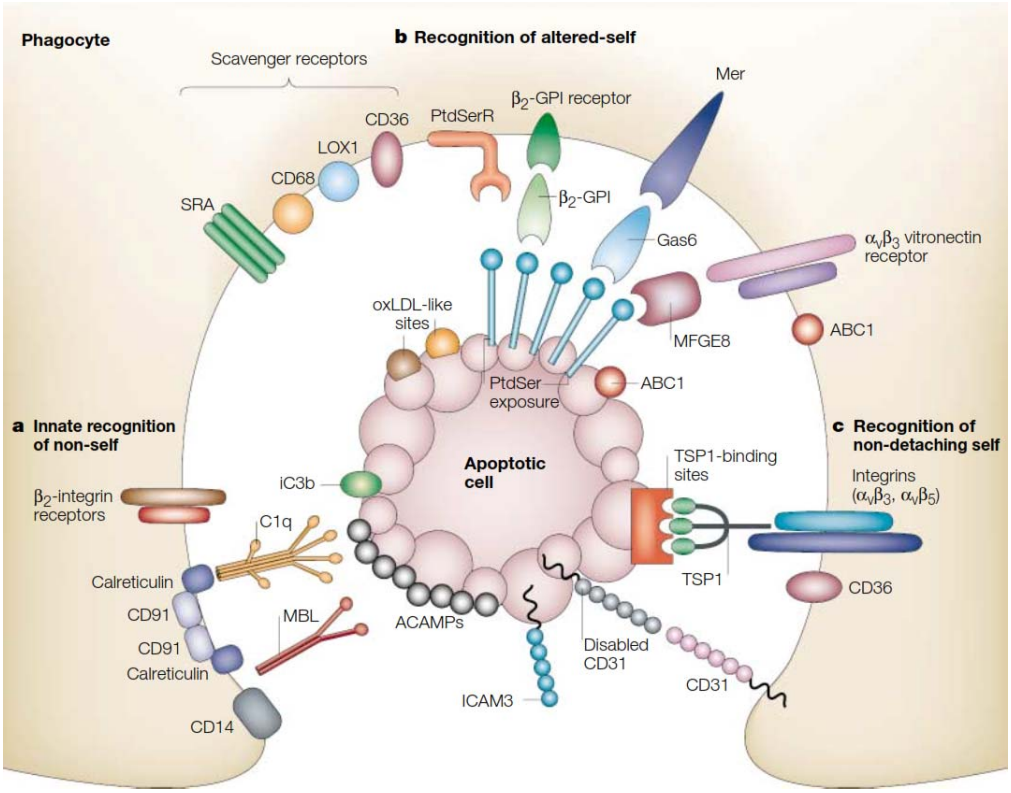

Figure 3. Three classes of mechanism for the recognition of apoptotic cells by phagocytes

(Adapted from Savill et al., 2002) **(a)** Innate recognition of non-self involves phagocyte CD14, β-integrins (which bind the opsonic complement fragment inactivated C3b, iC3b) and the CD91–calreticulin complex (which can bind the first component of complement, C1q, and mannose-binding lectin, MBL, which recognizes pathogen-like apoptotic-cell-associated molecular patterns, ACAMPs). **(b)** Recognition of altered-self involves an array of scavenger receptors, including the class-A scavenger receptor (SRA), CD68, LOX1 (oxidized low-density lipoprotein receptor 1) and CD36, which recognize oxidized sites on apoptotic cells that mimic oxidized low-density lipoprotein (oxLDL). Exposure of phosphatidylserine (PtdSer) on the surface of apoptotic cells is a key 'eat-me' flag. It is detected by phagocyte phosphatidylserine receptor (PtdSerR), receptors for the bridging plasma-protein β-glycoprotein I (β-GPI), the Mer kinase receptor for the bridging protein Gas6, and $\alpha_v\beta_3$ integrin (vitronectin receptor), which binds the bridging protein milk-fat globule epidermal growth factor 8 (MFGE8). Rearrangement of plasma-membrane lipids, i.e. PS exposure, in both the dying cell and the phagocyte by the ATP-binding cassette transporter ABC1 can contribute to this type of recognition. **(c)** Recognition of non-detaching self involves disabling the detachment signals that are conferred by apoptotic-cell CD31 and, possibly, similar alterations in another immunoglobulin-superfamily member, intercellular adhesion molecule 3 (ICAM3). Disabled apoptotic-cell CD31 binds tightly to phagocyte CD31, which may promote binding of the bridging protein thrombospondin-1 (TSP1) by phagocyte integrins.

1.1.3 Immune Response Regulation in Apoptosis

Sharing recognition and engagement mechanics, the process of apoptotic clearance resembled innate immune response. However, their difference was that apoptotic clearance did not trigger inflammation. This immune-quiescence, or non-immune response-triggering characteristic, was observed since the very discovery of apoptosis, and confirmed through experiments done on several different cell types (Meagher et al., 1992; Stern et al., 1996). No pro-inflammatory cytokines were released when iC3b (complement fragment inactivated C3b) opsonized apoptotic cells were taken up by macrophages through the $\alpha_m\beta_2$ and $\alpha_x\beta_2$ integrins (Marth and Kelsall, 1997; Wright and Silverstein, 1983). However, as the knowledge grew and research deepened, evidence showed that, rather than being neutral, apoptosis was sometimes immunosuppressive and anti-inflammatory. Upon recognition of and binding to apoptotic cells, the pro-inflammatory tumor-necrosis factor (TNF) secretion was inhibited, and expression of anti-inflammatory transforming growth factor-β1 (TGF-β1) and interleukin-10 (IL-10) was promoted even without actual engulfment in LPS (lipopolysaccharide) -stimulated monocytes to happen (Voll et al., 1997). Similar results were obtained by Fadok and colleagues using LPS-stimulated human monocyte-derived macrophages (Fadok et al., 1998). They found that phagocytosis of apoptotic neutrophils actively inhibited the production of interleukin (IL)-1b, IL-8, IL-10, granulocyte macrophage colony-stimulating factor, and tumor necrosis factor-a, as well as leukotriene C4 and thromboxane B2, by human monocyte-derived macrophages. In contrast, production of transforming growth factor (TGF)-β1, prostaglandin E2, and platelet-activating factor (PAF) was increased. Addition of exogenous TGF-b1, prostaglandin E2, or PAF resulted

in inhibition of lipopolysaccharide-stimulated cytokine production, and restoration of this secretion using anti–TGF-β antibody, indomethacin, or platelet activating factor (PAF) receptor antagonists suggested that binding and/or phagocytosis of apoptotic cells induces active anti-inflammatory or suppressive properties in human macrophages. This inhibitor studies also revealed insights in the paracrine and autocrine inhibition of TNF by TGF-β1, prostaglandin E2 and PAF.

Among these effectors, TGF-β1 seemed to be the central one. It performed multiple immunosuppressive actions, including the inhibition of many cytokines like interferon-γ, TNF-α, various interleukins, and cytokine receptors (Letterio and Roberts, 1998). Upon binding of apoptotic cells, different phagocyte receptors from monocytes / macrophages were activated by their corresponding ligands, and the downstream signaling would promote the secretion of TGF-β1 (Savill et al., 2002). CD36, $\alpha_v\beta_3$ and their mutual ligand TSP1 were shown to inhibit immune response through TGF-β1 production (Freire-de-Lima et al., 2000; Voll et al., 1997). PS receptor also triggered the anti-inflammatory signaling through TGF-β1 upon binding to exposed PS (Fadok et al., 2000). The activation of these receptors led to downstream up-regulation of TGF-β1 expression and secretion from bound macrophage. The released TGF-β1 might act autocrinely on the macrophage, or paracrinely in surrounding to create an immune-suppressed local environment (Savill et al., 2002). Moreover, bridged by Gas6 towards exposed PS, Mer-RTK was believed to suppress immune responses directly through intracellular signaling and alter the expression of various cytokines. This was demonstrated by the knockdown study in mice showing accumulation of anti-nuclear antibodies and defect in apoptotic clearance (Scott et al., 2001).

Similar to monocytes / macrophages, dendritic cells (DC) cells can also ingest unwanted cells and pathogens and elicit immune responses, but have different mode of action. They are professional antigen-presenting cells derived from phagocytic precursors. In response to 'danger' signals, these highly-phagocytic DC precursors were activated, took up the target, processed and presented the ingested materials on their surface to other cells in the immune system (Banchereau and Steinman, 1998; Savill et al., 2002). DCs could also phagocytose the apoptotic cells through surface receptors including CD36 and $\alpha_v\beta_5$ integrin with the bridging molecule TSP1 (Albert et al., 1998; Rubartelli et al., 1997). The immunosuppressive action associated was shown to be the suppression of the co-stimulatory molecule CD86 and IL-12, and the suppression of DC maturation (Stuart et al., 2002; Urban et al., 2001).

Therefore, both innate immune system and adaptive immune system were suppressed or inhibited by apoptotic cell recognition, preventing development of immunity towards self antigen.

1.1.4 Phosphatidylserine in Apoptosis

Downstream of caspase 3 activation is a full spectrum of cellular actions which give rise to the morphological events of apoptosis. As mentioned above, PS externalization and exposure are the most unique features that define apoptosis. The exposed PS functions as an 'eat me' signal and anchor point for clearances of the apoptotic bodies or cells (Fadok et al., 1992). Surrounding viable cells and 'professional' phagocytes can recognize this signal and be triggered to engulf and degrade the PS-exposing apoptotic cells (Savill and Fadok, 2000). Immunosuppressive actions during apoptotic clearance were also largely dependent on the recognition and binding to different receptors after PS exposure (Savill

et al., 2002). Therefore, the mechanism by which PS exposes and interacts to perform its functions has attracted much interest, and had been studied thoroughly.

Phosphatidylserine is a phospholipid with negatively charged amino-group of serine linked to the phosphate to form the head group. It is a constitutive part of the normal eukaryotic and prokaryotic cells, and composes about 2 - 10 % of the total lipid found in mammalian cell membrane depending on species and cell types (Vance and Steenbergen, 2005). Apart from the structural role as building blocks of cell membranes, PS also involved in the signaling pathways through recognition and interaction with protein kinase C (Stace and Ktistakis, 2006), or through localization of intracellular proteins and membrane surface charge (Yeung et al., 2008). This functional importance is reflected in the redundancy in the synthesis pathways that ensure a certain minimal level of PS production (Schutters and Reutelingsperger, 2010). In mammalian cells, phosphatidylcholine (PC) and phosphatidylethanolamine (PE) were enzymatically converted into PS through the serine exchange reaction. The enzymes that catalyzed the corresponding reactions were PS-synthase 1 (PSS1, catalyze the synthesis from PC) and PS-synthase 2 (PSS2, catalyze the synthesis from PE) (Arikketh et al., 2008; Bergo et al., 2002). PS is synthesized in the membrane of endoplasmic reticulum (ER), and distributed through vesicular transport or lipid-exchange by lipid-transfer protein (LTP) (Holthuis and Levine, 2005). The plasma membrane has an asymmetrical distribution of different types of phospholipids, with aminophospholipids (PE and PS) predominantly localized on the inner leaflet (Vance and Steenbergen, 2005). This is accomplished by the aminophospholipid transporter / translocase (APLT). It utilizes the energy from hydrolysis of ATP, and actively and constantly transports PE or PS against their

concentration gradients towards the cytosolic side of the membrane (Henson et al., 2001). In addition, an ATP-dependent enzyme called 'floppase' was found to regulate the localization of positively charged phospholipids like PC and sphingomyelin to the extracellular leaflet of plasma membrane, and phospholipid asymmetry was thus maintained by the collective efforts of the two (Tait and Gibson, 1994; van Heerde et al., 1995; Wood et al., 1996). This process was briefly illustrated in Figure 4.

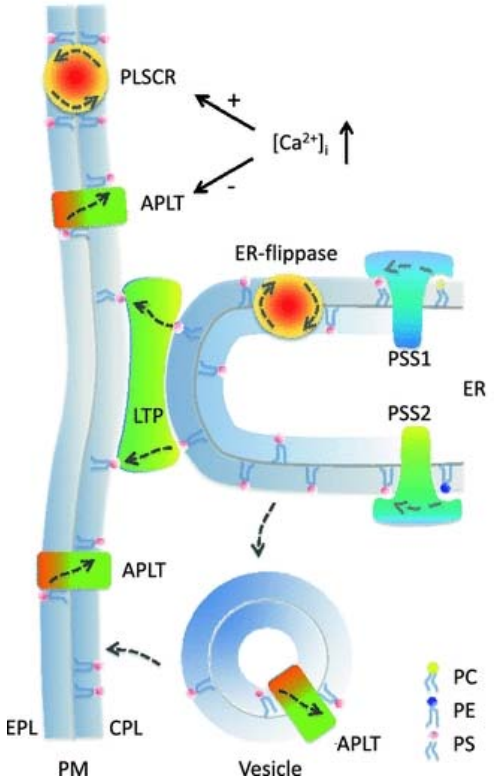

Figure 4. Synthesis and transportation of PS in mammalian cells
(Adapted from Schutters and Reutelingsperger, 2010) PS-synthase 1 and PS-synthase 2 are the main enzymes that synthesize PS from PC and PE by a serine exchange reaction in ER. After synthesis, PS is non-randomly distributed by vesicle transport, membrane fusion and exchange between juxtapositioned bilayers. Dotted arrows indicate pathways of PS-trafficking. Once located in the plasma membrane, PS is under the control of aminophospholipid translocase and phospholipid scramblase. Increase of cytosolic Ca^{2+}-concentration ($[Ca^{2+}]$) inhibits APLT and activates PLSCR.
APLT, aminophospholipid translocase; **CPL**, cytoplasmic leaflet; **EPL**, exoplasmic leaflet; **ER**, endoplasmatic reticulum; **LTP**, lipid transfer protein; **PC**, phosphatidylcholine; **PE**, phosphatidylethanolamine; **PLSCR**, phospholipid scramblase; **PM**, plasma membrane; **PS**, phosphatidylserine; **PSS**, PS-synthase.

During apoptosis, the oxidative stress and change in intracellular Ca^{2+} level disrupt the normal functioning of the APLT and floppase, inactivate the maintenance mechanism of the phospholipid asymmetry. Moreover, a third enzyme called 'scramblase' was believed to be activated by the increasing Ca^{2+} level, promoting the trans bilayer movement of the plasma membrane (Zhou et al., 1997), and thus resulted in the PS translocation towards the outer leaflet of the cell membrane (Wu et al., 2006). Previous research (Kagan et al., 2004) also suggested that the cytochrome *c* released might result in a gain-of-function peroxidase activity with specificity towards PS (Jiang et al., 2004). The exposed oxidized PS might also have additional effects to attract opsonins (Borisenko et al., 2004).Recently, PS externalization was also proposed to be part of a membrane repair mechanisms triggered by apoptosis, with fusion of lysosomes and plasma membrane involved (Mirnikjoo et al., 2009).

1.2 Phospholipid-Binding Domains

Among various intracellular organelles and structures, phospholipid membraneis one of the most important parts. This semi-permeable lipid bi-layer forms structural enclosure of the cell and its various compartments, separating the interior from extracellular matrices, and creating individual micro-environments that are suitable for the functions of different organelles. It is also the platform for wide variety of cellular functions. Proteins' association with the membrane is essential for these cellular processes across different aspects of the cell life, including cell-cell recognition, inter- and intra-cellular signaling, vesicular trafficking, cell structural maintenance, etc. One example is that the plasma membrane of most animal cells constantly associate with cytoskeleton to remain counteracting the outward pressure of cytoplasm, and the dynamics of membranes and

cytoskeleton also depend on their various interactions (Di Paolo and De Camilli, 2006; Sheetz et al., 2006). Besides, patches of specific lipid on certain cellular compartments could be used to differentiate organelles by the intracellular trafficking machinery (Behnia and Munro, 2005). Moreover, transient recruitment of various signaling proteins or molecules towards specific membrane patches upon stimulation of corresponding receptors is another example of the importance of protein-membrane association (Di Paolo and De Camilli, 2006; Teruel and Meyer, 2000). Over the years, numerous phospholipid-binding proteins and phospholipid-binding domains were discovered and studied in detail, revealing different binding targets and mechanisms.

1.2.1 Target Specificity

A wide variety of functions were performed by membrane binding domains and proteins through different mechanisms, allowing the exploitation of distinct modes of control for various cellular pathways and functions. Despite the differences in mechanisms, similarities in the selection of lipid targets were observed. These domains or proteins almost exclusively recognized acidic phospholipids as binding targets (Lemmon, 2008). Phosphatidylserine (PS), phosphatidic acid (PA) and phosphatidylinositol (PtdIns, or PI) were the main types of acidic phospholipids found in normal animal cell membranes. A small proportion of PtdIns was further phosphorylated to generate phosphoinositides. These phosphoinositides stand very minor portion of the total phospholipids, but had a disproportionally major role in membrane association with proteins and regulation of different pathways (Di Paolo and De Camilli, 2006).

There are more than 10 different phospholipid-binding domains studied. Some have highly specific binding targets, and involve high affinity stereospecific binding towards

the targets. Others are less-specific, and align more with the general physical properties of the membrane. Each domain has its unique phospholipid target (Lemmon, 2008). In this introduction, I will briefly discuss several domain types related to our research target.

1.2.2 C1 Domain

C1 domain is a group of small cysteine-rich structural units originally discovered as 'Conserved region-1' in protein kinases Cs (PKCs) isozyme family (Mochly-Rosen et al., 2012). It was found to be involved in the activation of the PKCs through recognizing phorbol esters, a plant-derived natural tumor promoting agonist, and diacylglycerol (DAG), a second messenger lipid produced by phospholipase C (PLC). It was responsible for the targeting of PKCs from cytosol to membrane in response to ligand generation from upstream effectors' activation (Colon-Gonzalez and Kazanietz, 2006). Two types of PKC C1 domain are there. First one is the C1 domains found in typical PKC isoforms which showed sensitive response towards phorbol ester and DAG. The other C1 domains from the atypical PKC isoforms did not interact with these two molecules, and were unknown about the functions (Lemmon, 2008). Typical C1 domain from PKC utilized a *Zinc-finger* configuration, and contained a conserved motif of $HX_{12}CX_2CX_nCX_2CX_4HX_2CX_7C$, where H is histidine, C is cysteine, X is any other amino acid, and n = 13 or 14 (Kazanietz et al., 1995). Crystal structure of the C1B (Cys2) domain from PKCδ had demonstrated the binding mechanism of C1 domain (Zhang et al., 1995). As shown in Figure 5, DAG/phorbol ester binding site was clustered within a group of hydrophobic residues (green), encircled by a band of positively charged residues (blue). The concerted actions from these three parts collectively contributed to the binding of DAG/phorbol ester embedded within membrane, and extensive membrane

penetration was observed. As the well accepted model, anionic phospholipid was considered as an essential cofactor for phorbol esters binding to PKC (Nelsestuen and Bazzi, 1991; Nishizuka, 1986), with phosphatidylserine being the most efficient (Kazanietz et al., 1992; Konig et al., 1985).

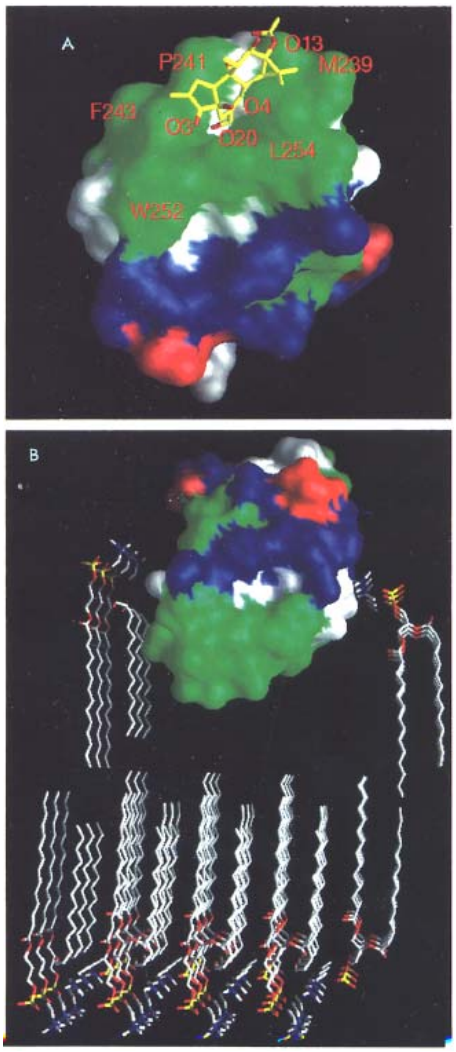

Figure 5. Molecular surface properties of the Cys2 domain
(Adapted from Zhang et al., 1995) **(A)** Molecular surface of the Cys2 domain colored by residue type: **green** represent the hydrophobic residues; **blue** represent the positively charged residues; **red** represent the negatively charged residues; and **white** represent the neutral polar residues. **(B)** Membrane insertion model of Cys2-phorbol ester complex.

1.2.3 Pleckstrin Homology (PH) domain

The term 'pleckstrin homology' demonstrated the origin of this protein domain. It was first identified in 1993 as a small protein sequence of around 100-120 residues with similarity towards the sequence occurred twice in pleckstrin, and was found in a large number of proteins with signaling functions (Lemmon and Ferguson, 2000; Mayer et al., 1993). Initially the PH domain was considered to have functions in cellular signaling pathways (Haslam et al., 1993; Mayer et al., 1993; Musacchio et al., 1993). Subsequent researches and publications discovered that PH domains participated in the membrane targeting of their host proteins by binding to phosphatidylinositols rather than the membrane-associated proteins (Bottomley et al., 1998; Gibson et al., 1994; Katan and Allen, 1999; Musacchio et al., 1993). One of the first examples was the finding that the N-terminal of the PH domain from pleckstrin binds specifically to phosphatidylinositol-4,5-biphosphate (PtdIns(4,5)P_2) (Harlan et al., 1994). A number of PH domains were subsequently studied, and their structures were examined. The crystal structures revealed a great amount of information regarding its binding to phosphatidylinositols (Figure 6) (DiNitto and Lambright, 2006). Different from C1 domain, PH domain did not have extensive membrane penetration (Ferguson et al., 1995). As Figure 6 shows, PH domains with stereospecificity utilize the variable loops between beta-strands to make contact with target. The β1/β2 loop between the two named strands was thought to create main interactions with the lipid head group (Isakoff et al., 1998). The sequence motif of KX_n(K/R)XR (K for Lysine and R for Arginine) found in this loop forms most lipid contacts. Other loops provided additional contacts to define ligand orientation and

phosphorylation pattern, and therefore, providing specificity towards their own targeted phospholipid type (Ferguson et al., 2000).

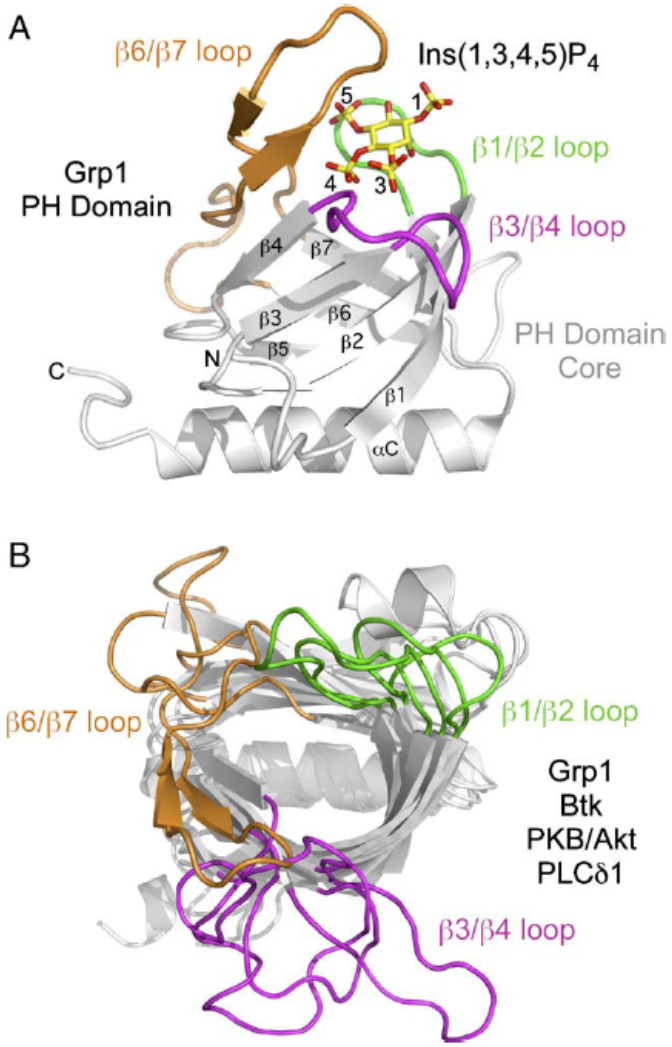

Figure 6. PH domain structure overview
(Adapted from DiNitto and Lambright, 2006) **(A)** Ribbon representation of the Grp1 PH domain complexed with a phosphoinositide head group (PDB ID: 1FGY). Gray represents the conserved structural core. Green, magenta and orange represent the hyper-variable specificity determining loops surrounding the head group binding site in the β1/β2 loop, β3/β4 loop, and β6/β7 loop respectively. The head group of PtdIns(3,4,5)P_3 is also shown with carbon and phosphorous atoms in yellow and oxygen atoms in red. **(B)** Superposition of representative PH domains (Grp1, PDB ID: 1FGY; PKB/Akt, PDB ID: 1H10; PLCδ1, PDB ID: 1MAI; Btk, PDB ID 1B55) specificity determining loop structures were highlighted for their diversity.

C1 domain and PH domain discussed above represent the group of phospholipid binding domains with high affinity and stereospecificity towards well-defined targets. However, there are another group of membrane-binding domains that show less target specificity, and their physiological targets are more ubiquitously distributed throughout cell membranes. C2 domains and Annexins were two examples of these type of membrane-binding domains, and they both target phosphatidylserine (Lemmon, 2008).

1.2.4 C2 domain of PKC

The protein kinases Chomology-2 (C2) domain was originally discovered as the second conserved domain of Ca^{2+}-dependent protein kinases C (PKC) (Nishizuka, 1988). It was not considered a lipid-binding domain until the characterization of the C2 domains in other proteins like synaptotagmin and group IVA cytosolic phospholipaseA2 (cPLA2α) (Clark et al., 1991; Perin et al., 1990), and was confirmed as Ca^{2+}-dependent, uniquely folded membrane binding domain. Since then, over a hundred proteins that contain C2 domain were identified or predicted, as suggested in a SMART genomic test (Schultz et al., 1998). Thereafter, only second to the PH domain, C2 domain represents one of the most abundant lipid binding domains (Cho and Stahelin, 2006).

Since its discovery, the C2 domain structures have been examined in various occasions, either as a domain alone or together with the whole protein. From these studies, a conserved secondary structure configuration of eight-stranded anti-parallel β-sandwich connected by surface loops has been found (Nalefski and Falke, 1996). This typical fold is demonstrated in Figure 7. Based on the dependency of Ca^{2+} ion, the C2 domain can be categorized into Ca^{2+}-dependent and Ca^{2+}-independent subpopulations. As for Ca^{2+}-dependent C2 domains, because of their interaction with Ca^{2+} ion in various sub-cellular

processes like signaling and vesicle trafficking (Rizo and Sudhof, 1998), most of them serve as effectors of various Ca^{2+}-mediated cellular processes. Whereas for those C2 domains that have limited or no affinity with Ca^{2+} ion, only limited portion of them would bind to lipid. The rest may be involved in protein-protein interactions or even not functional (Cho and Stahelin, 2006).

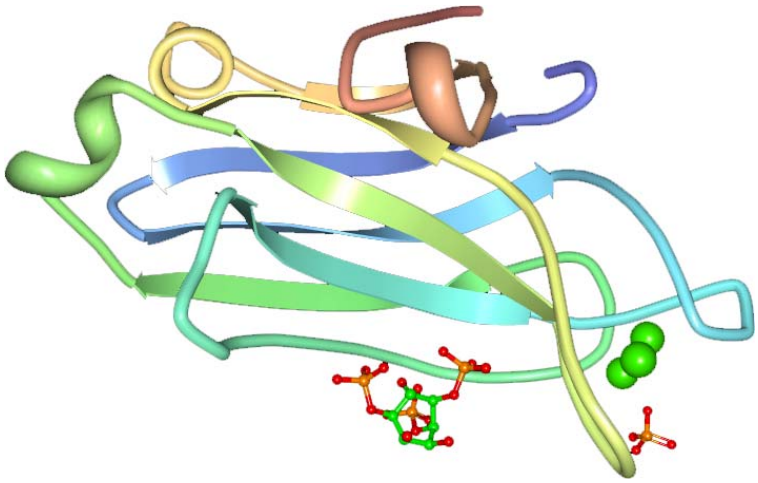

Figure 7. Crystal structure of PKCα C2 domain complexed with Ca^{2+} and Phosphatidylinositol-(4,5)-diphosphate
(Adapted from Guerrero-Valero et al., 2009) PDB accession number: 3GPE) C2 domain has a common fold of conserved eight-stranded anti-parallel β-sandwich connected by surface loops. Green spheres represent the bound Ca^{2+}.

In the well-studied Ca^{2+}-dependent lipid binding action shown in Figure 7, Ca^{2+} ions are found to participate in the interaction in several different ways: by changing electrostatic potentials of C2 domains (Shao et al., 1997), by playing a role as electrostatic bridge between the two binding partners (Verdaguer et al., 1999) and by inducing local conformational change in the C2 domain (Grobler et al., 1996). The canonical Ca^{2+}-dependent C2 domains generally contain three Ca^{2+}-binding loops (CBL1–3) positioned closely to each other at one side of the domain. The coordination of Ca^{2+} ions involves not only side chains like Asp, but also the peptide backbone (Cho and Stahelin, 2006),

and the number of Ca^{2+}ions coordinated at one time is not limited to single one. On the other hand, the mechanism of the binding between Ca^{2+}-independent C2 domain and lipid is still in the process of discovery.

1.2.5 C2 domain of discoidin or Factor V/VIII

C2 domain form PKC represents the PS binding domains that normally exist in cytosol. They participate in the intracellular functions like trafficking and signaling, and generally respond to intracellular Ca^{2+} levels and function as Ca^{2+} regulators, effectors, or sensors (Lemmon, 2008). Interestingly, there is another type of 'C2 domain' that differs greatly when compared with C2 domain form PKCs. Blood coagulation factors V and VIII contain 2 repeating domains in the C-terminus, each about 150 amino acids. These C-domains show similarities with N-terminal region of the cell adhesion protein discoidin found in slime mould *Dictyostelium discoideum*. This gives rise to a new type of extracellular module called discoidin (DS) or factors V and VIII (F5/8) type C domain (Baumgartner et al., 1998). This C2 domain is different from the C2 domain of PKC, despite the coincidence in nomenclature, structural characteristics and binding targets. They are generally secreted into extracellular compartments, recognize the anionic phospholipid exposed on the extracellular leaflet of the cell membrane and exert their functions in blood coagulation and apoptotic body clearances, etc (Lemmon, 2008). This group of membrane binding domains shares a common folding pattern of eight major anti-parallel β-strands arranged in two sheets of five and three strands packed against one another (Macedo-Ribeiro et al., 1999). Discoidin type C2 domains bind to phosphatidylserine in the absence of Ca^{2+}. As shown in Figure 8, Factor VIII C2 domain utilizes the loops region in between β-strands for the interaction with its physiological

targets and different inhibitors (Liu et al., 2010). These loops include the two spike loops (Met2199-Phe2200 and Leu2251-Leu2252), the loop containing Val2223, and the loop containing Trp2313-His2315 (Stoilova-McPhie et al., 2002). The residues with basic side chains like lysines and arginines are responsible for interacting with the anionic phospholipid head group. Residues with hydrophobic side chains, including Tryptophan, phenylalanine, and histidine, etc, also have important roles in the binding process. For example, $Trp^{2313}$was found to be mutated into arginine in some patients with hemophilia A, leading to a moderate to severe functional loss of Factor VIII (Kemball-Cook et al., 1998; Tagariello et al., 2000). This binding theme was further verified by the crystal structure of Factor V with ligand as shown in Figure 9 (Macedo-Ribeiro et al., 1999).

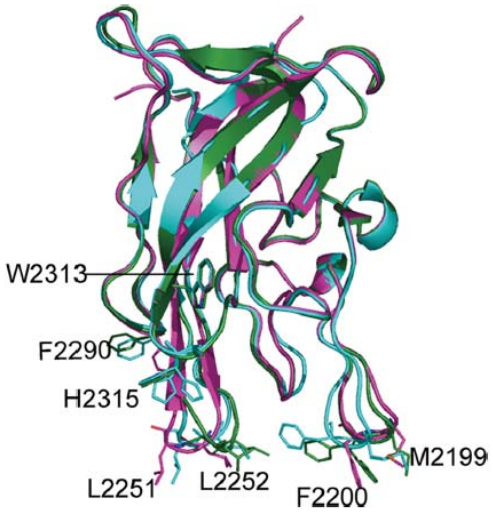

Figure 8. Structural superposition of FVIII C2 domain structures formed under different crystallization conditions
(Adapted from Liu et al., 2010) The C2 domain in the protein inhibitor complex from crystals formed in the presence of NaCl (PDB code3HNB) is shown in cyan; the C2 domain formed in the presence of ammonium sulfate (PDB code 1D7P) in magenta, the C2 domain from crystals formed inthe presence of PEG-MME (PDB code 3HOB) in green. The phenyl ring of residue Phe2200 was modeled in dual conformations. The conformations of Phe2200 are clearly different. The two membrane-binding spikes (2251–2252and 2199–2200) are more open in 1D7P (magenta) than in the structure ofF8C2–005B10 (cyan).

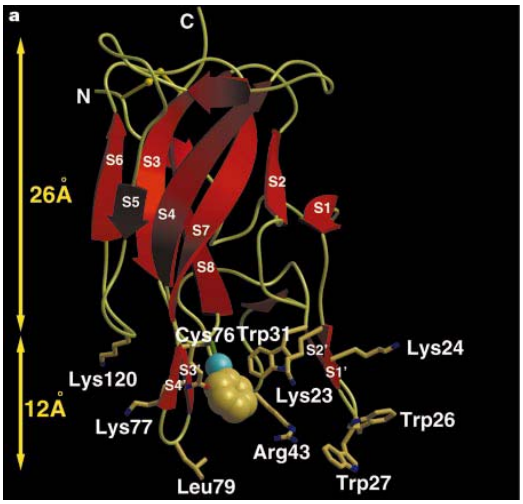

Figure 9. Structure of FVa-C2
(Adapted from Macedo-Ribeiro et al., 1999) Ribbon representation of the 'open' crystal form is displayed in the reference orientation, with the major secondary structure elements highlighted. The Cys1–Cys156 disulphide bridge and several noticeable side chains are displayed. The phenyl mercury molecule (space-filling model) used for structure determination is shown covalently attached to Cys76.

1.2.6 Annexin V

Annexin type of lipid-binding proteins is a protein family with over 160 members, found in over 65 species (Morgan and Pilar Fernandez, 1997; Morgan et al., 1999). They have a unique architecture of Ca^{2+} binding sites, and able to interact with negative charge membrane through these binding sites in a peripheral position (Gerke et al., 2005). There are two major components in an Annexin type protein, an N-terminal domain with sequence variations, and a C-terminal protein core conserved throughout the family, which harbored the Ca^{2+} binding sites. The annexin core comprises 4 annexin repeats (Raynal and Pollard, 1994), and forms a highly α-helical and tightly packed curvature structure. Its convex side contains Ca^{2+} binding sites of novel types (Swairjo et al., 1995), which is called the annexin-type or type-II Ca^{2+} binding sites (Weng et al., 1993). The more concave side is accessible to interact with the N-terminal domain and/or other cytoplasmic binding partners as it points away from the membrane (Gerke and Moss, 2002).

Most of their functions are associated with the reversible lipid-binding properties under tight regulation of Ca^{2+} level (Gerke et al., 2005). High resolution structures of several annexins have revealed the detailed binding mode: the Ca^{2+} ions are the key of annexin binding (Figure 10), they form coordination linkage on one side with carbonyl and carboxyl groups of annexin proteins, and on the other side with phosphoryl moieties of the glycerol backbone of membrane phospholipids (Swairjo et al., 1995). Most annexins recognize acidic phospholipids as the general targets, although some bind preferentially to PE or PC instead (Gerke et al., 2005). In addition to phospholipid, they also bind to cytoskeleton-associated proteins, EF hand type proteins, and other annexin ligands

ranging from proteins to RNA and smaller molecules (Davis et al., 1996; Kim et al., 2001). Although originally discovered as extracellular calcium trap to prevent clotting, this repertoire of targets allow annexins to participate in a wide range of functional pathways, including inhibition of coagulation, inhibition of phospholipase A (an inflammatory process component), and inhibition of protein kinase C (an intracellular signaling system) (Blankenberg, 2008).

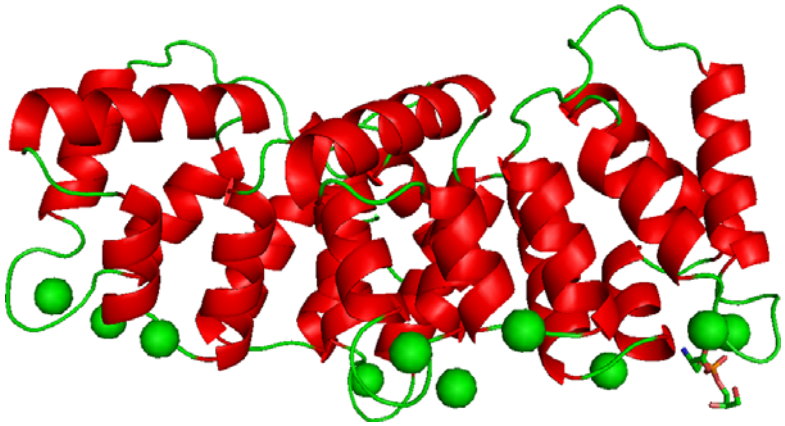

Figure 10. Annexin core from Annexin A5 bound with glycerolphosphoserine
(Adapted from Swairjo et al., 1995) (PDB code: 1A8A) Protein is shown as cartoon representation. A-helices are colored red, Calcium atoms are colored green, and glycerophosphoserine are shown as sticks.

1.3 MFG-E8 and Its Membrane Binding Domains

Milk fat globule-EGF factor 8 protein (MFG-E8), also known as lactadherin, is a soluble and heavy glycoprotein. It is produced and secreted by various cells including mammary epithelial cells, stimulated macrophages, stimulated endothelial cells in different tissues, such as brain, spleen, lymph nodes, and mammary glands, and is conserved across species and could be found in human, mice, pig, and cow (Butler et al., 1980; Hanayama et al., 2002; Hanayama et al., 2004; Silvestre et al., 2005). Its domain configuration is shown in Figure 11.

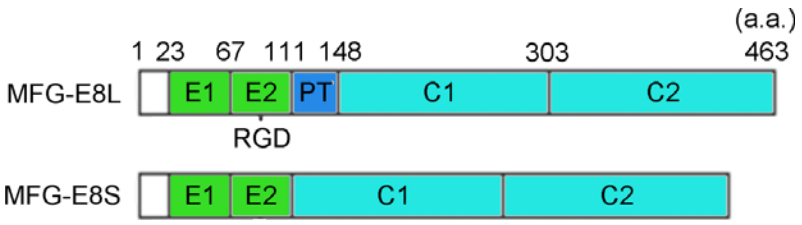

Figure 11. Domain structure of MFG-E8
MFG-E8 consists of two tandem EGF-like domains on the amino-terminal side, and two C domains on the carboxyl-terminal side. Two alternative splice variants (MFG-E8L and MFG-E8S) were identified differing on the existence of a P/T domain.

Two tandem EGF-like domains were located on the amino-terminal, whereas two discoidin like C domains (C1 and C2 domains) could be found on the Carboxyl-terminus. Two alternative splicing variants were discovered, and the presence a proline/threonine-rich domain (P/T) in the L form and the absence of it in the S form marked the difference (Hanayama et al., 2002).

1.3.1 RGD motif on EGF domain binds with integrin on the macrophages

The term 'integrin' was claimed in a review article published in 1987 (Hynes, 1987) to describe a family of structurally, immunochemically, and functionally related cell-surface heterodimeric receptors, which **integrated** the extracellular matrix with the intracellular cytoskeleton to mediate cell migration and adhesion (Plow et al., 2000). Mammalian genomes contain 18 α subunit and 8 β subunit genes, and to date 24 different α-β combinations have been identified at the protein level (Humphries et al., 2006). The number of integrins and the remarkable breadth of their cellular distribution support the statement that the phenotype of virtually every cell is uniquely influenced by its display of integrins. The efforts spend on finding minimal recognition sequences of the integrins gave rise to the Arg-Gly-Asp (RGD) motif (Plow et al., 2000). The RGD was originally identified as the sequence in fibronectin that engages the fibronectin receptor, integrin

$\alpha_v\beta_1$, but now is known to serve as a recognition motif in multiple ligands for several different integrins (Pierschbacher and Ruoslahti, 1984; Ruoslahti, 1996). Beside the RGD binding site, each integrin heterodimer also contains 3 to 5 divalent cation binding sites of relatively low affinity. The bound cations exert profound effects on integrin function. Collectively, these bound divalent ions can promot ligand binding, inhibit ligand binding, and change the ligand binding specificity.

In MFG-E8 protein, previous studies demonstrated the existence in the second EGF-like domain of the RGD motif. This well-characterized motif was shown to be the binding site for the integrin family of receptors $\alpha_v\beta_3$ and $\alpha_v\beta_5$ expressed on the surface of macrophages (Andersen et al., 2000; Hanayama et al., 2002; Tamm and Tatulian, 1997). And the RGE mutant of MFG-E8 was shown to inhibit phagocytosis significantly, proving the importance of the RGD motif (Hanayama et al., 2002).

1.3.2 C2 domain binds with PS on apoptotic cells

Homologous to the membrane-binding C2 domains of coagulation factor V and VIII, the C2 domain in MFG-E8 is also a discoidin type C domain (Cladera et al., 1997; Lin et al., 2007), and differs to the Ca^{2+}-binding C2 domains found in synaptotagmin, cPLA2 or PKC (Shao et al., 2008). It was proposed to be responsible for the recognition of PS-exposed membranes discussed earlier in the introduction (Andersen et al., 2000; Tamm and Tatulian, 1997). Experimental evidences were also provided to demonstrate the binding of C2 domain with PS (Hanayama et al., 2002). The common structural feature of discoidin type C domains is a β-sandwich scaffold consist of eight anti-parallel β-strands with a number of irregular inter-strand loops (Hurley and Misra, 2000; Schurholz,

1996). These flexible loops were less conserved across species and may contain amino acids compositing potential lipid-binding site which interact with the hydrophilic head group of PS in cellular membranes through stereospecific binding. The crystal structures of the C2 domains of factor V, factor VIII and MFG-E8 from other specie provided evidences for the proposition of binding mechanism that protruding water-exposed hydrophobic residues from loops region mediated membrane binding through membrane insertion (Macedo-Ribeiro et al., 1999; Pratt et al., 1999). In addition, hypothetical PS binding sites were also suggested from previous computational docking studies, and it differed among MFG-E8 and factor V or VIII (Shao et al., 2008).

1.3.3 MFG-E8 function in clearance of the apoptotic cells

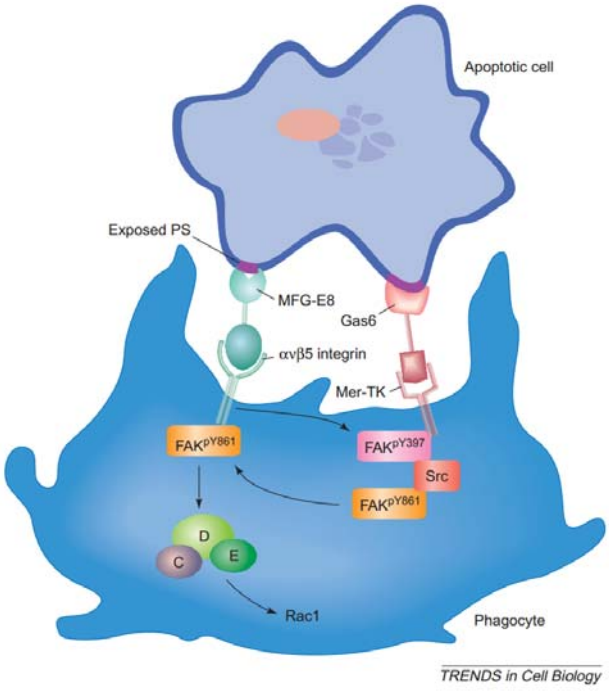

Figure 12. MFG-E8 function in the phagocyte clearance of apoptotic cells
(Adapted from Wu et al., 2006) PS exposed on the apoptotic cell is recognized by MFG-E8 C2 domain. The other side of this protein contact $\alpha_v\beta_3$ and $\alpha_v\beta_5$ integrin through RGD motif on the EGF domain. This binding triggers the post-receptor signaling leading to phagocytosis.

Combining these characteristics, MFGE8 functions as an opsonin to bridge the apoptotic cell with activated macrophage, connecting the exposed PS from apoptotic cells with C2 domain and macrophage using the RGD motif on the EGF domain, bringing the two in close proximity and facilitating the engulfment and clearance of the apoptotic cells (Figure 12) (Hanayama et al., 2002; Wu et al., 2006). Indeed, point mutation in the RGD motif prevented PS binding, and induced apoptotic cell accumulation in mice (Asano et al., 2004). In MFG-E8-deficent mice, the engulfment efficiency towards apoptotic lymphocytes from tingible body macrophages was decreased (Hanayama et al., 2004). Nonetheless, MFG-E8 deficiency was also identified to induce autoimmune diseases,

such as splenomegaly, glomerulonephritis, and atherosclerosis in mice (Hanayama et al., 2004; Silvius, 1992).

1.4 Phosphatidylserine in diagnosis

As discussed earlier, PS exposure was one of the early hall marks that demonstrated the onset of apoptosis, and signaled for clearance and corresponding immune response. In healthy tissue, PS exposed cells were believed to be cleared rapidly and constantly, therefore maintaining a steady-state of low-level overall PS exposure on cell surfaces. Whereas in pathological states, it either directly increased the amount of cell death, or indirectly interfered or blocked the apoptotic cell clearance, resulting in accumulation of PS-expressing cells or particles (Schutters and Reutelingsperger, 2010). Besides, in some special cases, cells might expose PS on their surface without the commitment of cell death. These were the endothelial cells of the tumor vasculature (Ran and Thorpe, 2002) and cardiomyocytes undergoing brief ischemia (Kenis et al., 2010). Surface expressed PS could be used as potential marker for various diseases, and its *in vivo* visualization would provide a valuable means for diagnosis, monitor and even treatment. Moreover, conventional radial- or chemo- therapies for tumors selectively induce programmed cell death in tumor tissue. PS exposure in such tissue will be good indicator for the therapeutical efficiency (Blankenberg, 2008).

So far, different PS binding entities were discovered, including proteins (Stace and Ktistakis, 2006), peptides (Burtea et al., 2009; Laumonier et al., 2006; Thapa et al., 2008) and small molecules (Hanshaw and Smith, 2005). Compared to large sized proteins, peptides and small molecules had the general advantage of fast clearance from specimen, but suffered from the low affinities. On the contrary, proteins could easily achieve high

affinity, but had much slower clearance kinetics (Schutters and Reutelingsperger, 2010). Several protein domains were shown to recognize specifically with PS exposed on the surface of cell membranes in high affinity, and Annexin A5 was the best characterized and most widely used. As shown in Figure 10, 4 annexin repeats composed the binding core of the Annexin A5, and utilized multiple Ca^{2+} ions coordinated with the residues in loop regions to bind to PS in a peripheral position. Its N-terminal concave side was genetically engineered to fuse with fluorescence tags, or labeled with different chelators of radionuclides (De Saint-Hubert et al., 2010), fluorochromes (Prinzen et al., 2007), nano-particles (Schellenberger et al., 2008) and liposomes (Garnier et al., 2009) through thiol linkages. It had been used in various preclinical researches and even clinical diagnosis to visualize PS exposure in assessment for various diseases conditions (Schutters and Reutelingsperger, 2010). Moreover, Annexin A5 could internalize into PS expressing cells, giving it potential to be vehicle for targeted drug delivery specifically to disease locus (Kenis et al., 2004). However, the complexities in the binding mechanism of Annexin A5 with PS had hindered the finding of smaller critical fragments with comparative affinity, and its relative large size withheld the development of a good pharmacokinetic profile for the safe use in clinical purposes.

1.5 Methods for studying protein-lipid interactions

Since an important part of my project is working on the study of protein-lipid interactions, it is worth discussing about various methodologies that could fulfill this purpose. With the advancement of technology and their application in the field of biological and biophysical area, a number of methods were available to gain insights in the protein-lipid

interactions with varying pros and cons. Here is a brief comparison between some selected methods.

Surface Plasmon Resonance (SPR) is an optical detection process that occurs when a polarized light, under condition of total internal reflection, hits a prism covered by a gold layer at the interface between media of different refractive index (Schasfoort RBM, 2008). It is a label-free method for analysis of molecular interactions in real time, and obtaining qualitative and quantitative data with low sample consumption. SPR is not useful for high throughput assays and not ideal for small analytes (MW< 1000Da).

Isothermal Titration Calorimetry (ITC) is a highly sensitive physical technique which is used to determine the thermodynamic parameters associated with biomolecular interactions in solution (Salim and Feig, 2009). It is a label-free, direct measurement under a specific temperature condition which could obtain the entire thermodynamic profile of a reaction from a single experiment. The disadvantages of ITC include the requirement of large quantities of proteins with high solubility, and the binding partners need to be soluble in same buffer system, with requirement in change of enthalpy.

Circular-dichroism (CD) spectroscopy is a powerful technique for studying the secondary-structure of proteins in solution. It has the great advantages of measuring both nonnative and native proteins at low concentration in a wide range of solution conditions containing lipids and detergents, and has been widely used for analyzing the structure and conformational changes of membrane proteins due to its sensitivity to local structures and short time for the detection. The drawback of CD spectroscopy is the low structural resolution it provided.

Nuclear Magnetic Resonance (NMR) spectroscopy is a competitive, elegant, and eminently viable technique for determining the solution structures of membrane proteins at the level of atomic resolution (Tamm and Tatulian, 1997). It offers a combination of several versatile strategies such as choice of NMR experiments, temperature, ionic strength, isotope labeling, and detergents, etc. Strategic combinations of these advancements together with availability of highly sensitive cryogenically cooled probes equipped high-field NMR spectrometers have overcome several of the conventional pitfalls associated with the NMR technique and membrane proteins such as low sensitivity, poor sample stability, spectral crowding, and a limited number of NOEs and other constraints for structure calculations. NMR spectroscopy provides information not only about the atomic coordinates of the structures but also dynamic motions of the backbone and side chains of membrane proteins solubilized in a large excess of mild detergents. In addition to structure and dynamics, NMR technique also offers unique opportunities to study the interactions of the membrane proteins with several other interacting partners.

Since the structure determination was done using NMR spectroscopy in this project. The sample was ready to be tested using the same method for functional characterization. Besides, we have shown that C2 domain of MFG-E8 binds to PS with much higher affinity when compared to binding with PC using 1D ^{31}P NMR spectroscopy (Reddy et al., 2007). To maintain consistency and comparability, we decided to continue using the method, with added characterization of the binding on protein side using 2D HSQC titration experiments. Moreover, as C2 domain's main function is performed

predominantly on cells, functional analysis in cell lines using flow cytometry was also proposed.

1.6 Research Objectives

In agreement with past results, we demonstrated preferential binding of MFG-E8 C2 domain with PS compared with PC, which is another participating phospholipid in the immune function of phagocytes (Hanayama et al., 2002; Reddy et al., 2007). And the molecular mechanism of the specific binding between the two could be possibly revealed by the three-dimensional structural information. Based on these, in our current study, we expressed and purified, both labeled and unlabeled mouse MFG-E8 C2 domain, and performed three-dimensional structural analysis using nuclear magnetic resonance (NMR) spectroscopy and binding site dynamics study using two-dimensional hetero nuclear single quantum correlation spectroscopy (HSQC). We also carried out mutagenesis studies on selected key residues to check for their involvement in the PS binding event both in solution by ^{31}P-NMR spectroscopy, and *in vitro* through FACS analysis using different methods. And these important residues were proved to be participating in the binding event with varying functions.

2 Materials and Methods

2.1 Materials

2.1.1 Chemicals

^{15}N-NH_4Cl and ^{13}C-Glucose were purchased from Cambridge Isotope Laboratories, Inc. (Andover, MA, USA).

Etoposide was purchased from Calbiochem (La Jolla, CA).

ProLong Gold antifade reagent with DAPI was purchased from Molecular Probes (Eugene, OR).

Ni^{2+}-NTA resin was from Qiagen (Hilden, Germany).

Phenylmethylsulfonyl fluoride (PMSF) was from Roche (Indianapolis, IN, USA).

Tris-(2-carboxyethyl)-phosphine (TCEP) was from Soltec Ventures (Massachusetts, USA),

1,4-Dithiothreitol (DTT), Isopropyl-Thio-B-D-galactopyranoside (IPTG) and kanamycin sulfate were purchased from USBiological (Massachusetts, USA).

Phosphatidylserine (PS) was purchased from Avanti Polar Lipids, Inc. (Alabama, USA).

CellTracker™ Green CMFDA (5-Chloromethylfluorescein Diacetate) and CellTracker™ Red CMTPX were purchased from Invitrogen, Life Technologies Corporation (CA, USA).

2.1.2 Protein molecular weight markers

The protein marker, Precision Plus Protein Standard Dual Color, was purchased from BioRad.

2.1.3 Bacterial strain

E. coli (Escherichia coli) DH5α strain was used for plasmid amplification and subcloning recovery.

E. coli (Escherichia coli) BL21 (DE3) strain was used for protein expression.

XL1 Blue super competent cell was used for the transformation of mutagenesis product.

2.1.4 Mammalian cell lines

HeLa (human cervical cancer cell line) were obtained from American type Culture Collection (Manassas, VA, USA).

THP-1 (human acute monocytic leukemia cell line) and Jurkat (immortalized line of T lymphocyte cells) cells were used for co-culture FACS analysis and obtained from American type Culture Collection (Manassas, VA, USA).

2.1.5 Plasmid

The cDNA coding for the C2 domain (His306-Cys463) of M. musculus MFG-E8L sequence (GenBank Accession No. AK171143) was subcloned into pET29b vector (Novagen) to create a C2 domain expression construct with 6 * Histidine tag at the C-terminal end as mentioned in the Method section.

C1C2 domain (Cys148-Cys463) was subcloned into pET-SUMO vector (Novagen) as mentioned below to create 6*His-tag – SUMO tag – C1C2 construct.

pGEX 4T-1 EGFP-MFGE8L C2 wild type was obtained from Dr. Choi Bo Hwa. MFGE8L C2 aromatic mutants were made by site-directed mutagenesis based on the template wild type construct. pGEX 4T-1 EGFP-MFGE8L C1C2 were produced by subcloning C1C2 sequence from pET29b MFGE8L full-length wild type plasmid and ligating into the pGEX 4T-1 vector with EGFP sequence inserted in advance.

Single mutations Lys331Arg (K24N, residue numbered within C2 domain), Try333Ala (W26A), Lys352Arg (K45N), Phe388Ala (F81A), and the double mutants K24N/K45N and W26A/F87A were produced by standard site-directed mutagenesis described in the Method section.

2.2 Methods

2.2.1 Subcloning

Target blank vector was digested with desired forward and reverse restriction enzyme (New England Biolabs) and purified by gel extraction using Gel Extraction Kit (Qiagen). The insert sequence was obtained by PCR using specific primers on its template. The reaction mixture was prepared in 50 µl total volume as follow: 5 µl 10 × Taq buffer (Roche), 2 µl forward primer, 2µl reverse primer, 1 µl dNTP mixture, 0.5 µl template, 1 µl Taq DNA polymerase (Roche), PCR grade water to top up. The PCR reaction was performed by heating the sample to 95 ˚C for 5 min followed by 28 cycles of 95 ˚C for 30 sec, 50 ˚C for 30 sec, and 68 ˚C for 1 min. The product was tested by agrose gel electrophoresis and purified by gel extraction. Restriction enzyme digestion was performed at 37 ˚C for 1 hour in 20 µl reaction mixture: 1 µl restriction enzyme, 2 µl enzyme specific buffer, 16 µl PCR product and PCR grade water top up. Ligation of PCR product into the target vector was performed at 16 ˚C overnight in 20 µl reaction mixture: 2 µl vector, 6 µl insert, 2 µl ligation buffer, 1 µl T4 ligase (New England Biolabs) and PCR grade water top up. The ligation product was chemically transformed into DH5α competent cell by heat-shock and plated on LB-plate with corresponding antibiotic and grown overnight. Single colony was picked and amplified to 2 ml LB culture. The amplified plasmid was purified using Plasmid Extraction Kit (Qiagen) and confirmed by sequencing service provided by 1st Base (Singapore).

2.2.2 Site-directed Mutagenesis

To obtain the target single residue mutation in the protein of interest, standard site-directed mutagenesis protocol was used. Pair of complimentary primers were designed in such way that the mutating residue was in the middle with 3-5 original flanking residue sequences at each side. The reaction mixture was prepared in 50 µl total volume as follow: 5 µl 10 × Pfu reaction buffer (Fermentas), 2.5 µl of each primer, 1 µl template, 1 µl dNTPs, 1 µl Pfu enzyme (Fermentas), and PCR grade water to top up. The amplification reaction was performed by heating up the mixture to 95 ˚C, followed by 18 cycles of 95 ˚C for 50 sec, 55 ˚C for 50 sec, and 68 ˚C for 7 mins. The product was verified using agrose gel electrophoresis and purified by Gel Extraction Kit (Axygen). The purified plasmid was chemically transformed into XL-1 blue super-competent cells by heat-shock and plated on LB-plate with corresponding antibiotic and grown overnight. Single colony was picked and amplified to 2 ml LB culture. The amplified plasmid was purified using Plasmid Extraction Kit (Qiagen) and confirmed by sequencing service provided by 1st Base (Singapore).

2.2.3 Mammalian Cell Culture Conditions

HeLa cells were maintained in DMEM described above, and cultured in a humidified 5% CO_2 incubator at 37 ˚C.

THP-1 cells and Jurkat cells were maintained in RPMI with serum, and cultured in a humidified 5% CO_2 incubator at 37 ˚C.

2.2.4 Preparation of recombinant proteins

Recombinant mouse MFG-E8 C2 domain was expressed and purified, as we previously described (Reddy et al., 2007). For NMR study, the isotopically labeled MFG-E8 C2 proteins were expressed in *Escherichia coli* (*E. coli*) BL21 (DE3) cells grown in M9 medium containing $^{15}NH_4Cl$, or $^{15}NH_4Cl$ plus [U-^{13}C]-glucose and purified using Ni^{2+}-NTA metal affinity chromatography followed by size-exclusion chromatography (Sephacryl Superdex-200 column). The purified MFG-E8L C2 was concentrated to 0.8 mM in the buffer containing 20 mM sodium phosphate ($NaPO_4$), pH 6.5, 20 mM NaCl, 0.01% sodium azide (NaN_3) and 10% or 100% D_2O. The concentration of the purified protein was determined by Bradford dye assay kit (Bio-Rad Laboratories).

To produce gst-EGFP-MFG-E8 C2 and its mutants, and gst-EGFP-MFG-E8 C1C2 for FACS analysis, the plasmids were transformed into *E. coli* BL21 cells to produce desired gst-tagged fusion proteins or mutants before being induced with 1 mM isopropyl-1-thio-β-D-galactopyranoside (IPTG) for 4 h at 25°C. Cells were lysed by sonication in a phosphate-buffered saline (PBS) containing 1 mM phenylmethanesulfonylfluoride (PMSF). After centrifugation at 20000 rpm in a Beckman Coulter JA25 rotor, supernatant was incubated with glutathione-sepharose beads (Amersham Biosciences, Little Chalfont, UK) for 1 h at 4°C. The beads were washed with PBS and the proteins were eluted from the beads with 10 mM reduced glutathione in 50 mM Tris, pH 8.0. The concentration of the purified protein was determined by Bradford dye assay kit (Bio-Rad Laboratories).

To produce SUMO-MFG-E8L-C1C2 domain, the plasmids were transformed into *E. coli* BL21 cells to produce desired gst-tagged fusion proteins or mutants before being induced with 1 mM isopropyl-1-thio-β-D-galactopyranoside (IPTG) for 4 h at 25°C. Cells were

lysed by sonication in the buffer containing 20 mM Tris, pH 8.2, 500 mM NaCl, 5 % Glycerol, and 5 mM TCEP. After centrifugation at 20000 rpm in a Beckman Coulter JA25 rotor, supernatant was purified using Ni^{2+}-NTA metal affinity chromatography and analyzed by 12% SDS-PAGE. Sample buffer was exchanged to the buffer containing 20 mM Tris, pH 8.2, 500 mM NaCl, 5 mM TCEP using PD-10 column.

2.2.5 Fluorescence Activated Cell Sorting (FACS)

Annexin V-FLUOS staining kit (Roche, Penzberg, Germany) was used as control to measure the binding of the protein with exposed phosphatidylserine on the outer leaflet of the plasma membrane. Briefly, HeLa cells grown in 6-well plates were treated with 100 μM etoposide for 24 hours to induce apoptosis. Whole cells were then harvested, washed using 1 × PBS and stained with annexin V or testing proteins together with propidium iodide (PI) at room temperature, followed by fluorescence activated cell sorter (FACS) analysis using a BD (Becton Dickinson, Franklin Lakes, NJ, USA) FACSCalibur flow cytometer according to the manufacturer's protocol. A population of at least 10,000 cells was used for each experiment.

2.2.6 Co-culture FACS analysis of C2 binding with PS

THP-1 and Jurkat cells were first labeled using red or green fluorescence dyes, respectively. 1 μl of 10 mM CellTracker™ Red or Green fluorescence dye stock solutions were diluted into 10 ml pre-warmed RPMI without serum to the final working concentration of 1 μM. The cells were harvested by centrifugation at 500 g for 2 mins, and resuspended using the aforementioned working solution respectively. After 45 mins incubation at 37 ˚C in normal growth condition, the cells were spanned down again and

resuspended using normal RPMI with serum and allowed 30 mins incubation for recovery. THP-1 cells were maintained in normal 10 cm patri-dish. Jurkat cells were split into 6-well plates and apoptosis in selected wells was then induced by adding etoposide to the final concentration of 100 µM. After 24 h incubation, both cells were harvested and washed by 1 × PBS to remove residual medium. Protein of interest was diluted to desired concentration using 1 × PBS, and cells from each well of the 6-well plates were resuspended using 100 µl of testing protein solution into 4 ml falcon tube. After 20 mins incubation, 100 µl of washed THP-1 cells in sample buffer were added in equal cell number and incubated at room temperature for 20 mins. Another 500 µl sample buffer were added before proceeding to the FACS analysis using a BD (Becton Dickinson, Franklin Lakes, NJ, USA) FACSCalibur flow cytometer according to the manufacturer's protocol. A population of at least 10,000 cells was used for each experiment.

2.2.7 NMR Experiments

NMR spectra were acquired on a Bruker Avance II 700 MHz NMR spectrometer equipped with four RF channels and a 5 mm z-gradient TXI CryoProbe (Bruker BioSpin) at 298 K. Spectra were processed with Topspin version 1.3 (Bruker) and analyzed using Sparky (Goddard T. D. & Kneller D. G., SPARKY3, University of California, San Francisco) and NMRview (Blevins, 1994). Backbone assignment was made from Heteronuclear Single Quantum Coherence (HSQC) HNCA, HNCO, HNCACB, CBCACONH and 3D ^{15}N-HSQC-nuclear Overhauser effect spectroscopy (NOESY) (Shao et al., 2008). Side-chain assignments were made from 3D HC(C)H-TOCSY, H(CC)(CO)NH, (H)CC(CO)NH and ^{13}C-HSQC-NOESY. Nuclear Overhauser effects (NOE) distance constraints were provided by 3D ^{15}N- and ^{13}C-edited NOESY spectra

acquired with mixing time of 120 ms and 3D aromatic ^{13}C-HMQC-NOESY spectra acquired with mixing time of 80 ms. The exchanging amide protons were monitored by dissolving the lyophilized protein in D_2O and acquiring a series of ^{15}N-HSQC spectra.

2.2.8 Structural Calculation

NMR spatial structures of the MFG-E8 C2 were calculated using CYANA. (Guntert, 2004) NOE distance constraints for the structure calculation were obtained from 3D ^{15}N- and ^{13}C-edited NOESY and 3D aromatic ^{13}C-HMQC-NOESY spectra. Dihedral angle restraints were calculated from chemical shifts suing Torsion Angle Likelihood Obtained from Shift and sequence similarity (TALOS) and the overall secondary structure was predicted from the Chemical Shift Index (CSI) and NOE pattern. (Cornilescu et al., 1999) Disulfide bond was predicted using the method described in previous paper. (Sharma, 2000) The slowly exchanging amide protons were assigned as hydrogen bond donors with related hydrogen-acceptor partners on the basis of preliminary structure calculated. The standard CYANA simulated annealing protocol was applied to 100 random structures and the resulting 20 energy-minimized structures with the lowest target function energy were selected for further analysis. Structures were analyzed using the program PROCHECK and visualized by MOLMOL, PyMOL (www.pymol.org) and Swiss-PdbViewer. (Cornilescu et al., 1999; Guex and Peitsch, 1997; Laskowski R A, 1993) The chemical shifts and the NMR-derived restraints and atomic coordinates of the protein ensemble have been deposited at BioMagResBank (www.bmrb.wisc.edu) with accession code BMRB 17477 and the Protein Data Bank (www.pdb.org) with accession code PDB 2L9L, respectively.

2.2.9 2D ^{1}H-^{15}N Heteronuclear Single Quantum Correlation (HSQC) titration with 06:0 PS

1,2-dihexanoyl-*sn*-glycero-3-phospho-L-serine (06:0 PS) (Avanti Polar Lipids, Inc.) was dissolved into buffer containing 20 mM $NaPO_4$, pH 6.5, 50 mM NaCl, 0.01% NaN_3, to make stock solution of 3 mM concentration. The ^{15}N labeled protein sample was expressed and purified as mentioned above, and concentrated to about 0.2 mM in the buffer containing 20 mM $NaPO_4$, pH 6.5, 50 mM NaCl, 0.01% NaN_3, 10% D_2O. 06:0 PS was added into protein sample to the final protein concentration of 0.12 mM and lipid concentration of 1.2 mM, with molar ratio of 1:10. ^{1}H-^{15}N HSQC spectra were acquired on a Bruker Avance II 700 MHz NMR spectrometer.

2.2.10 ^{31}P NMR spectroscopy

Phosphatidylserine (0.25 mM) and the wild type C2 domain and its mutants were prepared in a buffer containing 10 mM $NaPO_4$, pH 6.5, 10 mM NaCl, 10 mM CHAPS, 0.01% NaN_3 and 10% D_2O. ^{31}P NMR spectroscopy of PS was determined as we previously described.(Reddy et al., 2007) Binding constant (K_d) for PS with the C2 domain was determined by non-linear least square fitting on the plots of the chemical shift data vs. the protein concentration for the wild type, and line width at half height data as vs. protein concentration based on one binding site equation. (Peng et al., 2001)

2.2.11 Molecular docking study

To identify potential binding residues for the head group of PS, molecular dockings were performed using Gold 4.0 (Jones et al., 1997). Coordinates of PS were taken from its

complex with protein kinase C (PDB ID: 1DSY) and employed for docking PS with the mouse C2 domain. Alignment of different C2 members, factor V C2, factor VIII C2, human, bovine and mouse MFGE-8 C2 domains (Figure 20) suggests that residues in the spikes/loops region are conserved and could participate in membrane binding. Further binding site analysis also revealed potential sites at which PS docks at these spikes or loops. Gold molecular docking software was employed to dock PS with protruding loops or spikes of the C2 domain (Jones et al., 1997). A region around 10 Å from these spikes was defined to dock PS using annealing parameters of hydrogen bond and Van der Waal's interactions at 2.5 and 4.0 Å, respectively, with docking solutions within 1.5 Å RMSD considered. Electrostatic calculations were numerically solved from the linear Poisson-Boltzmann equation with the aid of APBS code associated with the PyMol software package (Baker et al., 2001).

3 Results

3.1 Expression and Purification of MFG-E8 C2 domain

In order to study the interaction between MFG-E8 C2 domain and PS, the protein segment corresponding to the amino acid sequence His306 to Cys463 of *mus musculus* MFG-E8 was cloned, expressed and purified as mentioned in the Method section. As shown in Figure 13, MFG-E8 C2 domain was expressed in *E. coli* and purified using affinity column (Ni^{2+}-NTA). Purification fractions were analyzed in SDS-PAGE and visualized by coomassie blue staining. It suggested that the protein of interest was well expressed in our expression system and could be purified with high yield. Elution fractions from affinity column (Ni^{2+}-NTA) were combined and further purified to homogeneity using size-exclusion column (Sephacryl Superdex-200), the peak eluted around 105 ml were analyzed using SDS-PAGE (Figure 14). The purified sample was also analyzed by MALDI-TOF/TOF to check the exact molecular weight. And database search was performed to confirm the identity by our in-house Mass spectrometry facility (data not shown). Together, these results suggested that the protein we cloned, expressed and purified was the correct one. In this Results section, the term 'C2 domain' will be referring to the C2 domain of mouse MFG-E8 protein from now on. C2 domains from other proteins or other species will be specified accordingly.

It is noteworthy that the construct of human MFG-E8 C2 domain was originally selected for characterization since it was more relevant with our aim of study. However, due to poor expression and solubility in our experimental conditions, construct of mouse MFG-E8 C2 domain was chosen instead.

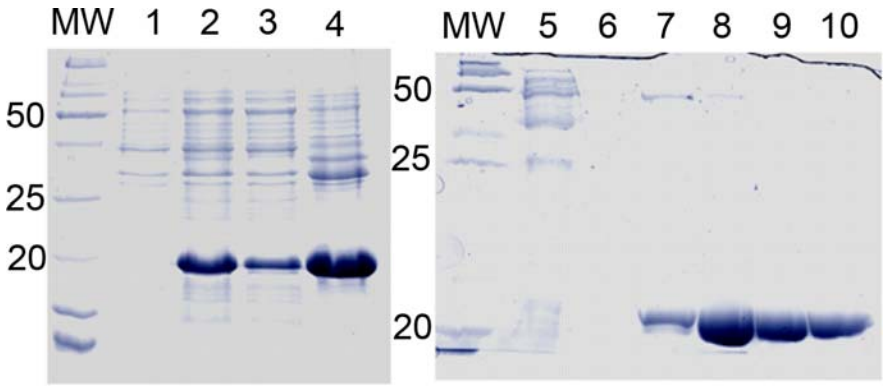

Figure 13. Purification of MFG-E8 C2 domain Using Affinity Column
MFG-E8 C2 domain was expressed in *E. coli* and purified using affinity column (Ni^{2+}-NTA). Purification fractions were analyzed in SDS-PAGE and visualized by coomassie blue staining. (**MW**: molecular weight standard; **Lane 1**: before IPTG induction; **Lane 2**: total lysate; **Lane 3**: supernatant; **Lane 4**: pellet; **Lane 5**: Flow through; **Lane 6**: wash; **Lane 7 to 10**: elution fractions)

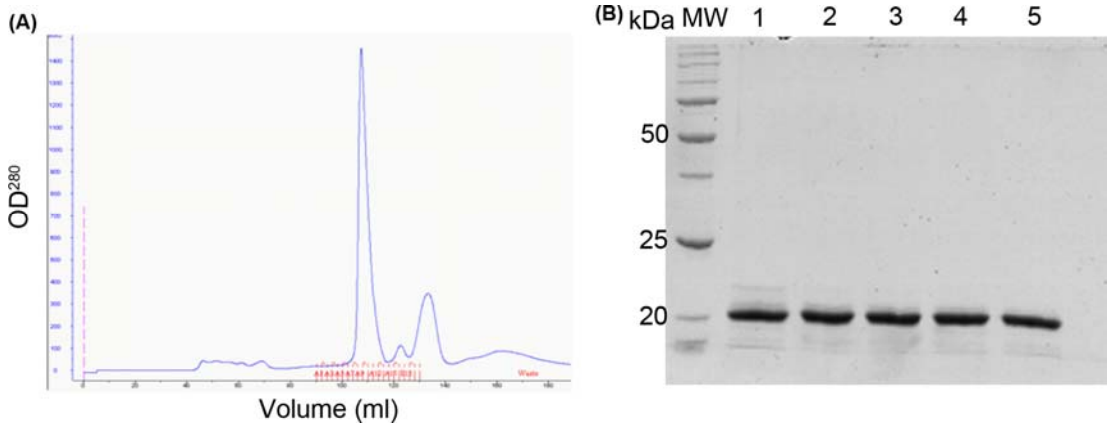

Figure 14. Purification of MFG-E8 C2 domain Using Size-exclusion Column
Elution fractions from affinity column (Ni^{2+}-NTA) were combined and further purified using size-exclusion column (Sephacryl Superdex-200), the peak eluted around 105 ml were analyzed using SDS-PAGE. **(A)** Size-exclusion column elution profile of MFG-E8 C2 domain. **(B)** SDS-PAGE analysis of the main elution peak from size-exclusion column. (**MW**: molecular weight standard; **Lane 1 to 5**: FPLC fractions collected; **OD^{280}**: Optical density at wavelength of 280 nm)

In order to verify the functionality of our purified protein, 1D ^{1}H NMR spectrum was collected (Figure 15). In agreement with our previously published data, the well separated peaks of methyl protons (-0.5–1.5ppm), α-protons (3.5–6ppm), and amide protons (6–10ppm) indicated that the purified protein was well folded and sui table for the following structural, biochemical and biological studies (Reddy et al., 2007).

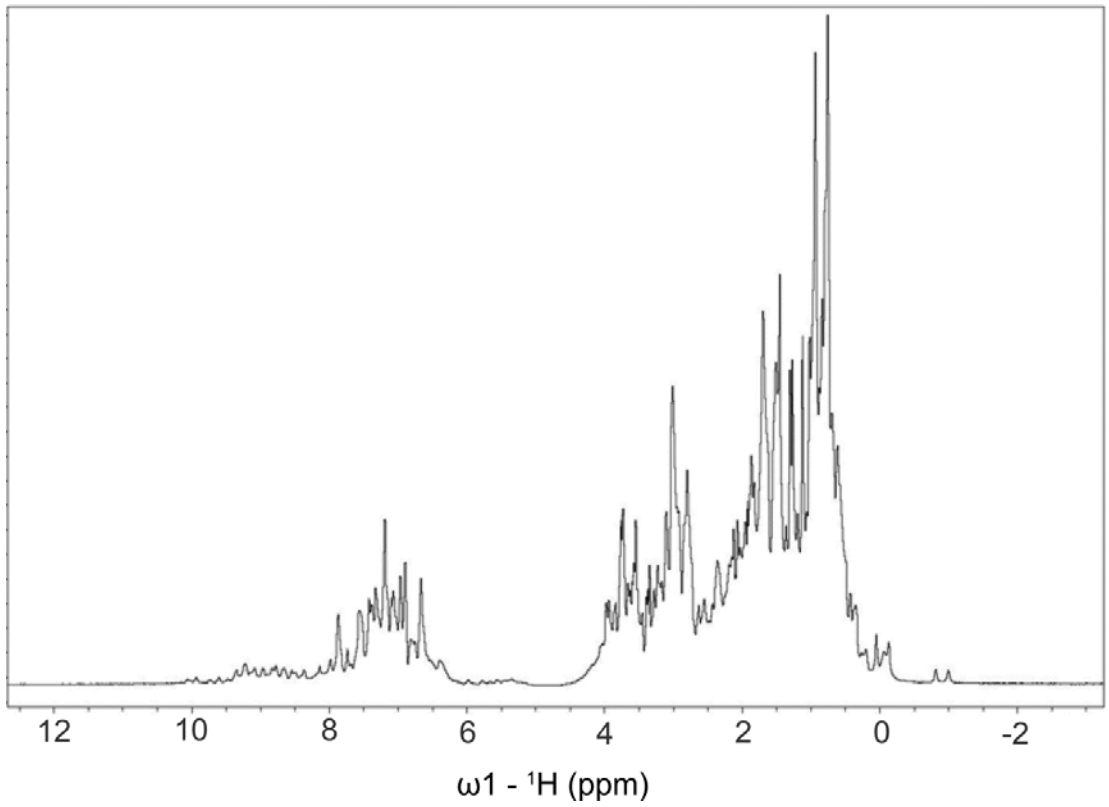

Figure 15. 1D ^{1}H NMR spectrum of MFG-E8 C2 domain
1D ^{1}H NMR spectrum of the purified MFG-E8 C2 domain was collected on an Avance 600 MHz NMR spectrometer. The well separated peaks of methyl protons (-0.5–1.5ppm), α-protons (3.5–6ppm), and amide protons (6–10ppm) suggested the protein was well folded.

3.2 NMR structural determination of MFG-E8 C2 domain

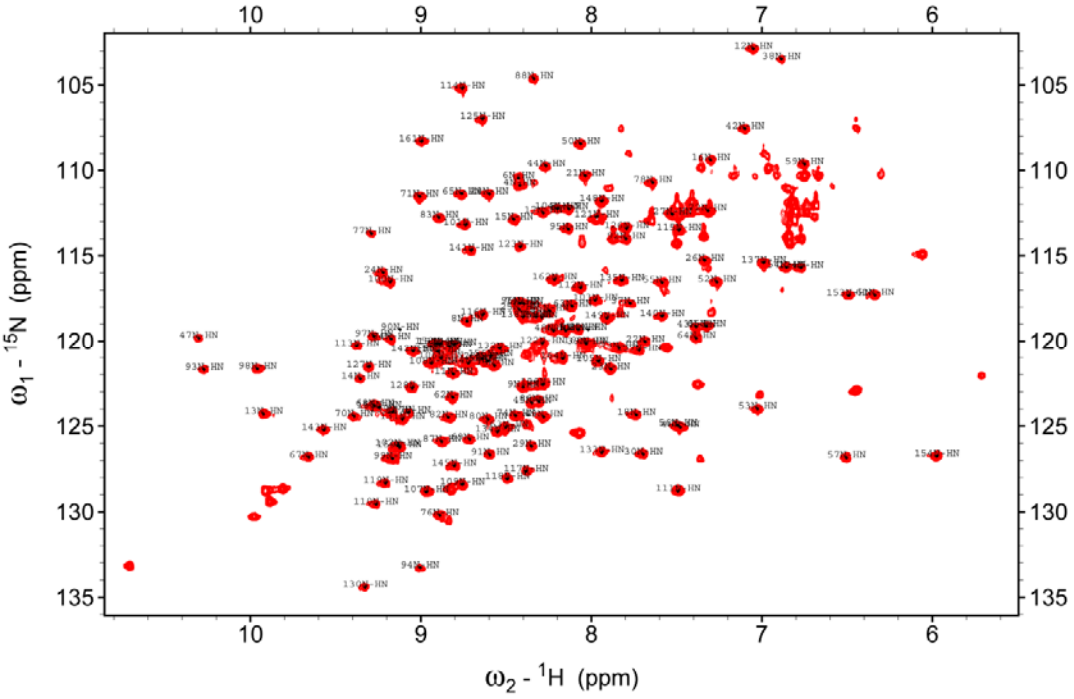

Figure 16. 2D ^{1}H-^{15}N HSQC spectrum of MFG-E8 C2 domain and its backbone assignment
The 2D HSQC were performed on an Avance 600 MHz NMR spectrometer. The MFG-E8 C2 domain showed well-dispersed peaks. Using a series of 2D and 3D spectra, backbone assignment was successful except for residues Thr25-Ala30.

The MFG-E8 C2 domain was concentrated to 0.5 mM, and series of 2D and 3D NMR spectra were collected and analyzed as mentioned in the method section. The 2D ^{1}H-^{15}N heteronuclear single quantum correlation (HSQC) spectrum gave good peak dispersion and minimal peak overlapping (Figure 16). The backbone assignment was successful through analysis of several 2D and 3D NMR spectra listed in the method section, except for residues Thr25-Ala30. The rest of the structural analysis was done mainly by Dr. Ye Hong.

Table 1 summarizes the structural statistics for the structure ensemble determined for MFG-E8 C2 domain through NMR spectroscopy. 110 backbone (φ, ψ) dihedral angle restraints, 99 hydrogen bond distance restraints, and 2067 NOE distance restraints were used for the NMR structure calculation as input data.

In previous study (Sharma, 2000), a database of cysteine ^{13}C C_α and C_β chemical shifts was constructed from the BioMagResBank (BMRB) (http://www.bmrb.wisc.edu), Sheffield (http://www.shef.ac.uk/uni/academic/1-M/mmb/nmr/chemshifts.html) databases, and published literature. Analysis on 316 cysteines revealed that ^{13}C chemical shifts of Cysteine C_α and C_β showed distinction between different redox states and in different secondary structure. Based on their finding, reduced cysteines have a C_β ^{13}C chemical shift in the range of around 25 to 35 ppm, and the oxidized ones have a C_β ^{13}C chemical shift in the range of around 35 to 50 ppm. From our experimental data, we have the following ^{13}C chemical shift for the two cysteine residues: C_β of cys1 is 45.248 ppm, while C_β of cys156 is 41.58 ppm, which fell into the range of oxidized category. Therefore, cys1 was predicted to form a disulfide bond with Cys156 based on these ^{13}C chemical shifts. The presence of this disulfide bond in our calculated structure agrees with detection of the disulfide bonds in the crystal structures of bovine MFG-E8 C2 and factor V and VIII. Therefore, our structural calculation also included this disulfide bond restraint.

It is also noteworthy of the conservation of these two cysteine residues across different homologous sequences and their location at the very extremities of N- and C-terminus of these proteins. And taking into account of the absence of additional cysteine residues in most of these protein sequences, these two cysteines at the terminus are believed to be

important in stabilizing the structure of the protein and/or maintaining a functioning conformation.

As a result, the structure of the ensemble as well as the one with lowest energy was shown in Figure 8. Similar to the structures of other C2 domains, there are also two major β-sheets consisting of five and three anti-parallel β-strands respectively and facing each other, plus four minor β-strands in our solution structure of mouse MFG-E8 C2 domain (Figure 17A). Relative to the mean coordinates of the 20 representative conformers, the average root-mean-square-deviation (RMSD) for the backbone atoms were determined to be 0.73 Å, and the RMSD of heavy atoms from residues in well-defined regions (17-20,59-96,102-104,112-156) were determined to be 1.40 Å (Table 1).

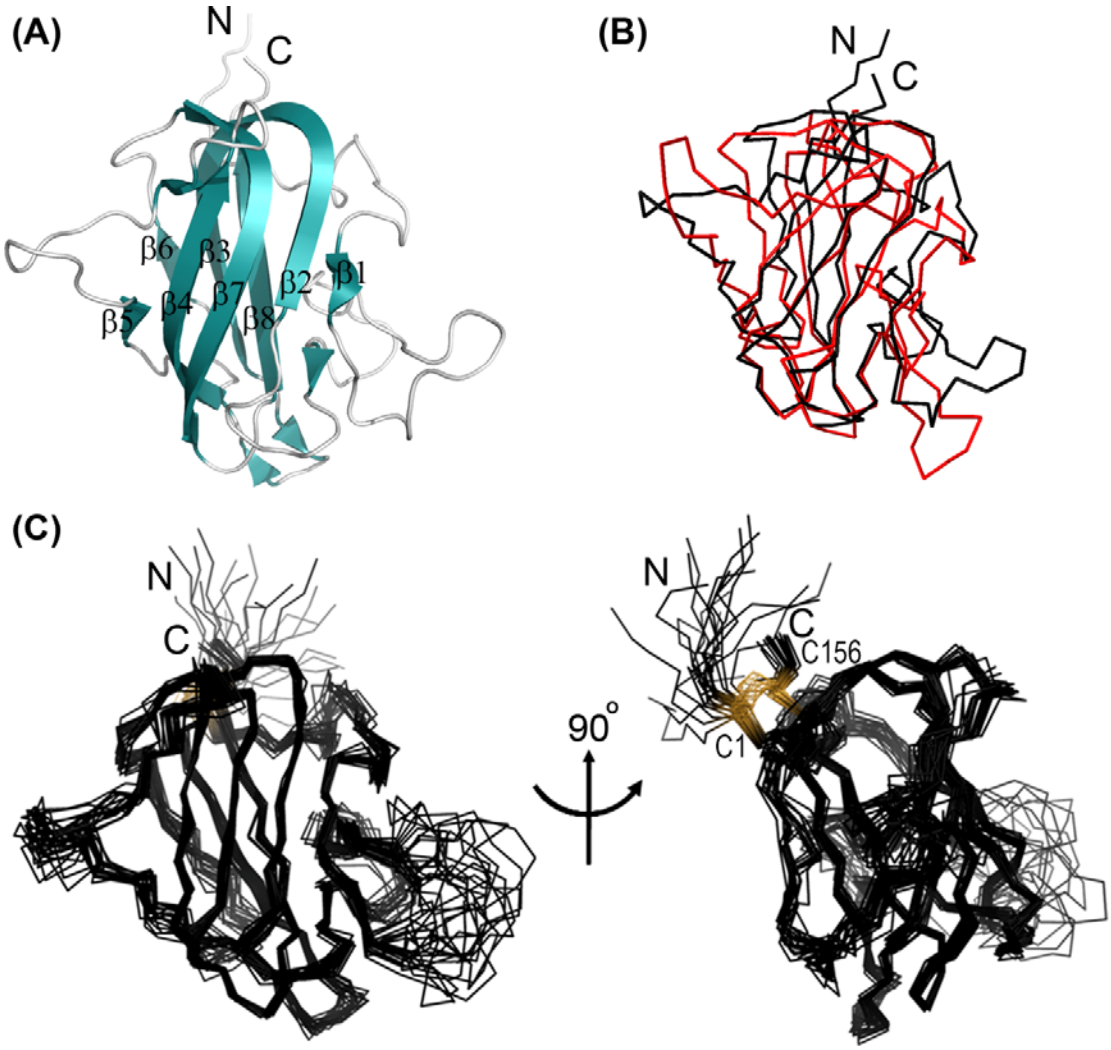

Figure 17. Solution structure of MFG-E8 C2 domain
(A) The lowest energy conformer structure of mouse MFG-E8 C2 domain. **(B)** Overlay of mouse MFG-E8 C2 domain solution structure (black; PDB code: 2L9L) and bovine MFG-E8 C2 domain crystal structure (red; PDB code: 3BN6). **(C)** Overlay of the top 20 conformers ensemble. The disulfide bridge between Cys1 and Cys156 is highlighted in yellow.

Table 1. Structural Statistics for Solution Structure of Mouse MFG-E8 C2 Domain

Unambiguous NOE restraints	2067
Intra-residual (i=j)	455
Sequential (|i-j|=1)	700
Medium Range (1<|i-j|<5)	188
Long Range (|i-j|≥5)	724
Dihedral angle restrains	
All	110
ϕ	56
ψ	54
Hydrogen bond restraints (upper / lower)	99/99
Disulfide bond	1
Total number of restraint violations > 0.4	0
Total number of dihedral angle violations > 5°	0
Average RMSD (Å) to Mean for the top 20 structures	
Residues 1-158	
Backbone atoms	1.5±0.25
All heavy atoms	2.18±0.23
Residues 17-20,59-96,102-104,112-156	
Backbone atoms	0.73±0.10
All heavy atoms	1.40±0.14
Residues 14-24,36-156	
Backbone atoms	0.92±0.16
All heavy atoms	1.55±0.16
Ramachandran analysis (%)	
Residues in most favored regions	59.9%
Residues in additional allowed regions	35.1%
Residues in generously allowed regions	3.7%
Residues in disallowed regions	1.4%

The amino acid sequences alignment between mouse and bovine MFG-E8 C2 domains demonstrates a sequence identity of 72.8% between the two, and suggests that the C2 domain sequence is highly conserved across these two species (Lin et al., 2007). Comparing our lowest energy NMR structure of mouse MFG-E8 C2 (PDB code: 2L9L) with the crystal structure of bovine MFG-E8 C2 (PDB code: 3BN6), the RMSD for the α-carbon atoms was 1.52 Å (Figure 17B). However, even with such a high sequence identity, these two structures were still considerably different, and these deviations mainly arises from the inter-strand loops between β-sheets, such as residues starting from Thr25 to Ala30 and the inter-strand loop between β5 and β6. In our study, peaks for residues Thr25-Ala30 were unable to be observed in the 2D ^{1}H-^{15}N HSQC spectrum (Figure 16). This may be due to that as these residues locate within the flexible loop region, they undergo fast exchange with surrounding solvent molecules, leading to severe line broadening and peak disappearance. This agrees with the highest average B-factor value of the C_{α} atoms observed from residues Thr25-Ala30 in the crystal structure of bovine MFG-E8 C2 domain (PDB ID: 3BN6) (Shao et al., 2008). Although they are unable to be well-defined, some possible conformations of this flexible region could be reflected from our solution structures which could be found in the structure ensemble with higher RMSD values (Figure 17C).

3.3 MFG-E8 C2 domain interaction with 06:0 PS examination by 2D ^{1}H-^{15}N Heteronuclear Single Quantum Correlation (HSQC)

In order to examine the binding event of MFG-E8 C2 domain, 2D ^{1}H-^{15}N HSQC titration experiments was performed. After the initial screening with different types and compositions of phospholipids (data not shown), 1,2-dihexanoyl-*sn*-glycero-3-phospho-L-serine (06:0 PS) (Avanti Polar Lipids, Inc.) was chosen to titrate into MFG-E8 C2 domain, because of its short carbon chain, high solubility in aqueous solution and low precipitation when bound with the target protein. The MFG-E8 C2 sample was titrated with 06:0 PS, and the final concentration of 0.12 mM for protein and 1.2 mM for PS. Following the method described in the method section, ^{1}H-^{15}N HSQC spectrum was recorded, and overlaid onto the free protein spectrum (Figure 18). The NMR signals exhibited an overall attenuation. Only about 40 to 50% of the original peak intensity was maintained. One possible explanation is that the binding with PS micelle caused general line broadening for all the residues. By analyzing this overlay, residues Tyr23, Lys24, Trp33, Asn42, Gly44, Lys45, Asn47, Ala48, Trp49, Gly77, Ala78, Gly82, Gln85, Asn116, Leu117, Asn119, Asn120 and Ser121 were found to have their corresponding peaks perturbed and shifted away from their original positions, and residues Phe31, Gly32, Ile46, Arg79, Phe81, and Arg150 could not be found for their corresponding peaks after the titration (Figure 19). Residue mapping was performed for these residues, and it was interesting to find out that almost all of these residues were located in close proximity as clusters within these loop regions, suggesting high involvement of these loops in the binding event and their importance.

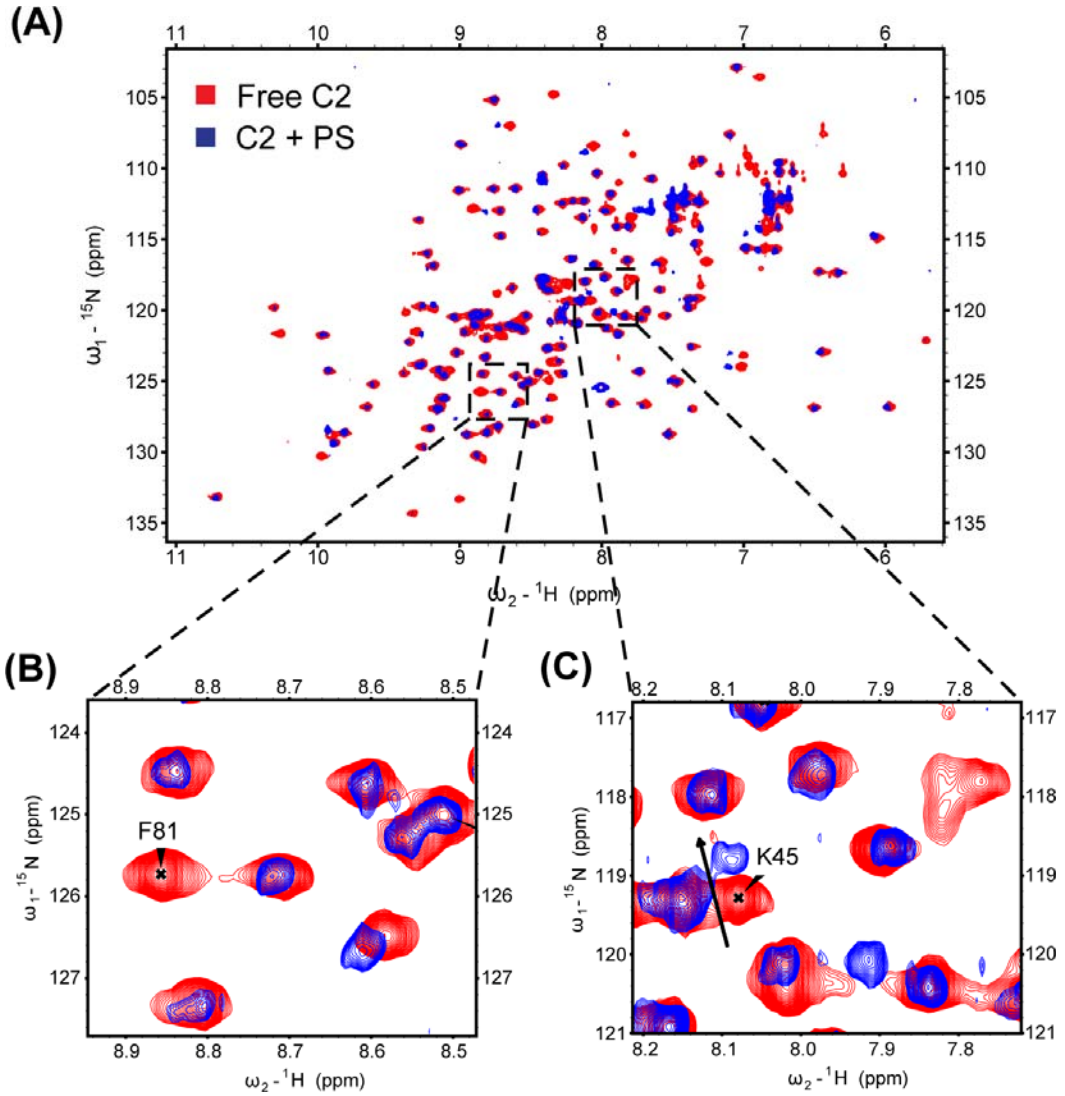

Figure 18. ^{1}H-^{15}N HSQC of MFG-E8 C2 domain binding with 06:0 PS
1.2 mM of 06:0 PS was titrated into 0.12 mM MFG-E8 C2 sample with the final concentration ratio to be 1:10 for Protein:PS. Following methods described in the method section, ^{1}H-^{15}N HSQC spectrum was acquired, and overlaid onto the free protein spectrum. This overlay made use of the free protein assignments shown in Figure 16, and omitted for the simplicity of the data presentation. Selected key residues were labeled in the zoom-in diagram. **(A)** Overlay of 1:10 molar ratio spectrum **(Blue)** with free protein spectrum **(Red)**. **(B and C)** Zoom-in on selected residues having significant changes. Left diagram shows the peak disappearance of Phe81. Right diagram shows the peak shift of Lys45, with arrow showing the direction of peak shift.

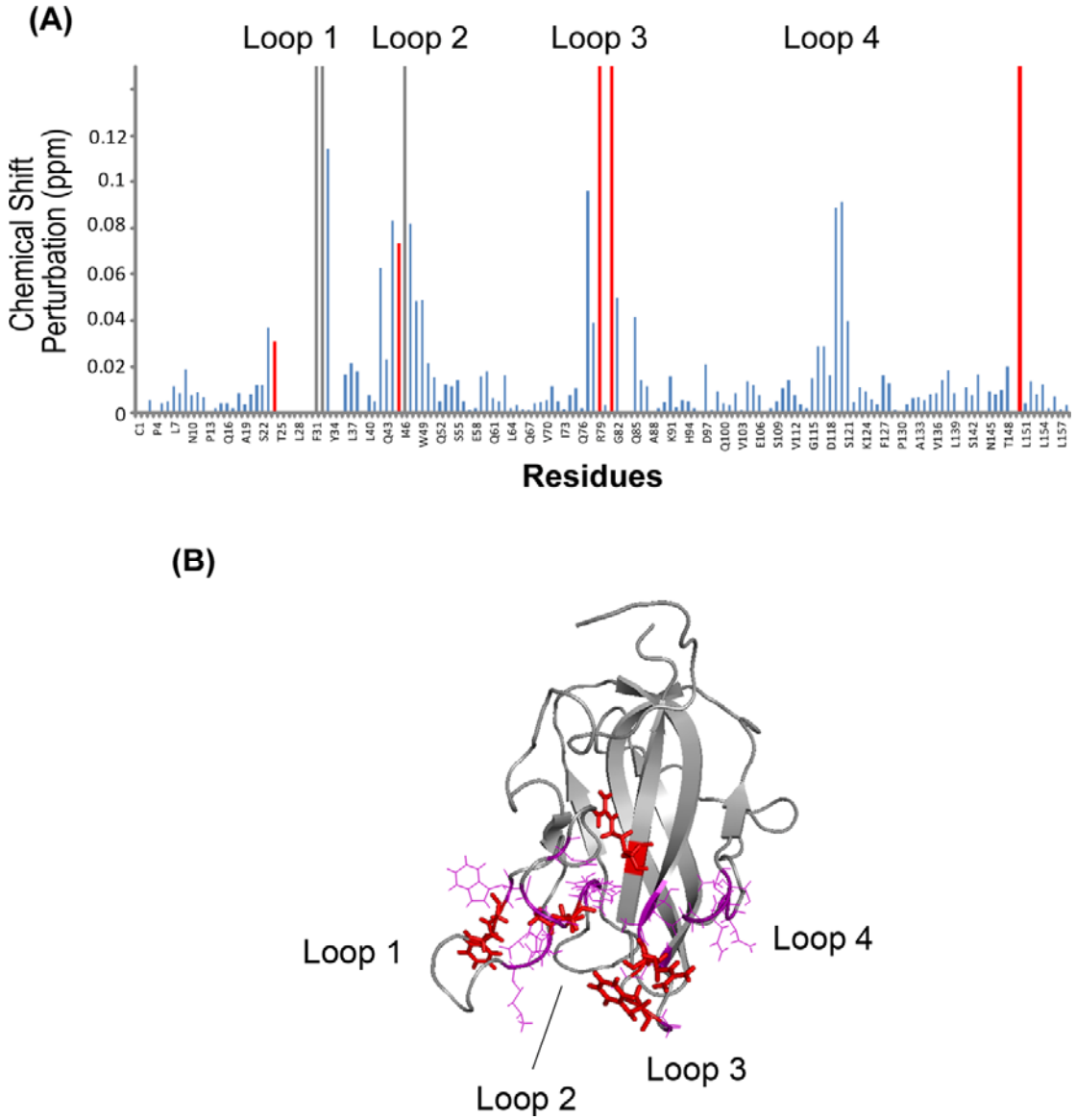

Figure 19. Analysis of HSQC titration results of C2 binding with PS and mapping of critical residues

1.2 mM of 06:0 PS was titrated into 0.12 mM MFG-E8 C2 sample with the final concentration ratio to be 1:10 for Protein:PS. Following methods described in the method section, ^{1}H-^{15}N HSQC spectrum was acquired. **(A)** Chemical shift perturbation analysis on HSQC spectra of MFG-E8 C2 domain after PS titration. Disappeared residues were incorporated into the chemical shift perturbation histogram by being treated as having chemical shift perturbation of 1 ppm with the color of Grey. Residues chosen to be mutated were colored red and may cover the original color of the bar. **(B)** Mapping of disappeared or shifted residues on MFG-E8 C2 domain structure selected from our structure ensemble. **Red** colored residues were disappeared ones; **Purple** colored residues were shifted ones.

3.4 *in silico* Study of Molecular interaction between MFG-E8 C2 domain and phosphatidylserine

In order to have better understanding about this protein, sequence alignment across different C2 family members was performed (Figure 20). A series of hydrophilic residues, including Lys24, Thr25, Arg29, Lys45, Gln77, Asp80, Glu85, Arg146, and Arg150, as well as hydrophobic residues, such as Trp33, Phe31, Phe81, Leu28, and Trp26 which might composing the potential PS-binding site were found to be conserved across the aligned proteins, suggesting their importance in the PS-binding.

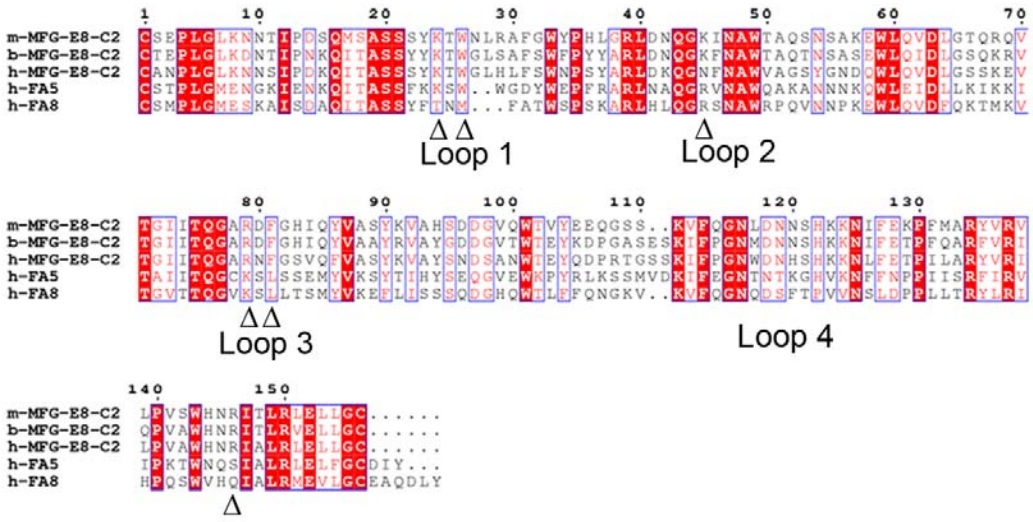

Figure 20. Sequence alignment of different C2 domains homologues
Amino acid sequence alignment between mouse MFG-E8 C2 domain and its homologous C2 domains was performed using the online alignment tool ESPript Web server. Residues colored in white with red background represent the identical residues conserved across all five sequences. Residues colored in red with white background represent those shared by more than two sequences. Δ pointed out the positions where mutagenesis attempts were made to analyzing mode of action of PS binding. Sequences used in this alignment were obtained from the UniProtKB data base entries listed as follows: P21956 for mouse MFG-E8 C2; Q95114 for bovine MFG-E8 C2; Q08431 for human MFG-E8 C2; P12259 for human factor V; P00451 for human factor VIII.

With the help from Dr. Amaravadhi Harikishore, molecular docking analysis was performed to study the mode of MFG-E8 C2 domain binding with PS. From the structure of MFG-E8 C2 domain, the surface charge distribution was very well-organized for the purpose of PS-binding. The electrostatic potential mapping revealed a uniformly positively-charged patch located in the loop region, which were the proposed PS binding site (Figure 21A). All those conserved polar residues found in the alignment study contributed to this unique charge distribution.

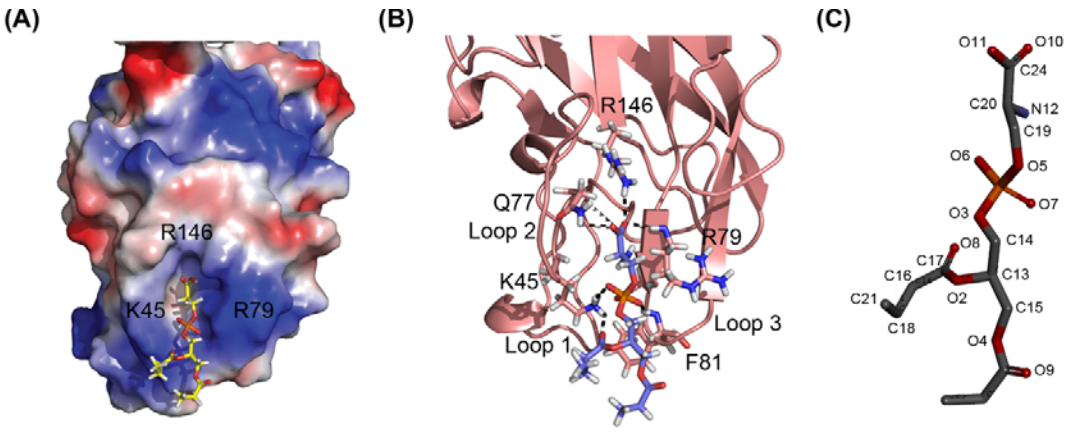

Figure 21. Docking analysis of MFG-E8 C2 domain binding with PS
(A) Electrostatic potential map of the C2 domain. The well-organized positive charges were important in driving the docking of PS head group into the loop regions of the C2 domain. C2 is shown as surface representation whereas PS is shown in stick representation. **(B)** Binding orientation of serine-carboxyl head group at the loops 2-3 regions. **(C)** Structure of PS ligand used in docking study

A more detailed docking result revealed that there are several hydrogen bonding contacts formed between C2 domain and bound PS (Figure 21B,C). Mainly, Gln77 and Arg146 formed weak salt bridge interaction through serine-carboxyl head group on PS (O10, O11 atoms). In addition, the main chain amide atoms of Arg79 are also engaging the head group of PS through hydrogen bonding. The interaction between the side chain amide atoms of Lys45 and Phe81 residues, which located at the tips of loop 2 and 3, and the

phosphoryl oxygen on PS (O6 and O7) further stabilized the PS binding. The side chain amide atoms of Lys45 interact with one of the carbonyl group on the acyl chains of PS (O8). In addition, the solvent-exposed residues such as Trp26 and Phe81 (loop 1, 3) also formed hydrophobic interactions with the acyl tails of PS. The list of simulated hydrogen bonding contacts between MFG-E8 C2 domain and PS molecule were shown in Table 2 below. Residues such as Trp33, Gln 43, Lys45, Asn47, Ala78, Arg79, Asp80, Phe81, G82, and Arg150 within a 5 Å region around the PS were also involved in non-bonding contacts

Table 2. Hydrogen bonding contact list for MFG-E8 C2 domain with PS obtained from molecular docking

PS Atoms	Hydrogen bonding contacts	
	C2 Residues	Distance (Å)
O10	R146 side chain NH atoms	2.69
O10	R79 main chain NH atoms	2.42
O11	Q77 side chain NH atoms	2.46
N12	R79 of main chain NH atoms	2.38
O6	K45 side chain NH atoms	2.46
H23	D80 side chain COOH atoms	1.98
O7	D80 side chain COOH atoms	2.83
O7	F81 main chain NH atoms	2.59
O7	G82 main chain NH atoms	2.5
O8	K45 side chain NH atoms	2.51

3.5 Electrostatic interaction is critical for PS binding

As shown in the 2D HSQC titration and *in silico* docking results, loop regions are the main region participating in the binding with PS, and possibly constructing the binding site. Those conserved residues located in these loops were therefore of greater interest to us. Being in the region with less contribution in structural feature maintenance, the conservation of these residues indicated their importance in binding functions of the protein. And those residues simulated to form hydrogen bond contacts were also believed to be the important ones. Combining these findings, it is worthwhile to test *in vitro* and *in vivo* on whether these residues really participated in the PS-binding event, and how they are functioning in the binding. Thus, different mutants were made through site-directed mutagenesis described in the Method Section. The positively charged residues Lys24, Lys45, Arg79 and Arg146 were selected to be mutated into neutral amino acids asparagine and glutamine respectively to change the electrostatic profile of the binding site. Mutations on these residues were supposed to disrupt the electrostatic potentials and theoretically decrease the binding affinity of C2 domain towards PS.

As described in method section, these mutants were made from site-directed mutagenesis based on the template of pET29b-MFG-E8 C2 wild type, and were sequenced, expressed and purified. Figure 22 summarized the purification of these proteins using affinity column. The structural statuses were examined using 1D 1H NMR spectroscopy. The overlay is shown below (Figure 23). There is no significant difference of the mutants spectra compared to the wild type spectrum, suggesting the maintenance of the proper folding of the mutants. Thus, the mutants were believed to be suitable for functional comparisons.

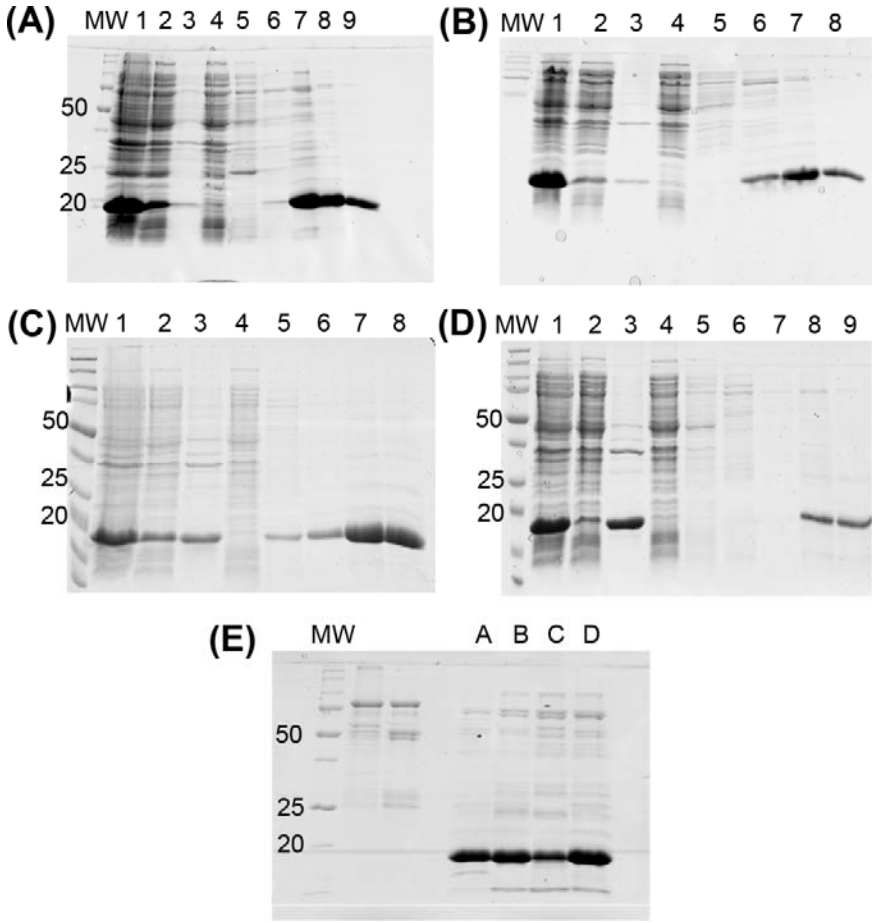

Figure 22. Purification of MFG-E8 C2 domain mutants for the positive-charged residues using affinity column

Plasmids containing MFG-E8 C2 domain mutants were transformed into *E. coli* and expressed by IPTG induction. The collected cells were lysed by sonication and centrifuged to remove cell debris. The supernatants were purified using affinity column (Ni^{2+}-NTA) and fractions were analyzed using SDS-PAGE: **(A)** K24N, **(B)** K45N, **(C)** R79Q, **(D)** R146Q, **(E)** All mutant samples concentrates before ^{31}P NMR experiments. (**MW**: molecular weight standards, unit: kilo Dalton (kDa); **Lane 1**: total lysate; **Lane 2**: supernatant; **Lane 3**: pellet; **Lane 4**: Flow through; **Lane 5**: wash; **Lane 6 to 8 or 9**: elution fractions)

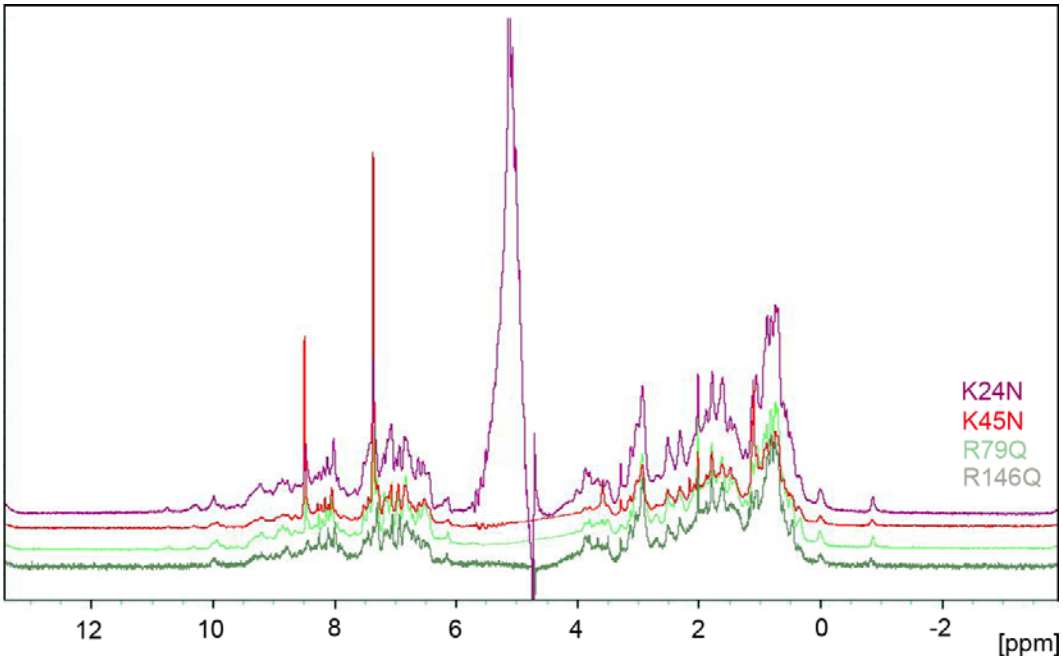

Figure 23. 1D ^{1}H NMR spectra overlay of C2 domain mutants.
1D 1H NMR spectra were collected as mentioned in M&M section for the 4 mutants on positively charged residues. Comparison using spectra overlay showed no significant differences between spectra, suggesting structural maintenance after mutagenesis. Peaks were colored as suggested by the legend. K24N, magenta; K45N, red; R79Q, light green; and R146Q, dark green.

As discussed in the introduction section, a number of methods and techniques are applicable in the study of protein-lipid interaction. Among these methods, NMR spectroscopy has the advantages like high resolution, versatility in detectable parameters, and being able to study interaction dynamics in close-to-reality scenario, etc. Moreover, since we have previously shown that MFG-E8 C2 domain preferentially binds to PS over PC using 1D ^{31}P-NMR spectroscopy (Reddy et al., 2007). To be consistent, 1D ^{31}P-NMR titration experiments were carried out to test the PS-binding activities of the different mutant C2 domains according to the method described in the method section.

^{31}P NMR experiments measures the chemical shift of phosphorus atoms in the solution. Since the protein is produced in bacteria without post-translational modifications, only phosphate buffer and phosphatidylserine have phosphorus atoms. So in free PS solution,

two peaks were observed as shown in Figure 24, WT panel bottom spectrum. A large central peak corresponding to the phosphorus atoms in phosphate buffer was manually centered at 0 ppm. A small peak corresponding to phosphorus atom in the phosphate backbone of PS in free-state was located at about -1.35 ppm. When WT C2 domain or its mutants were titrated into PS solution. C2-PS binding happens in solution, leading to local environment change at the phosphorus atoms in PS, resulting in changes of the detected peaks. Shown in Figure 24 WT panel, when wild type C2 domain was titrated, the original small peak remained and a new small peak corresponding to the C2 bound-state appeared at around -1.06 ppm, suggesting a strong binding of C2 with PS in slow-exchange regime. The original free-state peak and new bound-state peak were both showing chemical shift perturbations in response to C2 domain concentration increase. Whereas in mutant experiments (K24N, K45N, R79Q & R146Q) (Figure 24, right panels), neither new peaks appeared, nor chemical shift perturbation was observed. Instead, the peaks corresponding to the free-state were showing line-broadening and disappearing with the increase of C2 domain concentration, suggesting weaker binding between C2 mutants and PS in intermediate-exchange regime. Therefore, binding affinities of the mutants were lower than the wild type C2 domain, indicating the participation of these positively charged residues in the binding.

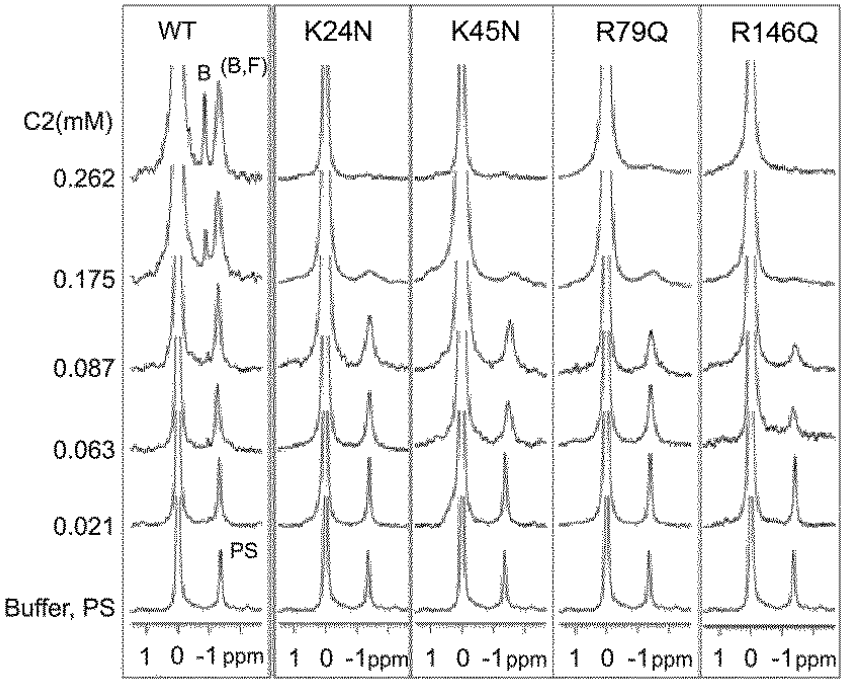

Figure 24. ^{31}P NMR spectrum of wild type or mutant C2 domain titration into PS

PS titration into different constructs of C2 domains (wild type or point mutants K24N, K45N, R79Q, R146Q) were observed on ^{31}P NMR spectra recorded on an Avance 400 MHz NMR spectrometer. Stacked plot gives the ^{31}P-NMR spectra of phosphate buffer (0 ppm), bound-state of PS (-1.06 ppm), and free-state of PS (-1.35 ppm).

As mentioned above, the wild type C2 domain and its mutants were binding with PS in different regimes. The dissociation constants (K_d) values was calculated differently based on the method described in our previous paper (Reddy et al., 2007). For wild type C2 domain, the chemical shift data of the appearing peak was plotted against protein concentrations (Figure 25A). For the mutants, the line-width at half height data was plotted against protein concentrations (Figure 25 B to E). Using one-site binding equation: K_d = [E] [L]/[EL], non-linear least square fitting was carried out on the plotted graphs to calculate the K_d values for each protein. The equation represents a dynamic equilibrium involving free protein [E], free lipid [L] and the protein–lipid complex [EL].

Table 3 summarized the K_d values calculated. There were 30- to 50-fold differences between K_d values of the mutants and that of the wild type C2. These values were indicating that the mutations on these selected positively charged residues reduced the binding affinity from C2 domain towards PS.

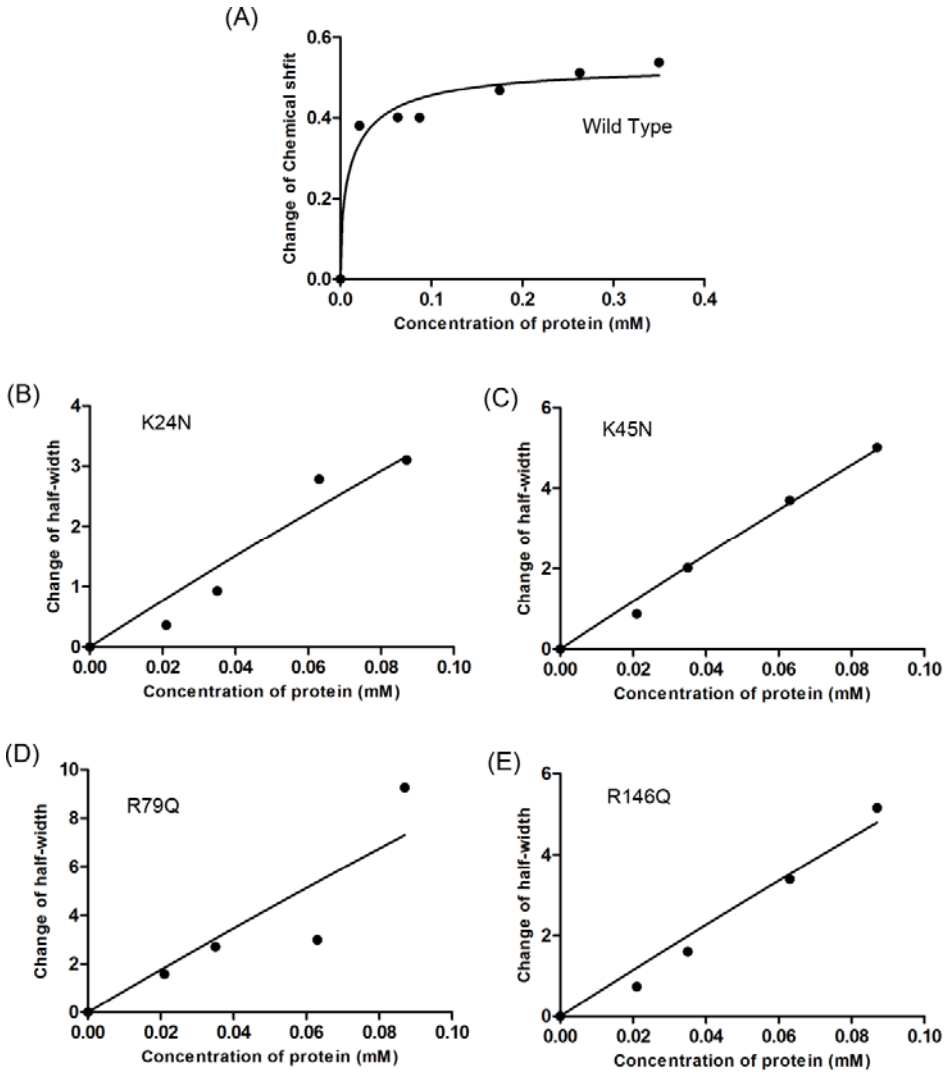

Figure 25. Curve Fitting for the calculation of K_d from ^{31}P NMR Titrations
Either chemical shift perturbation (A: wild type) or changes of half-width (B to E: mutants) were plotted against protein concentration. Non-linear least square regression analysis was carried out to calculate the K_d value for each mutant. **(A)** wild type C2 domain; **(B)** K24N; **(C)** K45N; **(D)** R79Q; **(E)** R146Q.

Table 3. The dissociation constants (K_d) of C2 domain wild type and mutants for the PS

C2	K_d (μM)
Wild Type	19 ± 0.07
K24 N	670 ± 30
K45 N	1400 ± 70
R79 Q	1030 ± 50
R146Q	1220 ± 60

3.6 C2 domain binds to PS-exposed apoptotic cells

Our previous results demonstrated the function of MFG-E8 C2 domain binding with PS molecule in solution. In order to evaluate the role of MFG-E8 C2 domain in PS-exposed cellular apoptosis event in a more biological relevant scenario, *in vitro* binding with PS-exposing apoptotic cells by C2 domain was detected by FACS analysis. An enhanced green fluorescence protein (EGFP) -tagged C2 domain was expressed and purified. After exposure to 100 μM etoposide for 24 h to induce apoptosis, HeLa cells were incubated with the fusion protein. As controls, etoposide-treated cells were also incubated with Annexin V-FLUOS and propidium iodide (PI). Annexin V-FLUOS was a modified Annexin V protein with a green fluorescence tag, FLUOS, linked at its N-terminal. It bound to surface exposed PS in high affinity, and detected the cells undergoing apoptosis with intact plasma membrane, thus was used as a positive control. PI was a red fluorescent DNA intercalating agent that bound to the nucleus only when membrane integrity was compromised, i.e. in necrosis or very late stage of apoptosis. In all samples,

co-staining with PI together with EGFP-C2 or Annexin V-FLUOS was made for the differentiation of apoptosis from necrosis.

Based on the status of the cell, different amount of the dyes would bind to the cell, leaving different fluorescence signal intensities on the cell. FACS machine employed a capillary mechanics to allow single cell detection of both the red and green fluorescence signal intensities. Pre-determined number of cells from each sample were tested and results were recorded. The processed data was used to generate dot plot diagrams with each dot representing a single cell. The horizontal axis represented the green fluorescence signal intensity and the vertical axis represented the red fluorescence signal intensity. During the data processing of the FACS results, 'gates' were created to facilitate data analysis. A 'gate' is a set of variable limits or boundaries to isolate specific population of cytometric events from the large general population. It can be created by drawing a series of data points in the diagrams using the computer software. Gates can be used to isolate target events, or discriminate different event populations for analytical purposes. Graphically, it could be either geometrics in the dot plots, i.e. the 4 quadrants separated by the two lines as shown in Figure 26A left panel, and the circles labeled 'R1' 'R2' 'R3' as shown in Figure 34A, or bars covering ranges in the x-axis in histograms as shown in Figure 26A right panel.

The dot plot diagrams were divided into four quadrants based on the location of the un-induced cells in the negative control sample, accommodating most of these dots within the left lower quadrant (LL), as shown in Figure 26A. In this way, the healthy cells would be located within the LL quadrant; the apoptotic and non-necrotic cells would fall inside right lower quadrant (RL), and the necrotic cells would be found within the right upper

quadrant (RU). The percentage of cells fallen within the RL quadrant was used to evaluate the binding affinity of C2 domain towards exposed PS in apoptotic cells. The same quadrant position was maintained throughout the whole experiments. All the experiments were done at least 3 times, and the numbers were shown in the form of mean ± standard deviation calculated.

As shown in Figure 26, after apoptosis induction with etoposide, increased amount of PS was detected, as stained by Annexin V-FLUOS. Cells stained positive for Annexin V but negative for PI was measured to approximately 28.9 ± 4.9 % in apoptotic condition (Figure 26A, top panel, RL quadrant), while cells stained positive for both annexin V and PI staining were measured to be 11.4 ± 2.3 % (RU quadrant). In the same experimental conditions, the C2 domain was also shown to bind apoptotic cells. Cells stained positive for C2 domain staining but negative for PI were measured to be about 23.3 ± 3.1 % (Figure 26A, bottom panel, RL quadrant), and cells stained with C2 domain and PI were measured to be 9.8 ± 2.4 % (RU quadrant). In the control and non-apoptotic cells, which were not stained with any fluorescence dyes, cells fall within RL quadrant were measured to be 2.3 ± 0.4 %. Collectively, these results demonstrated that MFG-E8 C2 domain could bind efficiently to PS-exposed apoptotic cells.

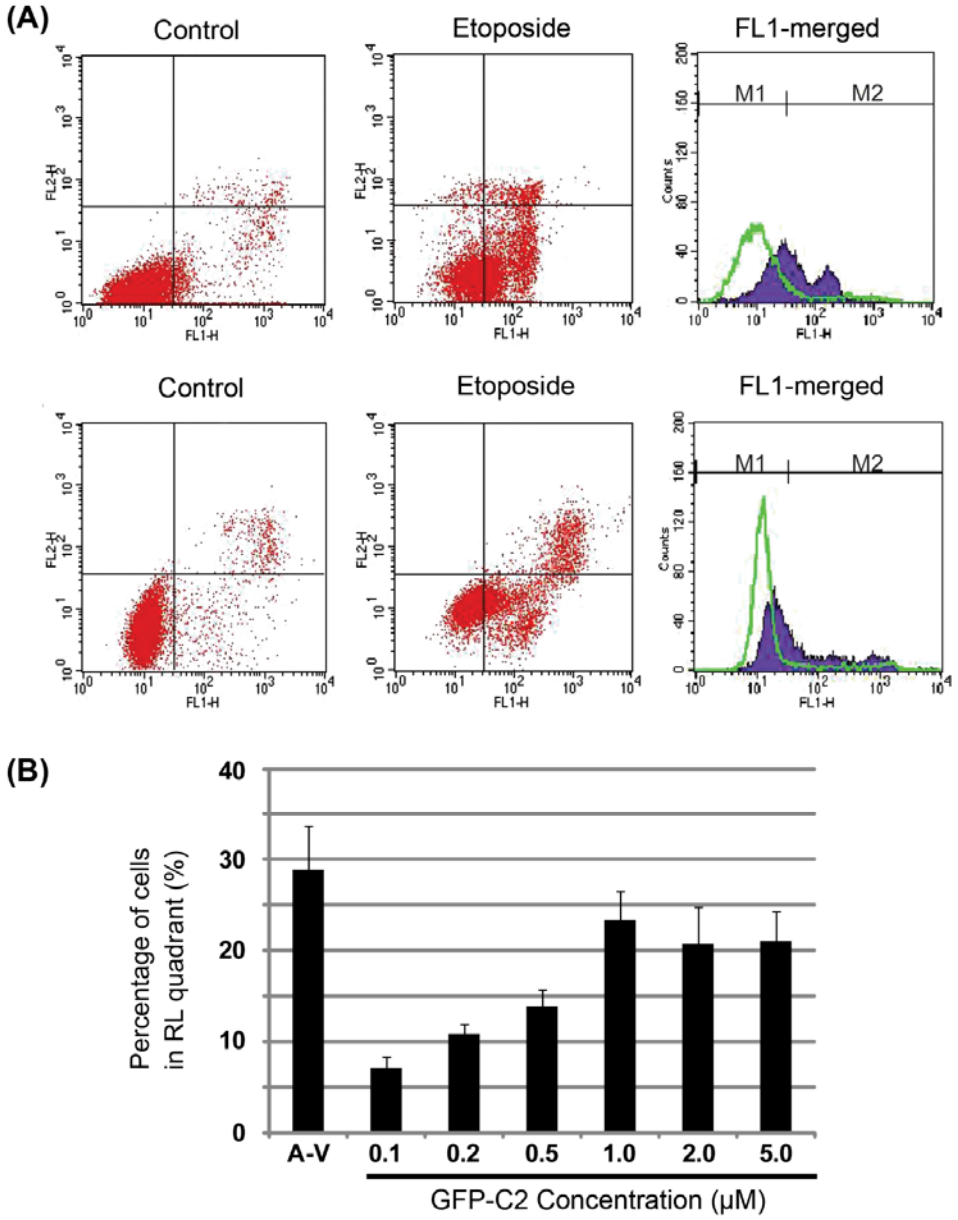

Figure 26. Binding of C2 domain to PS on the outer membrane of apoptotic cells

(A) HeLa cells exposed to 100 μM etoposide for 24 h, were incubated with either annexin V (top panel) or 1 μM EGFP-tagged wild type C2 domain (bottom panel), together with PI, and analyzed by FACS. Non-treated cells were used as negative controls in both conditions. Untreated cells were shown in green, and apoptotic cells are shown in purple. The gates marking the untreated population (M1 and M2) were placed as depicted in the each panel to aid the calculation. **(B)** Percentage of cells in the RL quadrant was calculated. Results are shown in the format of mean ± SE value from triplicate experiments. **A-V**, annexin V positive control cells.

Annexin V used in this study was from the commercial apoptosis detection kit, and used under the instruction of manufacturer's protocol. The used of Annexin V was to be a positive control to examine the feasibility of the testing system and provide a measurement of the real extend of apoptosis happening using a well established detection tool. Same procedures were performed in every Annexin V preparation to ensure exact concentration of Annexin V was used in each experiment, but the exact number of its concentration was not stated in the manual, nor tested by ourselves, and thus unknown in our experiment.

To further test binding characteristics of the binding between C2 domain and PS-exposed apoptotic cells, HeLa cells were firstly induced apoptosis by etoposide, followed by incubation with increasing concentrations of the C2 domain (0.1 – 5.0 μM). FACS analysis was performed on each sample. From the results, the amount of C2 domain bound with the PS-exposed apoptotic cells increased in a concentration-dependent manner, at the concentration of 1 μM and higher, the binding saturated (Figure 26B). Among all the cells tested, cells showing annexin V positive and PI negative staining were approximately 28.9 ± 4.9 % in apoptosis-inducing conditions. Cells showing C2 domain positive and PI negative staining were approximately 23.3 ± 3.1 %. These results suggested that the binding affinity of C2 domain towards PS-exposed cells was about 80% of the affinity of annexin V.

3.7 Positively charged residues in the C2 domain are involved in the binding to PS-exposed apoptotic cells

To evaluate the participations and functions of those positively charged residues in MFG-E8 C2 domain in the binding event towards PS-exposed apoptotic cells, we chose two lysine residues, Lys24 and Lys45, and mutated them into asparagines to change their electrostatic properties, and tested using the same experimental conditions including exposure durations, concentrations and FACS setup and procedures described above as compared to wild type protein. Before apoptosis induction, over 90% of cells were found within the LL quadrant (negative stain for both fluorescence dyes). After apoptosis induction using etoposide, the percentage of cells not bound to C2 wild type was 56.2 ± 0.4 %. When the wild type protein were substituted with the two single mutations, K24N and K45N, the percentage changed to 64.8 ± 1.7 % and 83.2 ± 0.9 %, respectively, suggesting the disruption of the binding event between C2 and apoptotic cells by these single mutations (Figure 27A, B). Especially when the K24N/K45N double mutant was tested, nearly no cell exhibited association with C2 domain, and nearly 95.7 ± 1.2 % of the cells were located in M1 (Figure 27B). From the dot plots, the population of double mutant positive and PI positive cells (RL quadrant) was shifted as compared with the case of the C2 wild type (Figure 27A), demonstrating a dramatic disruption of the binding. This trend of decreasing binding affinity towards PS provided added support to the conclusions made from the elevated K_d values of Lysine mutants against PS that these positively charged residues were critical in the recognition and association of the PS-exposed apoptotic cells.

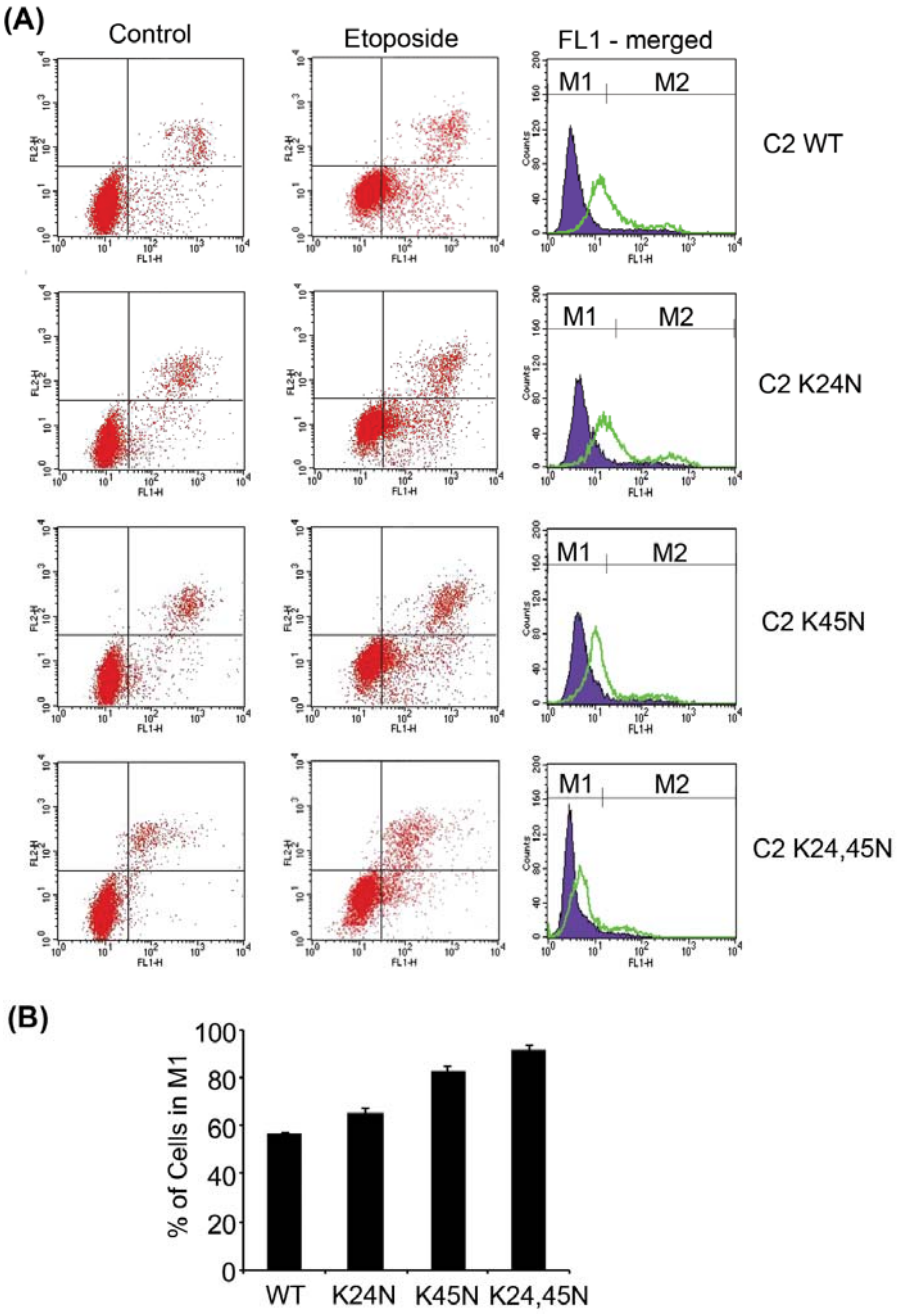

Figure 27. Positively charged residues in C2 domain are involved in the binding to PS-exposed apoptotic cells

(A) Etoposide induced HeLa cells were exposed to either 1 μM of EGFP-tagged C2 domain wild type, K24N, K45N, or K24N/K45N together with PI, and analyzed by FACS. Untreated cells were shown in purple, and apoptotic cells are shown in green. The gates marking the untreated population (M1 and M2) were placed as depicted in the each panel to aid the calculation. **(B)** Percentage of cells in the gated region of M1 was calculated as compared with each control. Results are shown in the format of mean ± SE value from triplicate experiments.

3.8 Hydrophobic residues in loop regions of the C2 domain contribute to the binding towards PS-exposed apoptotic cells

In the loop regions of C2 domain, it was noticed that several hydrophobic residues were identified through our computational modeling studies. To check their involvement in the binding event, two aromatic residues, Trp26 and Phe81, were selected to be mutated into alanines. The mutant proteins were tested on their binding towards PS-exposed cells by flow cytometer. The expression and purification of gst-EGFP-MFGE8 C2 mutants were shown in Figure 28.

The effect on binding to apoptotic cells from the single mutants W26A and F81A was comparatively similar to that of the wild type protein (Figure 29A). W26A showed 67.4 ± 2.5 %, and F81A showed 73.4 ± 2.1 % of cells not bound to any protein (gate M1) (Figure 29B). Compared to 71.8 ± 1.9 % measured from wild type C2 domain, there was not any significant differences. However, in the experiment on the double mutant W26A/F81A, cells in the M1 gate were measured to 83.1 ± 1.5 %, showing clear disruption of the binding event, and proved the participation of these two aromatic residues in the binding to PS-exposed apoptotic cells (Figure 29).

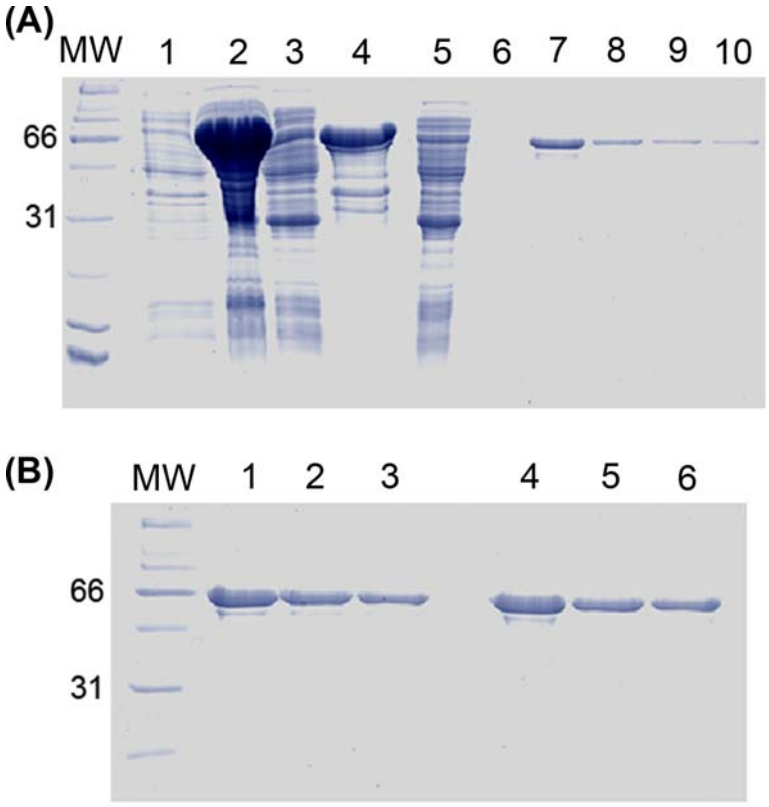

Figure 28. Purifications of gst-EGFP-MFGE8 C2 wild type and mutants using affinity column
Gst-EFGP-MFG-E8 C2 domain was expressed in *E. coli*. Supernatant of the cell lysate was purified using affinity column (glutathione-sepharose beads). **(A)** SDS-PAGE analysis of the purification fractions of gst-EGFP-MFGE8 C2 wild type protein. **(B)** Elution fractions of the two single mutants. (**MW**: molecular weight standards, unit: kilo Dalton (kDa); **(A) Lane 1**: before IPTG induction; **Lane 2**: total lysate; **Lane 3**: supernatant; **Lane 4**: pellet; **Lane 5**: flow through; **Lane 6**: wash. **(B) Lane 1 to 3**: F81A elutions fractions**; Lane 4 to 6**: W26A elution fractions)

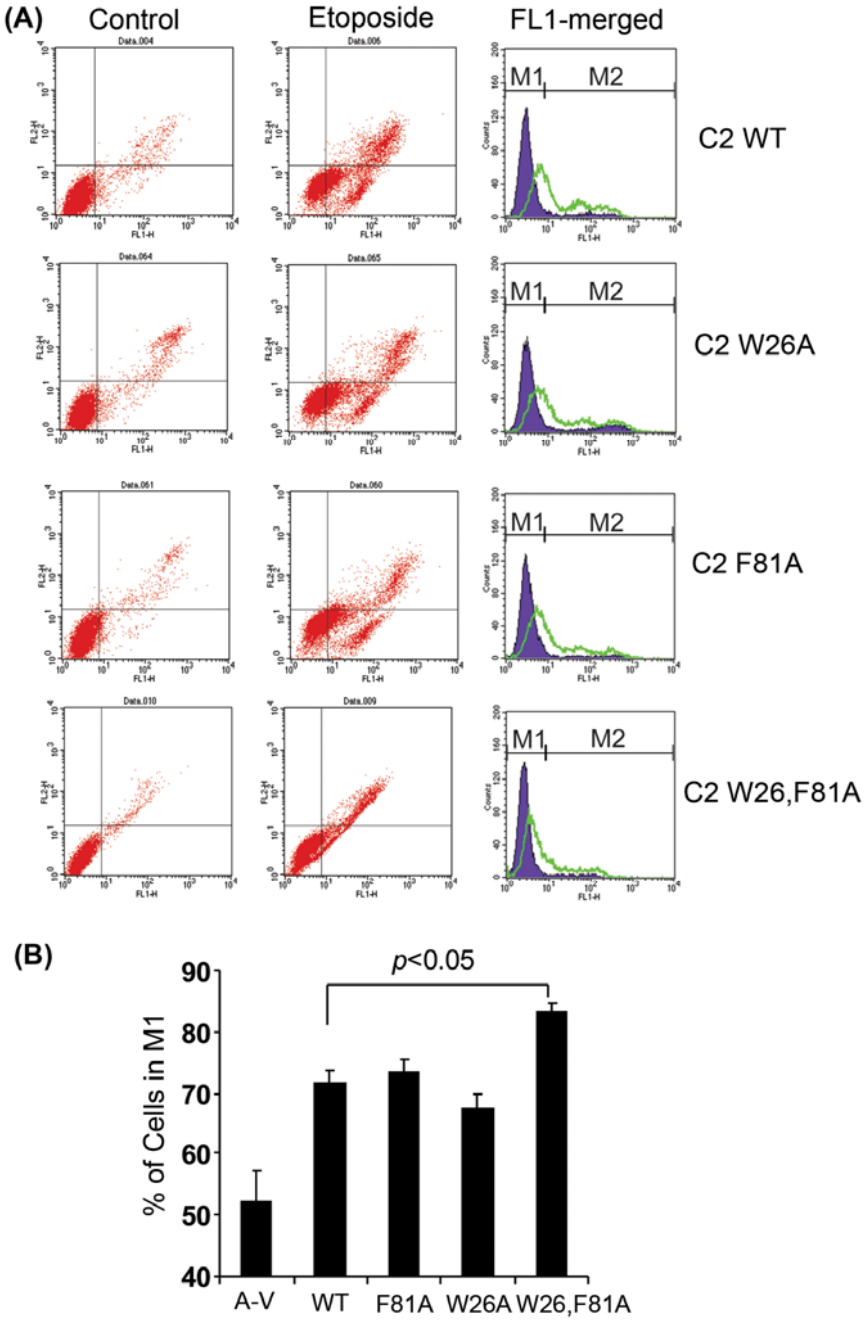

Figure 29. Hydrophobic residues in the binding loop of C2 domain contribute to the binding to PS-exposed apoptotic cells

(A) Etoposide induced HeLa cells were exposed to either 1 μM EGFP-tagged C2 domain wild type, W26A, F81A, or W26/F81A, and analyzed by FACS. Untreated cells were shown in purple, and apoptotic cells are shown in green. The gates marking the untreated population (M1 and M2) were placed as depicted in the each panel to aid the calculation. **(B)** Percentage of cells in the gated region of M1 was calculated as compared with each control. Results are shown in the format of mean ± SE value from triplicate experiments.

3.9 Subcloning, Expression and Purification of gst-EGFP-MFGE8L C1C2 domain

From the pET29b MFGE8L wild type plasmid, the C1C2 domain was obtained by PCR and subcloned into the pGEX 4T-1 vector that re-incorporated the EGFP sequence. The ligation product was then confirmed by sequencing and expressed in *E. coli* system. As shown in Figure 30, the protein was eluted with contaminants from the affinity column and thus passed through a size-exclusion column for further purification. Then final sample was buffer exchanged to 50 mM Tris pH 6.5, 150 mM NaCl, and adjusted to about 50 μM for the following FACS analysis.

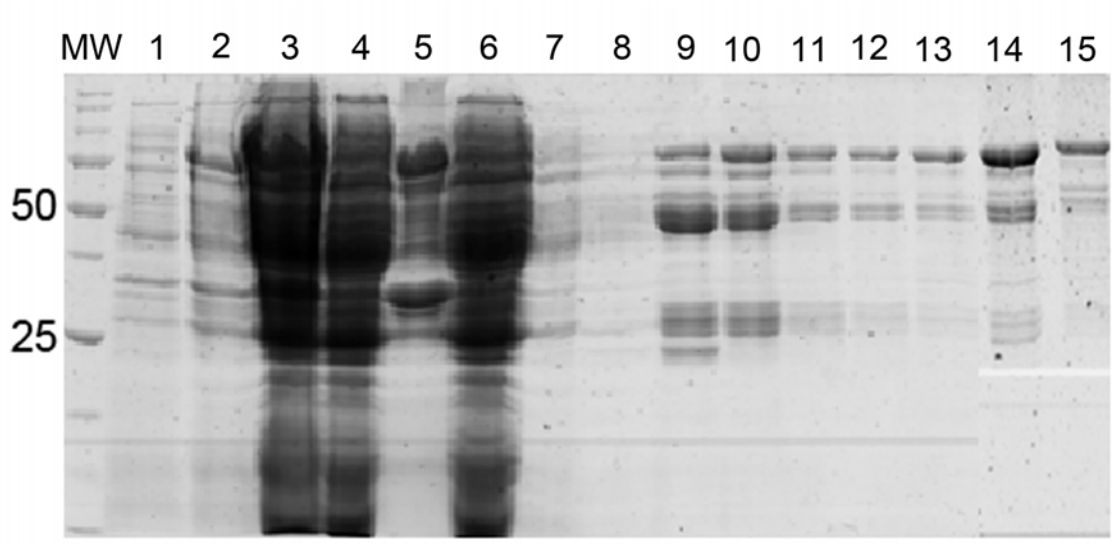

Figure 30. Purification of gst-GFP-MFGE8 C1C2 using affinity column
pGEX 4T-1 MFGE8L mouse C1-C2 domain were expressed and purified using affinity column (Ni^{2+}-NTA) as described in Method section. Size-exclusion column (Sephacryl Superdex-200) was used to further purify the elution fractions and later concentrated to about 50 μM stock concentration. Purification fractions were analyzed using SDS-PAGE and visualized by coomassie blue staining. (**MW**: molecular weight standards, unit: kilo Dalton (kDa); **Lane 1**: before IPTG induction; **Lane 2 & 3**: total lysate; **Lane 4**: supernatant; **Lane 5**: pellet; **Lane 6**: flow through; **Lane 7**: 50 mM imidazole wash; **Lane 8**: 100 mM imidazole wash; **Lane 9 to 13**: Elution fractions; **Lane 14**: Loading sample for size-exclusion column; **Lane 15**: elution concentrate after size-exclusion column)

3.10 C1 domain enhance the binding of MFGE8 C2 domain with PS

HeLa cells were treated with 100 µM Etoposide for 24h, and incubated with gst-GFP-C1C2 and Annexin V after harvest. As shown in Figure 31, the C1 domain did enhance the binding of C2 domain with PS, but only to a limited extent. Comparing with the C2 domain result shown in Figure 26, the extent of the green fluorescence signal shift increased. And about 300 nM C1C2 domain displayed about the same extent of that of C2 domain alone. This result confirmed that C1 domain also contribute to the binding process, but probably only in a supportive manner.

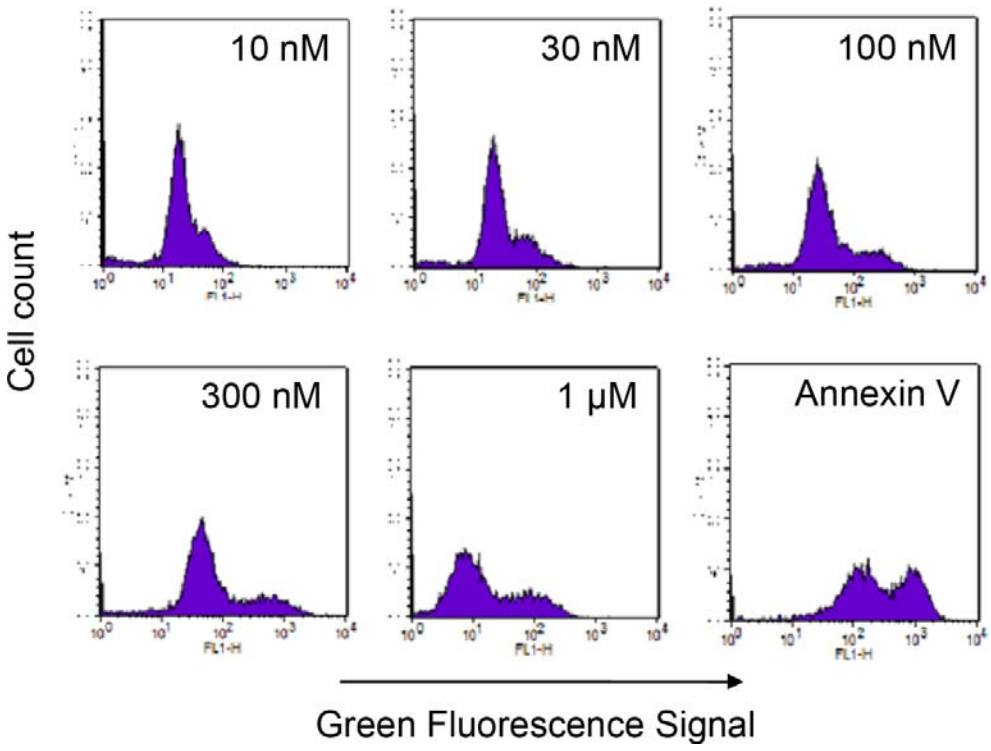

Figure 31. FACS analysis of gst-GFP-MFGE8 C1C2 domain
HeLa cells were treated with 100 µM Etoposide for 24 hours, and incubated with the purified protein and Annexin V after harvest. The x axis represent the green fluorescence signal detected from the scanned cells. With the increase of C1C2 domain concentration, the number of cells with enhanced green fluorescence signal increased, but only in a similar extend as that of C2 domain alone.

3.11 Subcloning, expression and purification of SUMO-MFG-E8 C1C2

Previous PS-exposed cell binding test using gst-GFP-MFGE8 C1C2 provided some information on the function of C1 domain in the PS-binding process. However, the result was not so promising, possibly due to the large gst-GFP tags which might influence the proper folding and functioning of the protein. Therefore, a new method was developed making use of labeling on the cells instead of the proteins for the FACS visualization and much smaller SUMO tag for the protein solubilization.

Based on the template of MFG-E8 full-length plasmid, C1C2 domain (Cys148-Cys463) was amplified using designed primers and inserted into pET-SUMO vector. The sequencing approved plasmid of pSUMO-MFGE8 C1C2 was then transformed into BL21 (DE3) cells and expressed as mentioned in the method section.

Figure 32 shows the affinity column procedures and the SDS-PAGE image of the purification process. This protein was only soluble in relatively high pH, and high salt condition (data not shown). Therefore, pH 8.2 and 500 mM NaCl was maintained throughout the purification. The fractions after HisTrap affinity column were collected, concentrated and further purified using size-exclusion column. The final protein was in buffer containing 20 mM Tris, pH 8.2, 500 mM NaCl, 5 mM TCEP (Figure 33).

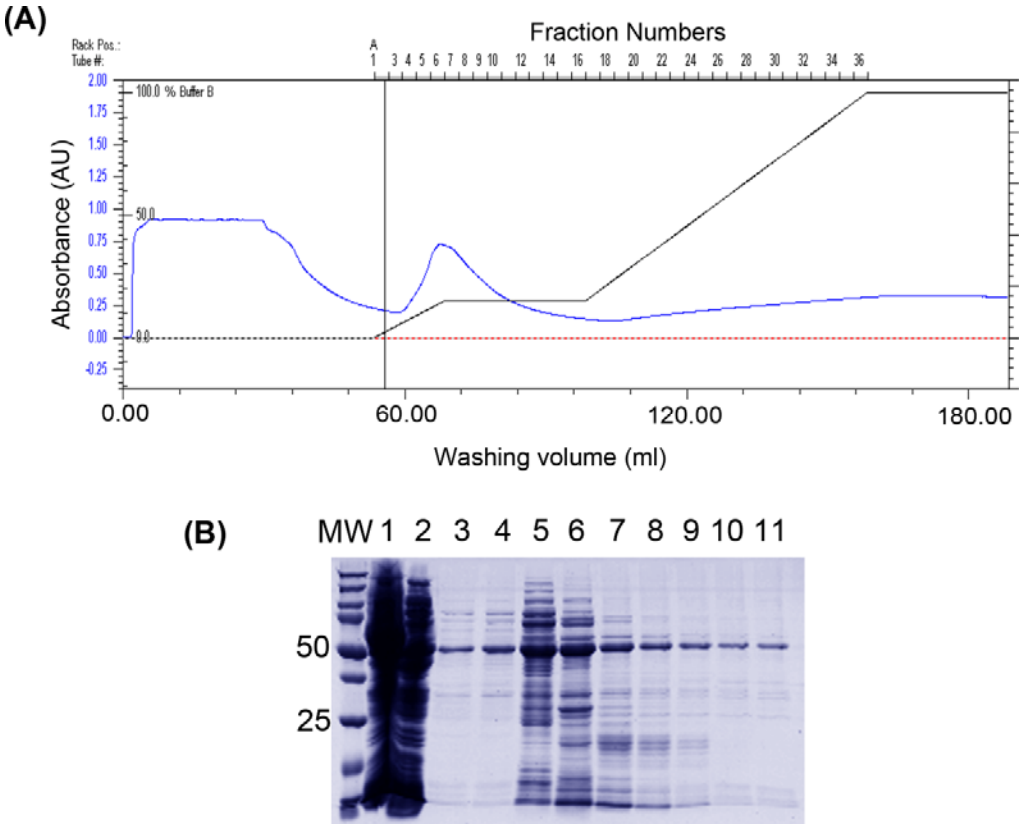

Figure 32. Purification of SUMO-MFGE8 C1C2 using affinity column
SUMO-MFGE8 C1C2 domain was expressed in *E. coli*. Supernatant of the cell lysate was purified by affinity chromatography (Histrap column) using an automated HPLC machine. The purification fractions were analyzed by SDS-PAGE and visualized by coomassie blue staining. **(A)** Affinity column result. Blue line is the absorbance reading, black line is the percentage of elution buffer. **(B)** SDS-PAGE analysis of the different fractions of affinity column purification. (**MW**: molecular weight standards, unit: kilo Dalton (kDa); **Lane 1**: total lysate; **Lane 2**: supernatant; **Lane 3 to 11**: Selected Histrap column fractions)

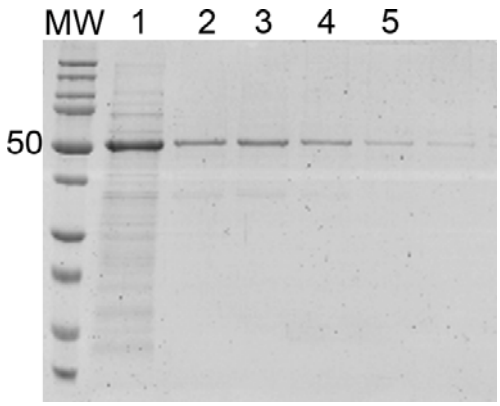

Figure 33. Purification of SUMO-MFGE8 C1C2 using size-exclusion column
Elution fractions from affinity column were combined and further purified using size-exclusion column (Sephacryl Superdex-200). The loading sample and elution fractions of peak around 40 ml were analyzed using SDS-PAGE and visualized by coomassie blue staining. (**MW**: molecular weight standards, unit: kilo Dalton (kDa); **Lane 1**: loading sample; **Lane 2 to 5**: size-exclusion column fractions from 35 ml to 45 ml)

3.12 Co-culture FACS analysis

To mimic the immune-scavenging event in human body, we designed a testing system making use of fluorescence labeling on the cell rather than on proteins for the FACS visualization. Two different cell lines were chosen. One is THP-1 cells, which is human acute monocytic leukemia cell line, the other one is Jurkat cells, which is the immortalized line of T lymphocyte cells. As a monocyte, THP-1 cells were able to express and secret endogenous opsonins including MFG-E8, and were phagocytic towards apoptotic Jurkat cell.

In order to monitor this process, these two cell lines were labeled with different commercial fluorescence dyes. THP-1 cells were labeled with red fluorescence using CellTracker™ Red CMTPX, thus give strong signal in FL2 channel (vertical axis). Jurkat cells were labeled with green fluorescence using CellTracker™ Green CMFDA, and showed high readings in the FL1 channel (horizontal axis) in FACS analysis. When these

two cell lines were mixed together and co-cultured, the cells could be well differentiated from each other in the two fluorescence channels in FACS analysis (Figure 34B).

Following the manufacturer's protocol, both cell lines were first labeled with the corresponding fluorescence dyes respectively, and allowed 24 h recovery. Jurkat cells were then treated with 100 uM Etoposide at normal growth condition to induce apoptosis, and THP-1 cells were grown at the same condition without any treatment. After 24 hours, both cell lines were harvested and resuspended using PBS. Then they were mixed together at equal cell number, and incubated for 30 mins at normal growth condition before FACS anaylsis using the BD FACSCalibur. Figure 34 shows the FACS results of the system testing trial.

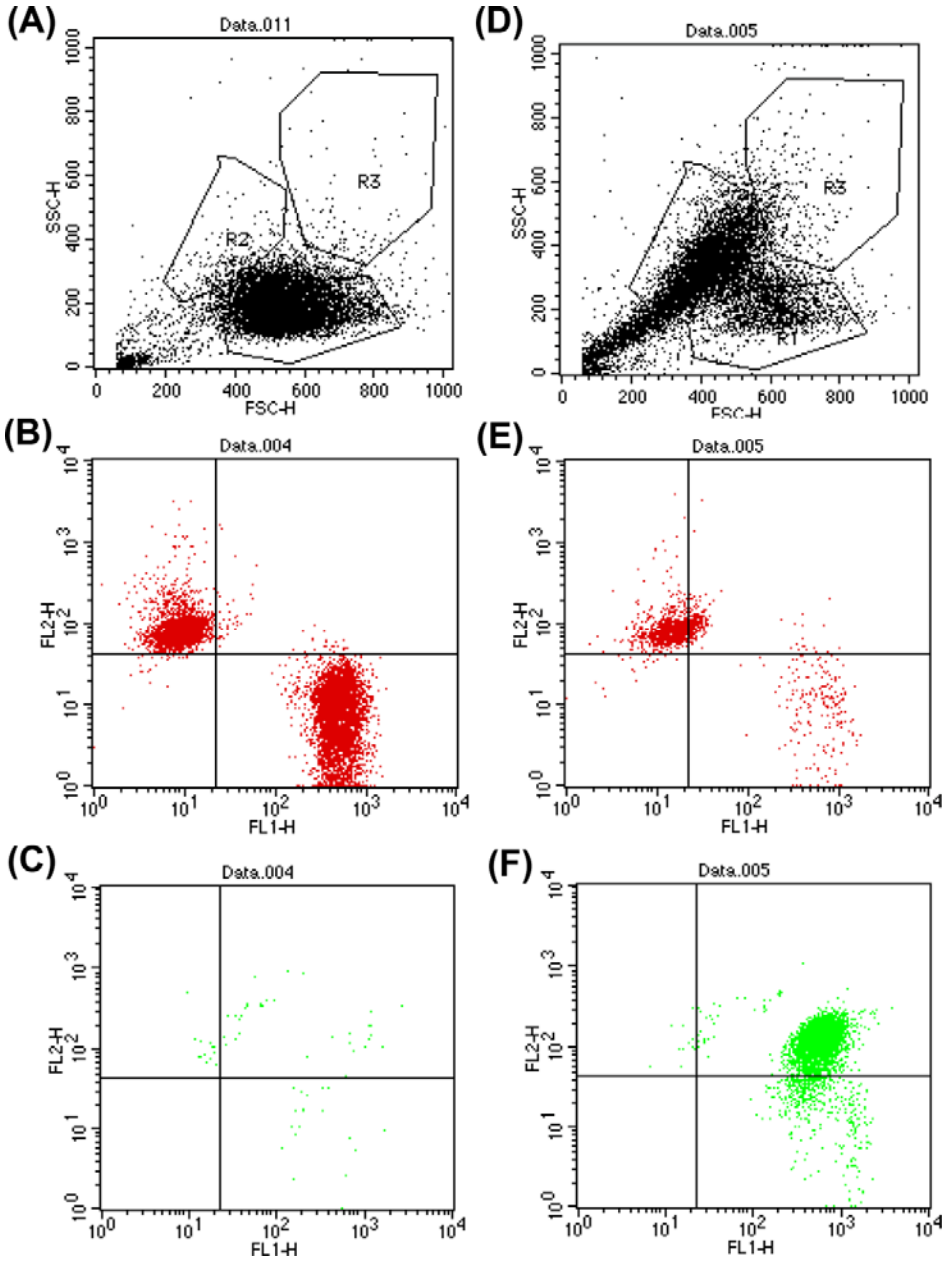

Figure 34. Co-culture FACS analysis test
Co-culture FACS system were tested using labeled THP-1 and Jurkat cells. Cells were labeled by different fluorescence dye individually. Jurkat cells were treated or not treated with 100 uM etoposide to have comparisons. After 24 h incubation, two cells were mixed together and analyzed using BD FACSCalibur machine. **(A-C)** negative control, in which the Jurkat cells were not induced apoptosis. **(B)** Cells from gate R1, **(C)** Cells from gate R2. **(D to F)** induced group, in which the Jurkat cells were induced apoptosis by 100 uM Etoposide for 24 h. (E) Cells from gate R1, **(F)** Cells from gate R2. (**FSC**: forward-scattering signal; **SSC**: side-scattering signal; **FL1**: Green fluorescence signal; **FL2**: Red fluorescence signal)

The left column of Figure 34 (A to C) shows the negative control that the Jurkat cells were not induced apoptosis. The right column (D to F) was the induced group. The circle lines in Figure 34 A and D were different gates, and only the particle falls within it were analyzed further. Figure 34 B and E represent the particles from gate 1 (R1), which is the lowest gate, of A and D respectively. And Figure 34 C and F represent the particles from gate 2 (R2), which is the left gate, of A and D respectively.

When Jurkat cells were not induced apoptosis (Figure 34A), both cell lines have similar morphological characteristics. Therefore most particles fall inside gate 1, and were analyzed in Figure 34B. And when no apoptosis induced, THP-1 cells were not interacting with Jurkat cells, thus the two populations were clearly separated from each other in the fluorescence channels: Jurkat cells only have green fluorescence label and fall inside the right lower quadrant (RL); THP-1 cells only have red fluorescence label and thus fall inside the left upper quadrant (LU).

When Jurkat cells were treated with etoposide and induced apoptosis, the jurkat cells became nuclear-condensed and fragmented, and showed cellular shrinkage and PS-exposure. These apoptotic cells were then taken up by THP-1 cells, leading to changes in side-scattering signal (SSC) and forward-scattering signal (FSC). Thus these cells migrated from gate 1 to gate 2, and were analyzed in Figure 34F. Each dot in this diagram actually represented the binding particle of THP-1 with Jurkat cell, or the THP-1 cell that already engulfed the dying Jurkat cell. Therefore, these binding/engulfing THP-1 cells possessed both green and red fluorescence signal, and were located in the right upper quadrant (RU) of the fluorescence plot (Figure 34F).

3.13 Co-culture FACS analysis of MFG-E8 domains

As described in the Introduction section, C2 domain can only recognize the exposed PS on the apoptotic cells. The absence of the EGF domains prevents it from binding with integrin on the phagocyte. Thus, C2 domain alone cannot function as opsonin to facilitate the phagocytosis. And its binding will compete with the endogenous opsonins, mask the "eat-me" signal and thus prevent phagocytosis. C1C2 domain would have a similar effect. As such, we decided to use the percentage of gated cells found in the RL quadrant as the indicator of C2 or C1C2 domain binding. Before mixing the two cell lines, Jurkat cells were first incubated with various samples diluted in PBS at 37 ˚C for 20 mins.

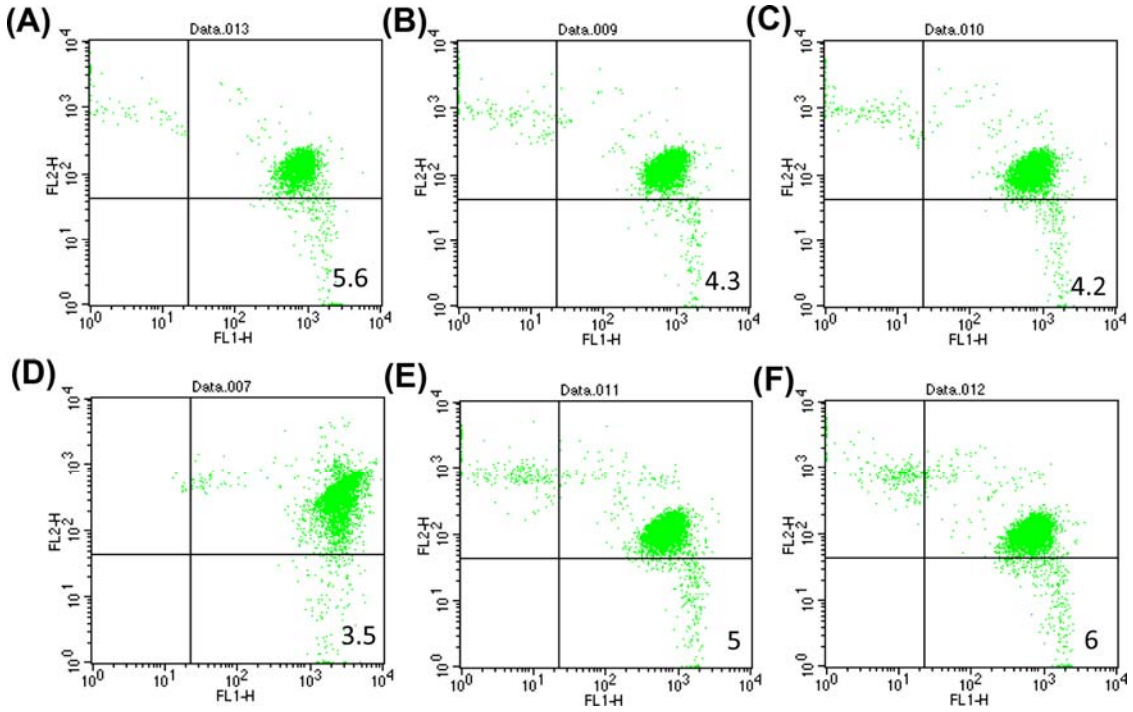

Figure 35. Dot plot of C2 domain co-culture FACS test
C2 domain alone were added at different concentration before mixing the two cells, and Co-culture FACS analysis were performed. **(A)** Induced, Buffer only; **(B)** Induced, 10 µM C2 wt; **(C)** Induced, 50 µM C2 wt; **(D)** Induced, Annexin V; **(E)** Induced, 100 µM C2 wt; **(F)** Induced, 200 µM C2 wt. Numbers represent the percentage of gated cells in LR quadrant, and are the average of three experiments. (**FL1**: Green fluorescence signal; **FL2**: Red fluorescence signal)

Results for C2 domain wild type test was shown in Figure 35. Most of the cells remain in the RU quadrant, suggesting that with up to 200 uM concentration, C2 domain alone could not compete with the physiological activity of the endogenous opsonins.

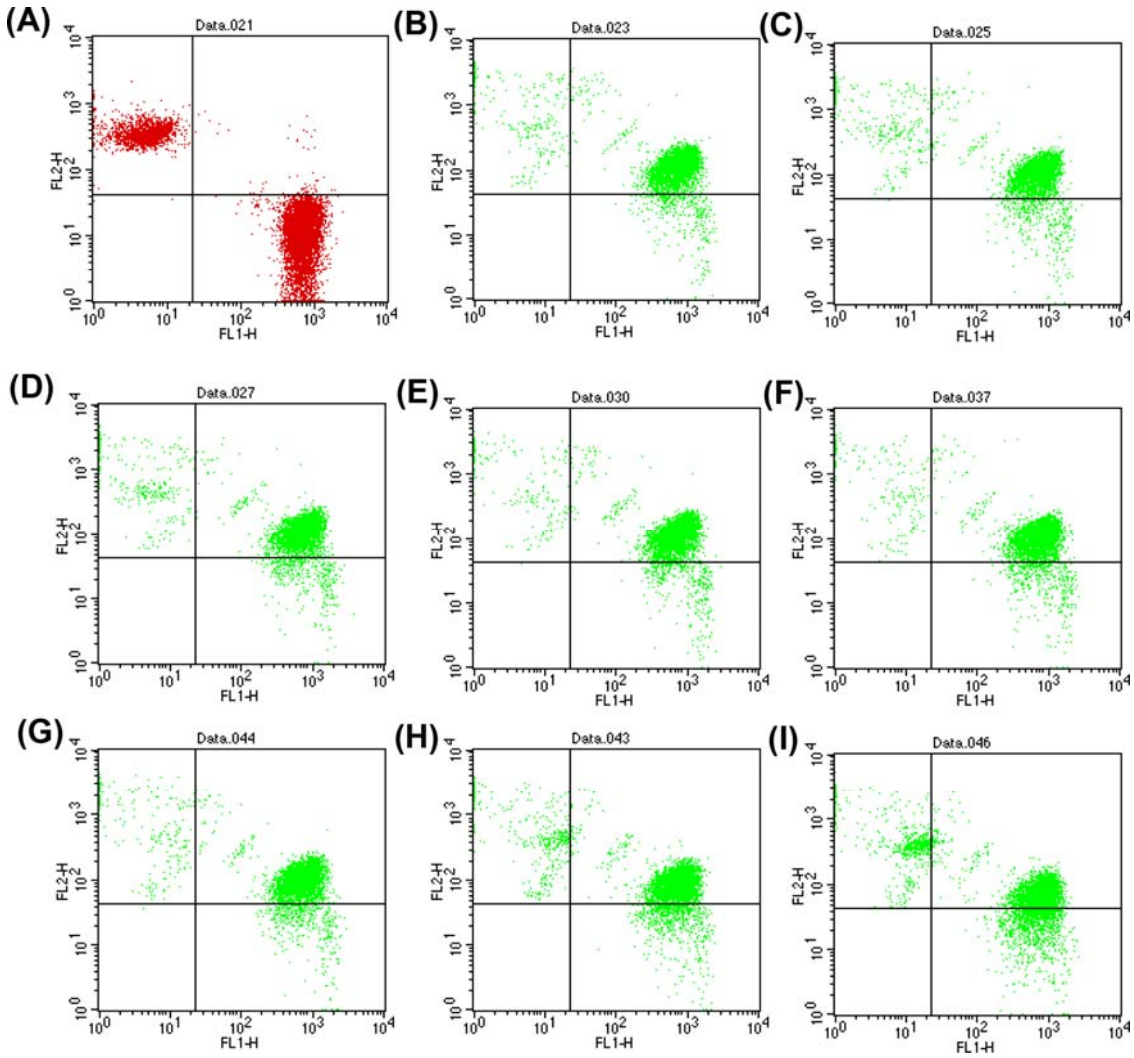

Figure 36. Dot plot of Co-culture FACS analysis of MFG-E8 C1C2 domain
SUMO-C1C2 domain, SUMO tag or blank buffer was tested using Co-culture FACS analysis. **(A)** Non-induced; **(B)** Induced, PBS only; **(C)** Induced, PBS with 10% v/v protein buffer; **(D)** Induced, PBS with SUMO tag in protein buffer; **(E)** Induced, PBS with 100 nM SUMO-C1C2; **(F)** Induced, PBS with 500 nM SUMO-C1C2; **(G)** Induced, PBS with 1 µM SUMO-C1C2; **(H)** Induced, PBS with 5 uM SUMO-C1C2; **(I)** Induced, PBS with 10 µM SUMO-C1C2. (**FL1**: Green fluorescence signal; **FL2**: Red fluorescence signal)

Interestingly, when SUMO-C1C2 was tested using this analysis, dose-dependent increase in the percentage of gated cells in RL quadrant was observed (Figure 36 and 37). SUMO-C1C2 domain was able to disrupt over 20% of the phagocytosis at only 10 μM concentration (Figure 37). Compared with the result from C2 domain alone, C1C2 domain together showed much higher binding affinity with the PS-exposed apoptotic cells, suggesting a very important role for the C1 domain in the PS recognition and binding. It was also noteworthy that Annexin V at its commercial working concentration could not trigger any significant disruption of the phagocytosis (Figure 35D).

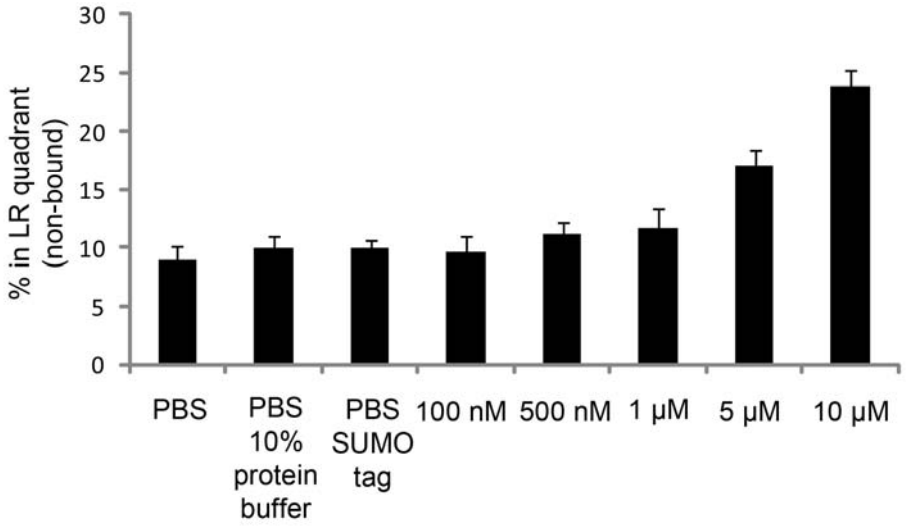

Figure 37. Histogram of SUMO-C1C2 in co-culture FACS analysis
Percentage cells within lower-right quadrant of the gate 2 graph were used to measure phagocytosis inhibition, i.e. SUMO-C1C2 binding with exposed PS. Results are mean ± SE value from three experiments.

4 Discussions

Since the discovery of PS recognition by the C2 domain of MFG-E8 (Hanayama et al., 2002), several studies had been performed pursuing the structure and function of MFG-E8 C2 domain (Lin et al., 2007; Shao et al., 2008). These studies both used X-ray crystallography to determine the crystal structure of bovine MFG-E8 C2 domain, employed computational simulation and docking methods to speculate the possible PS binding sites and binding mechanisms, with only basic mutational studies using biochemical assays. These high quality crystal structures had high resolutions (2.4 Å and 1.7 Å respectively), and provided valuable information for the upcoming studies. But the failure of ligand diffusion into crystal withheld the simulation results from experimental confirmation (Shao et al., 2008).

In current study, NMR spectroscopy was used to determine the solution structure of mouse MFG-E8 C2 domain. Our C2 domain solution structure had a RMSD value of 1.40 ± 0.14 Å for all backbone heavy atoms (Table 1), and was composed of two major β-sheets consisting of five and three anti-parallel β-strands respectively and facing each other, plus four minor β-strands (Figure 17A). Despite differences in the more dynamic and less conserved loop regions, this characteristic folding pattern was shared across the discoidin-like C2 domains, including Factor V (Kim et al., 2000), Factor VIII (Gilbert et al., 2002) and bovine MFG-E8 C2 domain (Shao et al., 2008). Two cysteines residues were located at the N- and C- terminal extremities of these proteins, and predicted to form a conserved disulfide-bond based on the ^{13}C chemical shift data (Sharma, 2000). The bottom loops region opposite the disulfide-bond were believed to accommodate the potential PS binding sites. There are three major loops at the bottom of the protein,

generally referred to as ‘spikes’ (spike 1: Tyr23–Trp33; spike 2: Gln43–Asn47; spike 3: Ala78–Gln85). In Factor V/VIII, spike 1 and 3 were shown to account for the high PS affinity in these proteins. Mutagenesis studies and antibody ligand binding demonstrated the solvent exposed hydrophobic residues in these loops to be critical (Gilbert et al., 2002; Kim et al., 2000). Recent Factor VIII C2 crystal structure also confirmed these findings, with the supplement of 2 other minor loops involved in the binding (Liu et al., 2010). Bovine MFG-E8 C2 domain was shown to agree with this binding model. The author claimed that in the lower loops, functional similarity as well as structural similarity were remained in bovine C2 domain as compared to Factor V/VIII C2 domain. However, the author also found that the spike 1 of bovine C2 domain had more organized structure than the same region of Factor V/VIII. Six hydrogen bonds were found in this loop, giving more structural rigidity and complexity, and thus contributing to the higher affinity of bovine C2 domain towards PS (Shao et al., 2008).

Compared to C2 domains from Factor V and Factor VIII, the crystal structure of bovine MFG-E8 C2 domain was of more relevance to our study. This homolog of mouse MFG-E8 C2 domain had sequence identity of 72.8%. The overlay of crystal structure of bovine C2 and our mouse C2 solution structure demonstrated overall structural similarity, with local variations. Comparing our lowest energy NMR structure of mouse MFG-E8 C2 (PDB code: 2L9L) with the crystal structure of bovine MFG-E8 C2 (PDB code: 3BN6), the RMSD for the α-carbon atoms was 1.52 Å (Figure 17B). This relative large deviation was mainly caused by the loop regions, namely the residues Thr25-Ala30 (spike 1) and loop between β5 and β6. In our study, the amides of residues Thr25-Ala30 were unable to be observed in the 2D ^{1}H-^{15}N HSQC spectrum (Figure 18 and 19). This may be due to

that these residues undergo fast exchange with the solvent, suggesting the highly dynamic property and flexibility of, which was somehow different from the conclusion drawn in the study of bovine C2. Since factor V C2 domain was found to be folded into two different conformations, and each of these forms represented either the circulating form or the membrane-bound form (Macedo-Ribeiro et al., 1999). Likewise, it is possible that spike 1 in mouse C2 domain might exist in different conformations at different physiological states, and conformational changes might be required during PS binding process. Our structure ensemble could provide some possible conformations that this loop might take up.

In X-ray crystallography, the structure was only a representation of certain structural state captured during crystallization process, and might not be the real physiological state. On the other hand, NMR spectroscopy aimed to determine the solution structure of a given protein, and with a well chosen protein buffer, it could record structural information when protein was in its physiological state, and allow protein dynamics, and thus was more biological relevant than that of crystal structure in some circumstances. Although they are unable to be well-defined, some possible conformations of this flexible region could be reflected from our solution structures which could be found in the structure ensemble with higher RMSD values (Figure 17C).

Phospholipids are lipids that form the major component of cell membranes. They normally form bilayers in aqueous solutions, or vesicles / liposomes upon sonication. In our previous published paper, PS was dissolved in the buffer containing 10 mM NaPO4, pH 6.5, 10 mM NaCl, 10 mM CHAPS to the final concentration of 0.25 mM, and titrated with varying concentrations of MFG-E8 C2 domain. According to previous studies

(Cladera et al., 1997; Silvius, 1992), the process to solubilize lipid bilayers by detergents composed 3 stages. Stage I involves partitioning of detergent monomers between the aqueous medium and the lipid bilayer. At the end of this stage, liposomes are saturated with detergent. During stage II, additional detergent gradually solubilizes the liposome. Micelles with mixed phospholipid-detergent contents begin to form. Stage III is characterized by complete solubilization of lipids into small mixed micelles. These stages were marked by some critical concentrations depending on the nature of the detergent and the molar ratio between lipid and detergent (Lichtenberg, 1985). CHAPS is a zwitterionic detergent with critical micelle ceoncentration (CMC) of 8 to 10 mM. It was shown to be able to dissolve various phospholipids at different concentrations, e.g. critical concentration of free detergent [Dw]c is measured to be 2.3 mM for phosphatidylcholine and 5.2 mM for a mixture of palmitoyloleoylphosphatidylcholine (POPC), phosphatidylethanolamine (PE) and phosphatidylglycerol (PG), POPC:PE:PG = 30:60:10 (mol.-%) (Schurholz, 1996). In the condition listed above, 10 mM CHAPS used in the buffer should completely dissolve the 0.25 mM of PS and form small mixed micelles. The molar ratio of CHAPS:PS was 40:1, and the aggregation number is 10 for CHAPS itself. Therefore, it is possible that each mixed micelle might contain just one PS molecule and binds with a single C2 protein molecule.

When we attempt to perform HSQC titrations of PS into C2 domain, problems rose in the preparation of PS stock solution. Since PS was titrated into protein solution, the stock should have much higher concentration to avoid significant change in sample volume, which is an important factor affecting NMR spectrum quality. Natural PS could not be well solubilized at concentrations beyond 1 mM and created protein precipitation when

added. The HSQC spectra were also affected showing severe overall line-broadening and peak intensity attenuation. Varying CHAPS concentrations or sonication were tried, but failed to solve the problem. Thus truncated forms of PS were used instead of natural long chain PS. 1,2-dihexanoyl-sn-glycero-3-phospho-L-serine (06:0 PS) was chosen because of its good solubility in water at up to 3 mM and causing minimal protein precipitation. It has a CMC of 1.2 mM and should be forming small unilamellar liposomes in our preparation of 3 mM with sonicatio in the absence of CHAPS. The presence of CHAPS did not show productive effect on PS stock preparation. This might be due to that the decreased CHAPS:PS molar ratio in 3 mM stock made it unable to completely dissolve PS, and thus partitioned at the PS-water interface and increased the liposome size, giving even worse spectra compared to 06:0 PS along.

However, even 06:0 PS was forming small liposomes with much larger size compared to single protein. Therefore, protein experienced an increase in tumbling time when bound to 06:0 PS, resulted in decrease of NMR spectra quality. Moreover, since the liposome was completely made of PS molecule, there were large number of binding sites on just one particle, attracting many protein molecules and creating chances for the protein to aggregate and eventually precipitate. This was the reason that we could only obtain 1:10 ratio HSQC spectra without the titration process. And overall peak intensities decreased to about half of that of the free protein spectrum. 3D NMR analysis was also impossible, preventing us from acquiring more detailed information about the binding event.

In bovine C2 domain, the solvent exposed hydrophobic residues Trp26, Leu28, Phe31, and Phe81 were shown to be in close proximity with each other and packed to a hydrophobic patch, similar to that of Factor V/VIII C2 domain. These residues in spike 1

and 3 were thought to be the most critical residues in Factor V/VIII C2 domain binding (Shao et al., 2008). In our study, due to the lack of structural information in spike 1, their functions were not thoroughly examined. However, 2D HSQC titration with 06:0 PS results showed signal disappearance for both Phe31 and Phe81 (Figure 19). Mutagenesis study using FACS also demonstrated minor decrease in apoptotic cell binding from F81A mutant, minor increase from W26A, and enhanced disruption of binding from the double mutant (Figure 29B). These findings proved involvement of hydrophobic residues in the binding event, especially the synergistic effect from multiple residues, and agreed with the previous models about lipid insertion of hydrophobic residues into membrane hydrophobic core. It is noteworthy that W26A showed slightly enhanced binding. We proposed that this may be due to the decrease in the area of hydrophobic patch leading to easier insertion into the membrane. As for F81A mutant, since Phe81 was shown in computer docking to have a hydrogen bond contact from its main chain amide proton to phosphoryl oxygen (O7 atom) on the PS molecule (Table 2), its absence would cause decrease in more than just hydrophobicity, and thus it should be more central in this binding event compared to other hydrophobic residues. The double mutation led to a more dramatic decrease in hydrophobic potential, rendering C2 to be unable to penetrate the hydrophilic bilayer surface or unable to stabilize the inserted conformation, thus showed much severe decrease or disruption of binding. Three of these hydrophobic residues were located within the flexible spike 1, forming a hydrophobic surface at the tip of this loop. The flexibility would allow searching for potential and possible membrane insertion sites, and changing in local conformation to better suit the site specifically. Therefore, we proposed that the hydrophobic residues in spike 1 functioned as initiators

in the binding, providing initial anchorage. The Phe81 located at spike 3 provided a support with added polar contact that further stabilizes the initial binding. We have to admit that there is one minor flaw that the influence of mutations on Trp26 and Phe81 were not tested in the same way as mutants for positively charged residues. This is due to the use of different constructs with gst and GFP tags. However, since these two residues were both located in the highly flexible loop 1 and 3, changes in these positions were not expected to have any major influence on the protein folding pattern and overall structure. Therefore, we believe that the tests using W26A and F81A were valid and could provide evidence for their corresponding conclusions.

The absence of spike 2 from Factor V/VIII C2 domain binding model was agreed in the bovine C2 domain study. However, from our 2D HSQC titration experiments, significant chemical shift perturbations or peak disappearance from residues Gly44-Trp49 within spike 2 were found, suggesting heavy involvement of spike 2 in the binding event. This result was further confirmed by the ^{31}P NMR spectra of K45N mutant experiments and by the simulated hydrogen bond between Lys45 with both phosphoryl oxygen (O6 atom) and acyl chains (O8 atom) in PS from computer docking (Table 2). Further *in vitro* testing using FACS analysis on Lys to Asn mutants also provided strong support for the critical roles of Lys24 and Lys45 residues. This mutation substitute positive side chain into zwitterionic, overall neutral side chain, losing electrostatic potential and thus losing affinity. Compared to those of Lys24, the higher chemical shift perturbation from Lys45 in HSQC titration experiments was in agreement with the stronger inhibition of apoptotic cell binding in K45N mutant in FACS analysis. This strongly suggested that Lys45 was more critical than Lys24 in the binding of mouse C2 domain towards PS. These were

only two examples of how positively charged residues in loop region functioned in the binding event. As shown in Figure 20 and Figure 21, a number of positively charged residues within these loops were found to be conserved across species, which gives rise to a very unique distribution of the surface electrostatic potential. They encompass an area large enough to cover the whole head group of the phospholipid. Therefore, these residues not only interact with the highly negatively charged phosphate group on the backbone of phospholipid, but also form contacts with the various functional groups in the head group. Since electrostatic interactions were energetically stronger than hydrophobic effect, here we proposed that these positively charged conserved residues on the loops were responsible for the high affinity in PS binding. Besides, comparing the structure of PS with PC, the serine-carboxyl group of PS head group provides an additional negative charge other than the phosphate group. Therefore, these positively charged residues could also be responsible for the selectivity for PS over PC.

Within these residues, two arginines Arg79 and Arg146 were proposed to be important in docking results from bovine C2 study. Our docking showed similar results (Table 2) that these two residues formed hydrogen bond with serine-carboxyl group (O10 atom) in PS. HSQC titration also found peak disappearance for both residues. Thus in our study, they were selected to be mutated into glutamine and tested using ^{31}P spectroscopy. Large decrease in the K_d for R79Q and R146Q mutants demonstrated their involvement in the PS binding. Moreover, since the chiral center in serine group was the C_α, Ptd-L-Ser differed from Ptd-D-Ser mainly on the relative position of backbone amide and carboxyl group. It was thus straight forward to speculate that residues having contacts with these groups might participate in the stereospecificity determination during the binding event.

Based on this speculation, Arg79 and Arg146, together with another residue Gln77 which also showed large chemical shift perturbation, were proposed to be part of the stereospecificity determining mechanism in our C2 domain. No experimental evidence was obtained so far, thus future testing on the stereo-selectivity using mutations on these residues might provide valuable information.

In summary, based on the experimental data obtained from our studies and some of previous research findings, we proposed the following binding mechanism for the binding of MFG-E8 C2 domain towards PS. First, hydrophobic residues Trp26, Leu28, and Phe31 in spike 1 form an initial hydrophobic patch. The flexibility of the loop allowed searching for possible insertion sites. Upon successful membrane insertion, Phe81 then join the hydrophobic patch formed by spike 1, and stabilize the binding through added hydrophobicity and additional hydrogen bond contacts with PS oxygen. Positively charged conserved residues like Lys24 and Lys45 then form salt-bridge interactions with the negatively charged phosphate backbone and the serine head group, account for the high binding affinity and possibly the ligand selectivity of PS over other phospholipids. Special residues like Gln77, Arg79 and Arg146 participated in the stereospecificity determining mechanism and thus preferred Ptd-L-Ser over Ptd-D-Ser.

In bovine C2 paper (Shao et al., 2008), the docking study yielded two binding sites for PS. Our docking predicted the same result. The binding site one was the one discussed above, utilizing mainly spikes 1, 2, and 3. The binding site two involved spikes 2, 3 and 4 on the other side of binding site one. As spike 1 was proposed to be responsible for the initial PS binding, its only participation in binding site one suggested that binding site one was the initial PS binding site. Upon binding of the first PS molecule, the second one (or even

other negatively charged phospholipids) might join and further stabilize the binding. This somehow could be proved by the 2D HSQC data (Figure 19), in which loop 4 (Gly115-Ser121) showed chemical shift perturbations for the entire loop, suggesting its active participation in the binding event. No previous data was associated with this region of loop, and our NMR titration could be the first report on the involvement of these residues, and it could demonstrate the possible binding of PS molecules in non-conventional binding site as predicted in our docking study.

Surface expressed PS could be used as potential marker for various diseases, and its *in vivo* visualization would provide a valuable means for diagnosis, monitor and even treatment. So far, Annexin V was the best characterized and most widely used molecular probe for PS detection (Blankenberg, 2008). As described in Introduction section, Annexin V binding was done through the coordinated Ca^{2+} ions in the loop regions, through near exclusively electrostatic interactions, with almost no membrane insertion. Thus somehow it was considered as superficial binding (Lemmon, 2008). It employed larger area of contact, required multiple PS molecules to bind at its full potential, so as to achieve high binding affinity. On the other side, judging from our proposed binding model for MFG-E8 C2 binding, it had relatively larger extend of membrane insertion, and required much less number of PS molecule to saturate. This could be proved by the higher minimal percentage of PS for Annexin V membrane binding of 8% compared to the much lower minimal percentage of C2 of 0.5% (Dasgupta et al., 2006; Shi et al., 2006). Compared to Annexin V, MFG-E8 C2 domain has the advantages of being stereospecific, due to its complex bonding contacts; small in size; and less demanding for minimal PS content. But it binds PS with less affinity, thus needs combined effort from

either another C2 domain or C1 domain. As demonstrated in our co-culture experiment, Annexin V failed to compete with endogenous opsonins, could not inhibit phagocytosis. C1C2 together showed disruption of phagocytosis in dose-dependent manner, although the effect was relatively weak. Nevertheless, Annexin V still possesses advantage of being able to be endocytosed upon binding, thus can be used as a means for targeted drug discovery.

C1 domain was found to help both direct binding of apoptotic cells, or disruption of phagocytosis (Figure 31 and 37). The former experiment displayed less effect. But the later one showed a transformation, from the non-disruptive effect in apoptotic cell clearance of C2 domain alone, to the dose-dependent disruption in SUMO-C1C2 construct. Although due to some drawbacks in the experiment, the results were not so convincing. For example, The test system we chose was not specifically modified cell lines, thus more than just PS-exposure was employed as the 'eat-me' signal the induced Jurkat cells, and other opsonins might also be released by THP-1 cells. The sensitivity of this system thus needed further calibration and adjustment. Besides, the SUMO-C1C2 protein we used was not in its monomeric form, and this slight aggregation might have increased the number of binding site on each particle, thus increasing the binding affinity. The function of C1 domain in the binding of C2 domain with PS should be further tested using other methods in the future. Nonetheless, this result still could infer the involvement of C1 domain in PS containing membrane binding. It was speculated that some C1 domains showed similarity towards C2 domain, thus like another C2, bound selectively to PS (Shao et al., 2008). Others proposed C1 function to bind to other general phospholipids, to enhance, stabilize the real specific PS binding from C2 (Takeshima et

al., 2003). For C1 domain from mouse MFG-E8, the alignment its C1 and C2 domain is shown below (Figure 38).

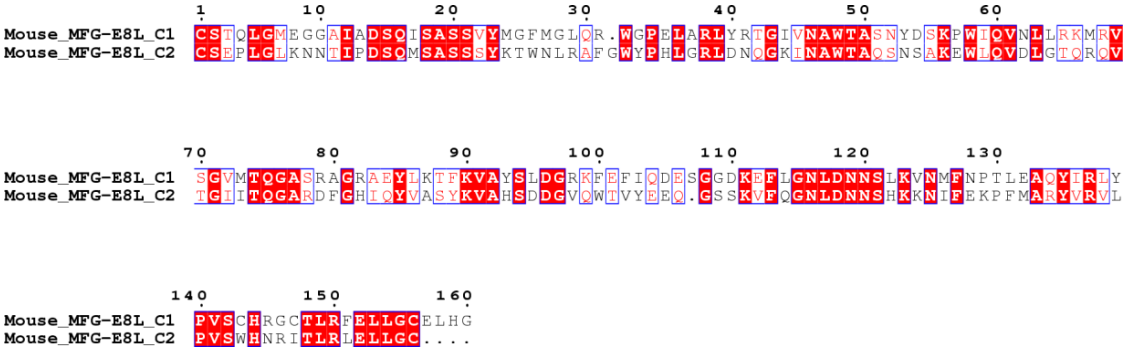

Figure 38. Sequence alignment of C1 and C2 domain from mouse MFG-E8
the sequence identity was only 44.1% and similarity was 55.9%. Some critical residues for C2-PS binding was not present in C1 domain, but the overall secondary structures are similar between the two domains.

It is noteworthy that, the sequence identity was only 44.1% and similarity was 55.9%. Therefore, substantial differences were there between these two homologous domains. Also, most of the residues chosen to be mutated including Lys24, Trp26, Lys45, Phe81, and Arg146 were not conserved in C1 domain, suggesting that the C1 domain might not be functioning in the exact way as C2 domain. Despite that, the main secondary structures were considerably similar, suggesting the similar overall folding pattern. So it could be possible that C1 domain functions by binding towards general phospholipid membrane and enhances the specific binding from C2 domain. However, our results could not differentiate the differences between these two hypotheses, and further studies are still needed.

As discussed in the Introduction section, the lipid binding domains utilized several binding schemes, including membrane insertion by hydrophobic residues, direct electrostatic interaction between positively charged residues and negatively charged phospholipids, and indirect electrostatic interaction mediated by calcium ion linking

negatively charged protein surface with negatively charged phospholipids. Different schemes may cooperate with each other and exhibit synergistic effect, leading to various binding events with different affinities towards different lipid targets. It is noteworthy that calcium mediation scheme mainly functions alone, or with only minor help from membrane insertion. This may be due to the relatively large space calcium ions take up at the center of the binding surface, preventing further membrane insertion into phospholipid core. Annexin V binding with PS is the best example of this type. On the other hand, lipid binding domains independent of calcium ion use the combined effort of membrane insertion and direct electrostatic interaction, but with varying involvements from these two schemes. This type of binding could be represented by PKC C1 domain, PH domain, and discoidin like C domains. Among the three, PKC C1 domain had the largest hydrophobic patch at its binding site (Figure 5), thus rely heavily on membrane penetration. PH domains and discoidin like C domains shared some similarities in their structural features, and both used more balanced ratio between the two schemes for the binding. Our study on and proposal of the mechanism of MFG-E8 C2 domain binding with PS provided insights into the general model for calcium independent lipid binding.

In conclusion, MFG-E8 has its integrin binding site on the EGF domains and its interaction is critical for the phagocyte-mediated engulfment in response to apoptotic stimuli, the functional role of PS binding via the C2 domain awaits more investigation. Its important participation in the pathology of autoimmunity, neurodegeneration made it valuable target for new drug discovery. Its anti-coagulation function could be worked on to develop novel anticoagulant. And further in depth researches on the binding mechanism of PS containing membrane binding would provide information for wide

usage. Future studies involving patient samples might provide new insight into the biological role of MFG-E8 in recognizing PS during apoptosis.

5 References

Albert, M.L., Pearce, S.F., Francisco, L.M., Sauter, B., Roy, P., Silverstein, R.L., Bhardwaj, N., 1998. Immature dendritic cells phagocytose apoptotic cells via alphavbeta5 and CD36, and cross-present antigens to cytotoxic T lymphocytes. J Exp Med 188, 1359-1368.

Andersen, M.H., Graversen, H., Fedosov, S.N., Petersen, T.E., Rasmussen, J.T., 2000. Functional analyses of two cellular binding domains of bovine lactadherin. Biochemistry 39, 6200-6206.

Arikketh, D., Nelson, R., Vance, J.E., 2008. Defining the importance of phosphatidylserine synthase-1 (PSS1): unexpected viability of PSS1-deficient mice. J Biol Chem 283, 12888-12897.

Asano, K., Miwa, M., Miwa, K., Hanayama, R., Nagase, H., Nagata, S., Tanaka, M., 2004. Masking of phosphatidylserine inhibits apoptotic cell engulfment and induces autoantibody production in mice. J Exp Med 200, 459-467.

Baker, N.A., Sept, D., Joseph, S., Holst, M.J., McCammon, J.A., 2001. Electrostatics of nanosystems: application to microtubules and the ribosome. Proc Natl Acad Sci U S A 98, 10037-10041.

Balasubramanian, K., Chandra, J., Schroit, A.J., 1997. Immune clearance of phosphatidylserine-expressing cells by phagocytes. The role of beta2-glycoprotein I in macrophage recognition. J Biol Chem 272, 31113-31117.

Banchereau, J., Steinman, R.M., 1998. Dendritic cells and the control of immunity. Nature 392, 245-252.

Baumgartner, S., Hofmann, K., Chiquet-Ehrismann, R., Bucher, P., 1998. The discoidin domain family revisited: new members from prokaryotes and a homology-based fold prediction. Protein Sci 7, 1626-1631.

Behnia, R., Munro, S., 2005. Organelle identity and the signposts for membrane traffic. Nature 438, 597-604.

Bergo, M.O., Gavino, B.J., Steenbergen, R., Sturbois, B., Parlow, A.F., Sanan, D.A., Skarnes, W.C., Vance, J.E., Young, S.G., 2002. Defining the importance of phosphatidylserine synthase 2 in mice. J Biol Chem 277, 47701-47708.

Blankenberg, F.G., 2008. In vivo detection of apoptosis. J Nucl Med 49 Suppl 2, 81S-95S.

Blevins, B.J.a.R., 1994. NMRView: A computer program for the visualization and analysis of NMR data. J. Biomol. NMR 4, 603-614.

Borisenko, G.G., Iverson, S.L., Ahlberg, S., Kagan, V.E., Fadeel, B., 2004. Milk fat globule epidermal growth factor 8 (MFG-E8) binds to oxidized phosphatidylserine: implications for macrophage clearance of apoptotic cells. Cell Death Differ 11, 943-945.

Bottomley, M.J., Salim, K., Panayotou, G., 1998. Phospholipid-binding protein domains. Biochim Biophys Acta 1436, 165-183.

Brown, S., Heinisch, I., Ross, E., Shaw, K., Buckley, C.D., Savill, J., 2002. Apoptosis disables CD31-mediated cell detachment from phagocytes promoting binding and engulfment. Nature 418, 200-203.

Burtea, C., Laurent, S., Lancelot, E., Ballet, S., Murariu, O., Rousseaux, O., Port, M., Vander Elst, L., Corot, C., Muller, R.N., 2009. Peptidic targeting of phosphatidylserine for the MRI detection of apoptosis in atherosclerotic plaques. Mol Pharm 6, 1903-1919.

Butler, J.E., Pringnitz, D.J., Martens, C.L., Crouch, N., 1980. Bovine-associated mucoprotein: I. Distribution among adult and fetal bovine tissues and body fluids. Differentiation 17, 31-40.

Canton, J., Neculai, D., Grinstein, S., 2013. Scavenger receptors in homeostasis and immunity. Nat Rev Immunol 13, 621-634.

Cho, W., Stahelin, R.V., 2006. Membrane binding and subcellular targeting of C2 domains. Biochim Biophys Acta 1761, 838-849.

Cladera, J., Rigaud, J.L., Villaverde, J., Dunach, M., 1997. Liposome solubilization and membrane protein reconstitution using Chaps and Chapso. Eur J Biochem 243, 798-804.

Clark, J.D., Lin, L.L., Kriz, R.W., Ramesha, C.S., Sultzman, L.A., Lin, A.Y., Milona, N., Knopf, J.L., 1991. A novel arachidonic acid-selective cytosolic PLA2 contains a Ca(2+)-dependent translocation domain with homology to PKC and GAP. Cell 65, 1043-1051.

Colon-Gonzalez, F., Kazanietz, M.G., 2006. C1 domains exposed: from diacylglycerol binding to protein-protein interactions. Biochim Biophys Acta 1761, 827-837.

Cornilescu, G., Delaglio, F., Bax, A., 1999. Protein backbone angle restraints from searching a database for chemical shift and sequence homology. J Biomol NMR 13, 289-302.

Dasgupta, S.K., Guchhait, P., Thiagarajan, P., 2006. Lactadherin binding and phosphatidylserine expression on cell surface-comparison with annexin A5. Transl Res 148, 19-25.

Davis, A.J., Butt, J.T., Walker, J.H., Moss, S.E., Gawler, D.J., 1996. The Ca2+-dependent lipid binding domain of P120GAP mediates protein-protein interactions with Ca2+-dependent membrane-binding proteins. Evidence for a direct interaction between annexin VI and P120GAP. J Biol Chem 271, 24333-24336.

De Saint-Hubert, M., Mottaghy, F.M., Vunckx, K., Nuyts, J., Fonge, H., Prinsen, K., Stroobants, S., Mortelmans, L., Deckers, N., Hofstra, L., Reutelingsperger, C.P., Verbruggen, A., Rattat, D., 2010. Site-specific labeling of 'second generation' annexin V with 99mTc(CO)3 for improved imaging of apoptosis in vivo. Bioorg Med Chem 18, 1356-1363.

Devitt, A., Moffatt, O.D., Raykundalia, C., Capra, J.D., Simmons, D.L., Gregory, C.D., 1998. Human CD14 mediates recognition and phagocytosis of apoptotic cells. Nature 392, 505-509.

Di Paolo, G., De Camilli, P., 2006. Phosphoinositides in cell regulation and membrane dynamics. Nature 443, 651-657.

DiNitto, J.P., Lambright, D.G., 2006. Membrane and juxtamembrane targeting by PH and PTB domains. Biochim Biophys Acta 1761, 850-867.

Fadok, V., Voelker, D.R., Campbell, P.A., Cohen, J.J., Bratton, D.L., Henson, P.M., 1992. Exposure of phosphatidylserine on the surface of apoptotic lymphocytes triggers specific recognition and removal by macrophages. J. Immunol. 148, 2207-2216.

Fadok, V.A., Bratton, D.L., Konowal, A., Freed, P.W., Westcott, J.Y., Henson, P.M., 1998. Macrophages that have ingested apoptotic cells in vitro inhibit proinflammatory cytokine production through autocrine/paracrine mechanisms involving TGF-beta, PGE2, and PAF. J Clin Invest 101, 890-898.

Fadok, V.A., Bratton, D.L., Rose, D.M., Pearson, A., Ezekewitz, R.A., Henson, P.M., 2000. A receptor for phosphatidylserine-specific clearance of apoptotic cells. Nature 405, 85-90.

Ferguson, K.M., Lemmon, M.A., Schlessinger, J., Sigler, P.B., 1995. Structure of the high affinity complex of inositol trisphosphate with a phospholipase C pleckstrin homology domain. Cell 83, 1037-1046.

Ferguson, K.M., Kavran, J.M., Sankaran, V.G., Fournier, E., Isakoff, S.J., Skolnik, E.Y., Lemmon, M.A., 2000. Structural basis for discrimination of 3-phosphoinositides by pleckstrin homology domains. Mol Cell 6, 373-384.

Freire-de-Lima, C.G., Nascimento, D.O., Soares, M.B., Bozza, P.T., Castro-Faria-Neto, H.C., de Mello, F.G., DosReis, G.A., Lopes, M.F., 2000. Uptake of apoptotic cells drives the growth of a pathogenic trypanosome in macrophages. Nature 403, 199-203.

Garnier, B., Bouter, A., Gounou, C., Petry, K.G., Brisson, A.R., 2009. Annexin A5-functionalized liposomes for targeting phosphatidylserine-exposing membranes. Bioconjug Chem 20, 2114-2122.

Gerke, V., Moss, S.E., 2002. Annexins: from structure to function. Physiol Rev 82, 331-371.

Gerke, V., Creutz, C.E., Moss, S.E., 2005. Annexins: linking Ca2+ signalling to membrane dynamics. Nat Rev Mol Cell Biol 6, 449-461.

Gershov, D., Kim, S., Brot, N., Elkon, K.B., 2000. C-Reactive protein binds to apoptotic cells, protects the cells from assembly of the terminal complement components, and sustains an antiinflammatory innate immune response: implications for systemic autoimmunity. J Exp Med 192, 1353-1364.

Gibson, T.J., Hyvonen, M., Musacchio, A., Saraste, M., Birney, E., 1994. PH domain: the first anniversary. Trends Biochem Sci 19, 349-353.

Gilbert, G.E., Kaufman, R.J., Arena, A.A., Miao, H., Pipe, S.W., 2002. Four hydrophobic amino acids of the factor VIII C2 domain are constituents of both the membrane-binding and von Willebrand factor-binding motifs. J Biol Chem 277, 6374-6381.

Grobler, J.A., Essen, L.O., Williams, R.L., Hurley, J.H., 1996. C2 domain conformational changes in phospholipase C-delta 1. Nat Struct Biol 3, 788-795.

Guerrero-Valero, M., Ferrer-Orta, C., Querol-Audi, J., Marin-Vicente, C., Fita, I., Gomez-Fernandez, J.C., Verdaguer, N., Corbalan-Garcia, S., 2009. Structural and mechanistic insights into the association of PKCalpha-C2 domain to PtdIns(4,5)P2. Proc Natl Acad Sci U S A 106, 6603-6607.

Guex, N., Peitsch, M.C., 1997. SWISS-MODEL and the Swiss-PdbViewer: an environment for comparative protein modeling. Electrophoresis 18, 2714-2723.

Guntert, P., 2004. Automated NMR structure calculation with CYANA. Methods Mol Biol 278, 353-378.

Hanayama, R., Tanaka, M., Miwa, K., Shinohara, A., Iwamatsu, A., Nagata, S., 2002. Identification of a factor that links apoptotic cells to phagocytes. Nature 417, 182-187.

Hanayama, R., Tanaka, M., Miyasaka, K., Aozasa, K., Koike, M., Uchiyama, Y., Nagata, S., 2004. Autoimmune disease and impaired uptake of apoptotic cells in MFG-E8-deficient mice. Science 304, 1147-1150.

Hanshaw, R.G., Smith, B.D., 2005. New reagents for phosphatidylserine recognition and detection of apoptosis. Bioorg Med Chem 13, 5035-5042.

Harlan, J.E., Hajduk, P.J., Yoon, H.S., Fesik, S.W., 1994. Pleckstrin homology domains bind to phosphatidylinositol-4,5-bisphosphate. Nature 371, 168-170.

Haslam, R.J., Koide, H.B., Hemmings, B.A., 1993. Pleckstrin domain homology. Nature 363, 309-310.

Hengartner, M.O., 2000. The biochemistry of apoptosis. Nature 407, 770-776.

Henson, P.M., Bratton, D.L., Fadok, V.A., 2001. The phosphatidylserine receptor: a crucial molecular switch? Nat Rev Mol Cell Biol 2, 627-633.

Holthuis, J.C., Levine, T.P., 2005. Lipid traffic: floppy drives and a superhighway. Nat Rev Mol Cell Biol 6, 209-220.

Hughes, J., Liu, Y., Van Damme, J., Savill, J., 1997. Human glomerular mesangial cell phagocytosis of apoptotic neutrophils: mediation by a novel CD36-independent vitronectin receptor/thrombospondin recognition mechanism that is uncoupled from chemokine secretion. J Immunol 158, 4389-4397.

Humphries, J.D., Byron, A., Humphries, M.J., 2006. Integrin ligands at a glance. J Cell Sci 119, 3901-3903.

Hurley, J.H., Misra, S., 2000. Signaling and subcellular targeting by membrane-binding domains. Annu Rev Biophys Biomol Struct 29, 49-79.

Hynes, R.O., 1987. Integrins: a family of cell surface receptors. Cell 48, 549-554.

Isakoff, S.J., Cardozo, T., Andreev, J., Li, Z., Ferguson, K.M., Abagyan, R., Lemmon, M.A., Aronheim, A., Skolnik, E.Y., 1998. Identification and analysis of PH domain-containing targets of phosphatidylinositol 3-kinase using a novel in vivo assay in yeast. EMBO J 17, 5374-5387.

Jacobson, M.D., Weil, M., Raff, M.C., 1997. Programmed cell death in animal development. Cell 88, 347-354.

Jiang, J., Kini, V., Belikova, N., Serinkan, B.F., Borisenko, G.G., Tyurina, Y.Y., Tyurin, V.A., Kagan, V.E., 2004. Cytochrome c release is required for phosphatidylserine peroxidation during Fas-triggered apoptosis in lung epithelial A549 cells. Lipids 39, 1133-1142.

Jones, G., Willett, P., Glen, R.C., Leach, A.R., Taylor, R., 1997. Development and validation of a genetic algorithm for flexible docking. J Mol Biol 267, 727-748.

Kagan, V.E., Borisenko, G.G., Tyurina, Y.Y., Tyurin, V.A., Jiang, J., Potapovich, A.I., Kini, V., Amoscato, A.A., Fujii, Y., 2004. Oxidative lipidomics of apoptosis: redox catalytic interactions of cytochrome c with cardiolipin and phosphatidylserine. Free Radic Biol Med 37, 1963-1985.

Katan, M., Allen, V.L., 1999. Modular PH and C2 domains in membrane attachment and other functions. FEBS Lett 452, 36-40.

Kazanietz, M.G., Krausz, K.W., Blumberg, P.M., 1992. Differential irreversible insertion of protein kinase C into phospholipid vesicles by phorbol esters and related activators. J Biol Chem 267, 20878-20886.

Kazanietz, M.G., Barchi, J.J., Jr., Omichinski, J.G., Blumberg, P.M., 1995. Low affinity binding of phorbol esters to protein kinase C and its recombinant cysteine-rich region in the absence of phospholipids. J Biol Chem 270, 14679-14684.

Kemball-Cook, G., Tuddenham, E.G., Wacey, A.I., 1998. The factor VIII Structure and Mutation Resource Site: HAMSTeRS version 4. Nucleic Acids Res 26, 216-219.

Kenis, H., van Genderen, H., Bennaghmouch, A., Rinia, H.A., Frederik, P., Narula, J., Hofstra, L., Reutelingsperger, C.P., 2004. Cell surface-expressed phosphatidylserine and annexin A5 open a novel portal of cell entry. J Biol Chem 279, 52623-52629.

Kenis, H., Zandbergen, H.R., Hofstra, L., Petrov, A.D., Dumont, E.A., Blankenberg, F.D., Haider, N., Bitsch, N., Gijbels, M., Verjans, J.W., Narula, N., Narula, J., Reutelingsperger, C.P., 2010. Annexin A5 uptake in ischemic myocardium: demonstration of reversible phosphatidylserine externalization and feasibility of radionuclide imaging. J Nucl Med 51, 259-267.

Kerr, J.F., 2002. History of the events leading to the formulation of the apoptosis concept. Toxicology 181-182, 471-474.

Kerr, J.F., Searle, J., 1972. A suggested explanation for the paradoxically slow growth rate of basal-cell carcinomas that contain numerous mitotic figures. J Pathol 107, 41-44.

Kerr, J.F., Wyllie, A.H., Currie, A.R., 1972. Apoptosis: a basic biological phenomenon with wide-ranging implications in tissue kinetics. Br J Cancer 26, 239-257.

Kim, S.W., Quinn-Allen, M.A., Camp, J.T., Macedo-Ribeiro, S., Fuentes-Prior, P., Bode, W., Kane, W.H., 2000. Identification of functionally important amino acid residues within the C2-domain of human factor V using alanine-scanning mutagenesis. Biochemistry 39, 1951-1958.

Kim, S.W., Rhee, H.J., Ko, J., Kim, Y.J., Kim, H.G., Yang, J.M., Choi, E.C., Na, D.S., 2001. Inhibition of cytosolic phospholipase A2 by annexin I. Specific interaction model and mapping of the interaction site. J Biol Chem 276, 15712-15719.

Konig, B., Di Nitto, P.A., Blumberg, P.M., 1985. Phospholipid and Ca++ dependency of phorbol ester receptors. J Cell Biochem 27, 255-265.

Kroemer, G., El-Deiry, W.S., Golstein, P., Peter, M.E., Vaux, D., Vandenabeele, P., Zhivotovsky, B., Blagosklonny, M.V., Malorni, W., Knight, R.A., Piacentini, M., Nagata, S., Melino, G., 2005. Classification of cell death: recommendations of the Nomenclature Committee on Cell Death. Cell Death Differ 12 Suppl 2, 1463-1467.

Laskowski R A, M.M.W., Moss D S, Thornton J M,, 1993. PROCHECK - a program to check the stereochemical quality of protein structures. Journal of Applied Crystallography 26, 283-291.

Laumonier, C., Segers, J., Laurent, S., Michel, A., Coppee, F., Belayew, A., Elst, L.V., Muller, R.N., 2006. A new peptidic vector for molecular imaging of apoptosis, identified by phage display technology. J Biomol Screen 11, 537-545.

Lemmon, M.A., 2008. Membrane recognition by phospholipid-binding domains. Nat Rev Mol Cell Biol 9, 99-111.

Lemmon, M.A., Ferguson, K.M., 2000. Signal-dependent membrane targeting by pleckstrin homology (PH) domains. Biochem J 350 Pt 1, 1-18.

Letterio, J.J., Roberts, A.B., 1998. Regulation of immune responses by TGF-beta. Annu Rev Immunol 16, 137-161.

Lichtenberg, D., 1985. Characterization of the solubilization of lipid bilayers by surfactants. Biochim Biophys Acta 821, 470-478.

Lin, L., Huai, Q., Huang, M., Furie, B., Furie, B.C., 2007. Crystal structure of the bovine lactadherin C2 domain, a membrane binding motif, shows similarity to the C2 domains of factor V and factor VIII. J Mol Biol 371, 717-724.

Liu, Z., Lin, L., Yuan, C., Nicolaes, G.A., Chen, L., Meehan, E.J., Furie, B., Huang, M., 2010. Trp2313-His2315 of factor VIII C2 domain is involved in membrane binding: structure of a complex between the C2 domain and an inhibitor of membrane binding. J Biol Chem 285, 8824-8829.

Macedo-Ribeiro, S., Bode, W., Huber, R., Quinn-Allen, M.A., Kim, S.W., Ortel, T.L., Bourenkov, G.P., Bartunik, H.D., Stubbs, M.T., Kane, W.H., Fuentes-Prior, P., 1999. Crystal structures of the membrane-binding C2 domain of human coagulation factor V. Nature 402, 434-439.

Marth, T., Kelsall, B.L., 1997. Regulation of interleukin-12 by complement receptor 3 signaling. J Exp Med 185, 1987-1995.

Mayer, B.J., Ren, R., Clark, K.L., Baltimore, D., 1993. A putative modular domain present in diverse signaling proteins. Cell 73, 629-630.

Meagher, L.C., Savill, J.S., Baker, A., Fuller, R.W., Haslett, C., 1992. Phagocytosis of apoptotic neutrophils does not induce macrophage release of thromboxane B2. J Leukoc Biol 52, 269-273.

Mevorach, D., Mascarenhas, J.O., Gershov, D., Elkon, K.B., 1998. Complement-dependent clearance of apoptotic cells by human macrophages. J Exp Med 188, 2313-2320.

Mirnikjoo, B., Balasubramanian, K., Schroit, A.J., 2009. Suicidal membrane repair regulates phosphatidylserine externalization during apoptosis. J Biol Chem 284, 22512-22516.

Mochly-Rosen, D., Das, K., Grimes, K.V., 2012. Protein kinase C, an elusive therapeutic target? Nat Rev Drug Discov 11, 937-957.

Moffatt, O.D., Devitt, A., Bell, E.D., Simmons, D.L., Gregory, C.D., 1999. Macrophage recognition of ICAM-3 on apoptotic leukocytes. J Immunol 162, 6800-6810.

Morgan, R.O., Pilar Fernandez, M., 1997. Distinct annexin subfamilies in plants and protists diverged prior to animal annexins and from a common ancestor. J Mol Evol 44, 178-188.

Morgan, R.O., Jenkins, N.A., Gilbert, D.J., Copeland, N.G., Balsara, B.R., Testa, J.R., Fernandez, M.P., 1999. Novel human and mouse annexin A10 are linked to the genome duplications during early chordate evolution. Genomics 60, 40-49.

Musacchio, A., Gibson, T., Rice, P., Thompson, J., Saraste, M., 1993. The PH domain: a common piece in the structural patchwork of signalling proteins. Trends Biochem Sci 18, 343-348.

Nalefski, E.A., Falke, J.J., 1996. The C2 domain calcium-binding motif: structural and functional diversity. Protein Sci 5, 2375-2390.

Nelsestuen, G.L., Bazzi, M.D., 1991. Activation and regulation of protein kinase C enzymes. J Bioenerg Biomembr 23, 43-61.

Nishizuka, Y., 1986. Studies and perspectives of protein kinase C. Science 233, 305-312.

Nishizuka, Y., 1988. The molecular heterogeneity of protein kinase C and its implications for cellular regulation. Nature 334, 661-665.

O'Rourke, M.G., Ellem, K.A., 2000. John Kerr and apoptosis. Med J Aust 173, 616-617.

Parnaik, R., Raff, M.C., Scholes, J., 2000. Differences between the clearance of apoptotic cells by professional and non-professional phagocytes. Curr Biol 10, 857-860.

Peng, J.W., Lepre, C.A., Fejzo, J., Abdul-Manan, N., Moore, J.M., 2001. Nuclear magnetic resonance-based approaches for lead generation in drug discovery. Methods Enzymol 338, 202-230.

Perin, M.S., Fried, V.A., Mignery, G.A., Jahn, R., Sudhof, T.C., 1990. Phospholipid binding by a synaptic vesicle protein homologous to the regulatory region of protein kinase C. Nature 345, 260-263.

Pierschbacher, M.D., Ruoslahti, E., 1984. Cell attachment activity of fibronectin can be duplicated by small synthetic fragments of the molecule. Nature 309, 30-33.

Platt, N., Suzuki, H., Kodama, T., Gordon, S., 2000. Apoptotic thymocyte clearance in scavenger receptor class A-deficient mice is apparently normal. J Immunol 164, 4861-4867.

Platt, N., Suzuki, H., Kurihara, Y., Kodama, T., Gordon, S., 1996. Role for the class A macrophage scavenger receptor in the phagocytosis of apoptotic thymocytes in vitro. Proc Natl Acad Sci U S A 93, 12456-12460.

Plow, E.F., Haas, T.A., Zhang, L., Loftus, J., Smith, J.W., 2000. Ligand binding to integrins. J Biol Chem 275, 21785-21788.

Pratt, K.P., Shen, B.W., Takeshima, K., Davie, E.W., Fujikawa, K., Stoddard, B.L., 1999. Structure of the C2 domain of human factor VIII at 1.5 A resolution. Nature 402, 439-442.

Prinzen, L., Miserus, R.J., Dirksen, A., Hackeng, T.M., Deckers, N., Bitsch, N.J., Megens, R.T., Douma, K., Heemskerk, J.W., Kooi, M.E., Frederik, P.M., Slaaf, D.W., van Zandvoort, M.A., Reutelingsperger, C.P., 2007. Optical and magnetic resonance imaging of cell death and platelet activation using annexin a5-functionalized quantum dots. Nano Lett 7, 93-100.

Ran, S., Thorpe, P.E., 2002. Phosphatidylserine is a marker of tumor vasculature and a potential target for cancer imaging and therapy. Int J Radiat Oncol Biol Phys 54, 1479-1484.

Raynal, P., Pollard, H.B., 1994. Annexins: the problem of assessing the biological role for a gene family of multifunctional calcium- and phospholipid-binding proteins. Biochim Biophys Acta 1197, 63-93.

Reddy, N.R.P., Vivekanandan, S., Yoon, H.S., 2007. Expression, purification and characterization of C2 domain of milk fat globule-EGF-factor 8-L. Protein Expr. Purif. 52, 329-333.

Ren, Y., Silverstein, R.L., Allen, J., Savill, J., 1995. CD36 gene transfer confers capacity for phagocytosis of cells undergoing apoptosis. J Exp Med 181, 1857-1862.

Rich, T., Allen, R.L., Wyllie, A.H., 2000. Defying death after DNA damage. Nature 407, 777-783.

Rizo, J., Sudhof, T.C., 1998. C2-domains, structure and function of a universal Ca2+-binding domain. J Biol Chem 273, 15879-15882.

Rubartelli, A., Poggi, A., Zocchi, M.R., 1997. The selective engulfment of apoptotic bodies by dendritic cells is mediated by the alpha(v)beta3 integrin and requires intracellular and extracellular calcium. Eur J Immunol 27, 1893-1900.

Ruoslahti, E., 1996. RGD and other recognition sequences for integrins. Annu Rev Cell Dev Biol 12, 697-715.

Salim, N.N., Feig, A.L., 2009. Isothermal titration calorimetry of RNA. Methods 47, 198-205.

Savill, J., Fadok, V., 2000. Corpse clearance defines the meaning of cell death. Nature 407, 784-788.

Savill, J., Hogg, N., Ren, Y., Haslett, C., 1992. Thrombospondin cooperates with CD36 and the vitronectin receptor in macrophage recognition of neutrophils undergoing apoptosis. J Clin Invest 90, 1513-1522.

Savill, J., Dransfield, I., Gregory, C., Haslett, C., 2002. A blast from the past: clearance of apoptotic cells regulates immune responses. Nat Rev Immunol 2, 965-975.

Schasfoort RBM, T.A., 2008. Handbook of surface plasmon resonance. The Royal Society of Chemistry, Cambridge, UK.

Schellenberger, E., Schnorr, J., Reutelingsperger, C., Ungethum, L., Meyer, W., Taupitz, M., Hamm, B., 2008. Linking proteins with anionic nanoparticles via protamine: ultrasmall protein-coupled probes for magnetic resonance imaging of apoptosis. Small 4, 225-230.

Schultz, J., Milpetz, F., Bork, P., Ponting, C.P., 1998. SMART, a simple modular architecture research tool: identification of signaling domains. Proc Natl Acad Sci U S A 95, 5857-5864.

Schurholz, T., 1996. Critical dependence of the solubilization of lipid vesicles by the detergent CHAPS on the lipid composition. Functional reconstitution of the nicotinic acetylcholine receptor into preformed vesicles above the critical micellization concentration. Biophys Chem 58, 87-96.

Schutters, K., Reutelingsperger, C., 2010. Phosphatidylserine targeting for diagnosis and treatment of human diseases. Apoptosis 15, 1072-1082.

Scott, R.S., McMahon, E.J., Pop, S.M., Reap, E.A., Caricchio, R., Cohen, P.L., Earp, H.S., Matsushima, G.K., 2001. Phagocytosis and clearance of apoptotic cells is mediated by MER. Nature 411, 207-211.

Shao, C., Novakovic, V.A., Head, J.F., Seaton, B.A., Gilbert, G.E., 2008. Crystal structure of lactadherin C2 domain at 1.7A resolution with mutational and computational analyses of its membrane-binding motif. J Biol Chem 283, 7230-7241.

Shao, X., Li, C., Fernandez, I., Zhang, X., Sudhof, T.C., Rizo, J., 1997. Synaptotagmin-syntaxin interaction: the C2 domain as a Ca2+-dependent electrostatic switch. Neuron 18, 133-142.

Sharma, D.a.R., K., 2000. 13C NMR chemical shifts can predict disulfide bond formation. Journal of B. NMR 18, 165-171.

Sheetz, M.P., Sable, J.E., Dobereiner, H.G., 2006. Continuous membrane-cytoskeleton adhesion requires continuous accommodation to lipid and cytoskeleton dynamics. Annu Rev Biophys Biomol Struct 35, 417-434.

Shi, J., Shi, Y., Waehrens, L.N., Rasmussen, J.T., Heegaard, C.W., Gilbert, G.E., 2006. Lactadherin detects early phosphatidylserine exposure on immortalized leukemia cells undergoing programmed cell death. Cytometry A 69, 1193-1201.

Silvestre, J.S., Thery, C., Hamard, G., Boddaert, J., Aguilar, B., Delcayre, A., Houbron, C., Tamarat, R., Blanc-Brude, O., Heeneman, S., Clergue, M., Duriez, M., Merval, R., Levy, B., Tedgui, A., Amigorena, S., Mallat, Z., 2005. Lactadherin promotes VEGF-dependent neovascularization. Nat Med 11, 499-506.

Silvius, J.R., 1992. Solubilization and functional reconstitution of biomembrane components. Annu Rev Biophys Biomol Struct 21, 323-348.

Stace, C.L., Ktistakis, N.T., 2006. Phosphatidic acid- and phosphatidylserine-binding proteins. Biochim Biophys Acta 1761, 913-926.

Stern, M., Savill, J., Haslett, C., 1996. Human monocyte-derived macrophage phagocytosis of senescent eosinophils undergoing apoptosis. Mediation by alpha v beta 3/CD36/thrombospondin recognition mechanism and lack of phlogistic response. Am J Pathol 149, 911-921.

Stoilova-McPhie, S., Villoutreix, B.O., Mertens, K., Kemball-Cook, G., Holzenburg, A., 2002. 3-Dimensional structure of membrane-bound coagulation factor VIII: modeling of

the factor VIII heterodimer within a 3-dimensional density map derived by electron crystallography. Blood 99, 1215-1223.

Stuart, L.M., Lucas, M., Simpson, C., Lamb, J., Savill, J., Lacy-Hulbert, A., 2002. Inhibitory effects of apoptotic cell ingestion upon endotoxin-driven myeloid dendritic cell maturation. J Immunol 168, 1627-1635.

Swairjo, M.A., Concha, N.O., Kaetzel, M.A., Dedman, J.R., Seaton, B.A., 1995. Ca(2+)-bridging mechanism and phospholipid head group recognition in the membrane-binding protein annexin V. Nat Struct Biol 2, 968-974.

Tagariello, G., Belvini, D., Salviato, R., Are, A., De Biasi, E., Goodeve, A., Davoli, P., 2000. Experience of a single Italian center in genetic counseling for hemophilia: from linkage analysis to molecular diagnosis. Haematologica 85, 525-529.

Tait, J.F., Gibson, D., 1994. Measurement of membrane phospholipid asymmetry in normal and sickle-cell erythrocytes by means of annexin V binding. J Lab Clin Med 123, 741-748.

Takeshima, K., Smith, C., Tait, J., Fujikawa, K., 2003. The preparation and phospholipid binding property of the C2 domain of human factor VIII. Thromb Haemost 89, 788-794.

Tamm, L.K., Tatulian, S.A., 1997. Infrared spectroscopy of proteins and peptides in lipid bilayers. Q Rev Biophys 30, 365-429.

Taylor, P.R., Carugati, A., Fadok, V.A., Cook, H.T., Andrews, M., Carroll, M.C., Savill, J.S., Henson, P.M., Botto, M., Walport, M.J., 2000. A hierarchical role for classical pathway complement proteins in the clearance of apoptotic cells in vivo. J Exp Med 192, 359-366.

Teruel, M.N., Meyer, T., 2000. Translocation and reversible localization of signaling proteins: a dynamic future for signal transduction. Cell 103, 181-184.

Thapa, N., Kim, S., So, I.S., Lee, B.H., Kwon, I.C., Choi, K., Kim, I.S., 2008. Discovery of a phosphatidylserine-recognizing peptide and its utility in molecular imaging of tumour apoptosis. J Cell Mol Med 12, 1649-1660.

Thornberry, N.A., Rano, T.A., Peterson, E.P., Rasper, D.M., Timkey, T., Garcia-Calvo, M., Houtzager, V.M., Nordstrom, P.A., Roy, S., Vaillancourt, J.P., Chapman, K.T., Nicholson, D.W., 1997. A combinatorial approach defines specificities of members of the caspase family and granzyme B. Functional relationships established for key mediators of apoptosis. J Biol Chem 272, 17907-17911.

Urban, B.C., Willcox, N., Roberts, D.J., 2001. A role for CD36 in the regulation of dendritic cell function. Proc Natl Acad Sci U S A 98, 8750-8755.

van Heerde, W.L., de Groot, P.G., Reutelingsperger, C.P., 1995. The complexity of the phospholipid binding protein Annexin V. Thromb Haemost 73, 172-179.

Vance, J.E., Steenbergen, R., 2005. Metabolism and functions of phosphatidylserine. Prog Lipid Res 44, 207-234.

Verdaguer, N., Corbalan-Garcia, S., Ochoa, W.F., Fita, I., Gomez-Fernandez, J.C., 1999. Ca(2+) bridges the C2 membrane-binding domain of protein kinase Calpha directly to phosphatidylserine. EMBO J 18, 6329-6338.

Voll, R.E., Herrmann, M., Roth, E.A., Stach, C., Kalden, J.R., Girkontaite, I., 1997. Immunosuppressive effects of apoptotic cells. Nature 390, 350-351.

Wajant, H., 2002. The Fas signaling pathway: more than a paradigm. Science 296, 1635-1636.

Weng, X., Luecke, H., Song, I.S., Kang, D.S., Kim, S.H., Huber, R., 1993. Crystal structure of human annexin I at 2.5 A resolution. Protein Sci 2, 448-458.

Wood, B.L., Gibson, D.F., Tait, J.F., 1996. Increased erythrocyte phosphatidylserine exposure in sickle cell disease: flow-cytometric measurement and clinical associations. Blood 88, 1873-1880.

Wright, S.D., Silverstein, S.C., 1983. Receptors for C3b and C3bi promote phagocytosis but not the release of toxic oxygen from human phagocytes. J Exp Med 158, 2016-2023.

Wu, Y., Tibrewal, N., Birge, R.B., 2006. Phosphatidylserine recognition by phagocytes: a view to a kill. Trends Cell Biol 16, 189-197.

Wyllie, A.H., Kerr, J.F., Currie, A.R., 1973. Cell death in the normal neonatal rat adrenal cortex. J Pathol 111, 255-261.

Yeung, T., Gilbert, G.E., Shi, J., Silvius, J., Kapus, A., Grinstein, S., 2008. Membrane phosphatidylserine regulates surface charge and protein localization. Science 319, 210-213.

Zhang, G., Kazanietz, M.G., Blumberg, P.M., Hurley, J.H., 1995. Crystal structure of the cys2 activator-binding domain of protein kinase C delta in complex with phorbol ester. Cell 81, 917-924.

Zhou, Q., Zhao, J., Stout, J.G., Luhm, R.A., Wiedmer, T., Sims, P.J., 1997. Molecular cloning of human plasma membrane phospholipid scramblase. A protein mediating

transbilayer movement of plasma membrane phospholipids. J Biol Chem 272, 18240-18244.